İmalat Teknolojileri ve Uygulamaları
Manufacturing Technologies and Applications
(MATECA)
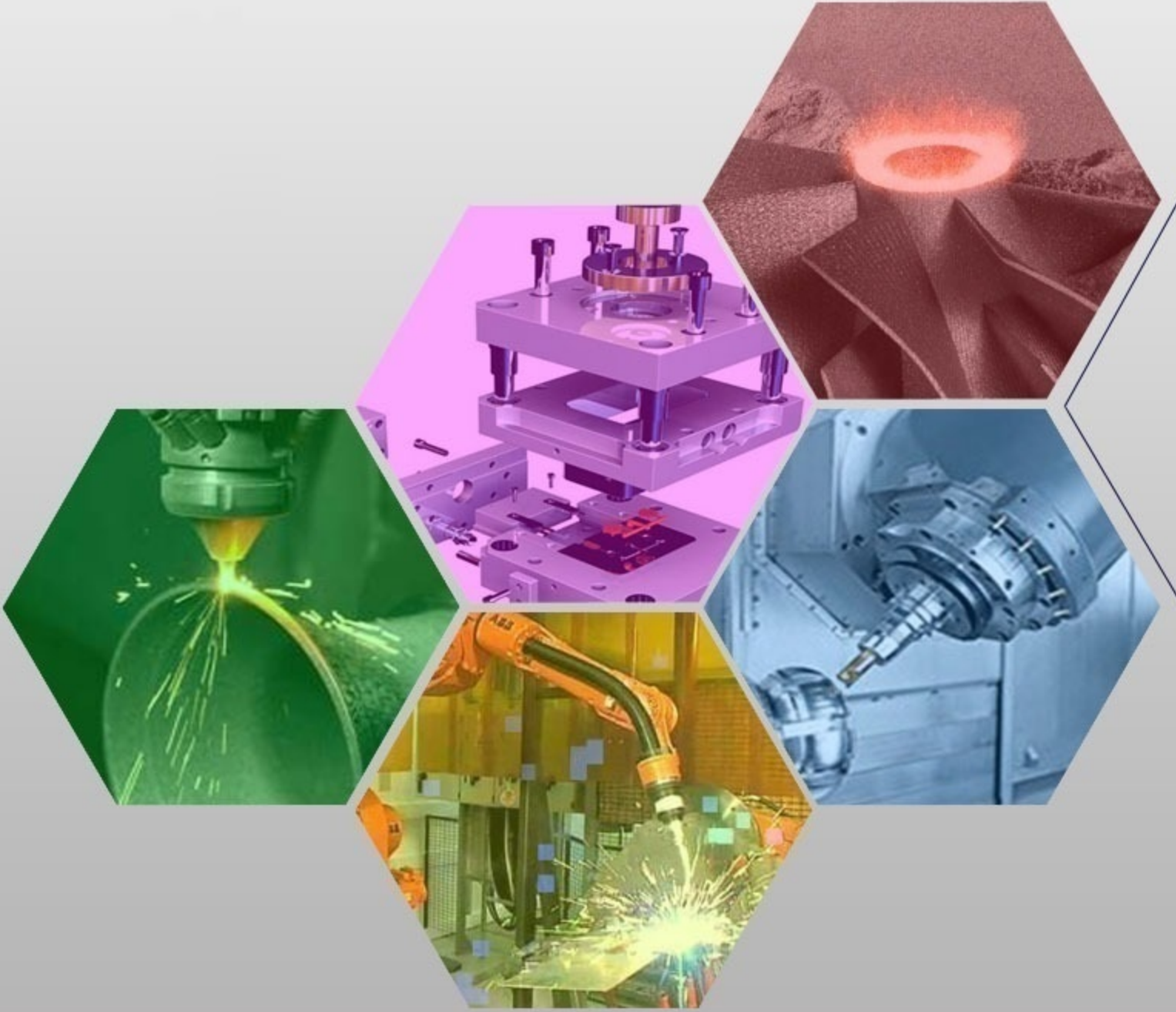
https://dergipark.org.tr/tr/pub/mateca

İÇİNDEKİLER (CONTENTS)

Measurement and Evaluation of Machinability Characteristics in Turning of Train Wheel Steel via CVD Coated-RCMX Carbide Tool

Recep DEMİRSÖZ[1*] (iD), Mehmet BOY[2] (iD)

[1*]*Karabük Üniversitesi, Mühendislik Fakültesi, Karabük, Türkiye*

[2]*Karabük Üniversitesi, TOBB Teknik Bilimler MYO, Karabük, Türkiye*

ABSTRACT

ER7 quality steels produced according to EN13262 standard used in European railway lines can be produced at Kardemir A.Ş Railway Wheel Production Facilities. These wheels, which are produced by pressing and rolling, are included in the machining process to be brought to their final dimensions after the production process. In this experimental study, the effects of cutting speed (CS) and feed rate (FR) on surface roughness (SR), power consumption (PC) and cutting temperature (CT) were investigated during turning of ER7 wheel material with 1mm depth of cut value under dry test conditions using MT-TiCN+Al$_2$O$_3$ CVD coated-RCMX 1606M0 K15 quality tool. Analysis of Variance (ANOVA) method was used to determine the effect rates of the input parameters on the results. In addition, estimation equations were obtained using the Response Surface Method (RSM). As a result of this study, the effective parameter for SR is FR with 57.158%, while the effective parameter for PC and CT is found to be CS, and it is found to be 58.071% and 64.977%, respectively.

CVD Kaplamalı-RCMX Karbür Takım ile Tren Tekerleği Çeliğinin Tornalanmasında İşlenebilirlik Özelliklerinin Ölçülmesi ve Değerlendirilmesi

ÖZET

Avrupa demir yolu hatlarında kullanılmakta olan EN13262 standardına göre üretilmiş ER7 kalite çelikleri Kardemir A.Ş Demir Yolu Tekeri Üretim Tesislerinde üretilebilmektedir. Pres ve haddeleme ile üretilen bu tekerlekler üretim prosesinin ardından nihai ölçülerine getirilmek üzere talaşlı imalat sürecine girmektedir. Bu çalışmada MT-TiCN+Al$_2$O$_3$ CVD kaplamalı-RCMX 1606M0 K15 kalite takım kullanılarak kuru test koşullarında ER7 tekerlek malzemesinin 1mm kesme derinliği değeri ile tornalanması sırasında ilerleme hızı (FR) ve kesme hızı (CS) parametrelerinin yüzey pürüzlülüğü (SR), güç harcaması (PC) ve kesme sıcaklığı (CT) üzerindeki etkileri araştırılmıştır. Giriş parametrelerinin sonuçlar üzerindeki etki oranlarının tespitinde varyans analizi (ANOVA) yöntemi kullanılmıştır. Ayrıca Cevap Yüzey Metodu kullanılarak tahmin denklemleri elde edilmiştir. Bu çalışmanın sonucunda yüzey pürüzlülüğü için etkili parametre %57.158 ile ilerleme hızı olurken, güç harcaması ve kesme sıcaklığı için etkili parametrenin kesme hızı olduğu tespit edilmiş olup sırası ile %58.071 ve %64.797 olarak bulunmuştur.

1. INTRODUCTION (GİRİŞ)

By using a vacuum degassing process and continuous casting method, the semi-finished products (thick round) of the items to be manufactured are created in the necessary steel quality (ER7) [1]. One of the most encountered problems in railway management is wheel flats. "Flat spots" or "wheel flats" are a defect that occurs in railway wheels. There are many factors in the formation of flattening points and wheel flats [2]. To eliminate these factors, dry machining of these train wheels via round insert are performed to obtain much better surface quality. While coolant is used in most

Nomenclature			
Adj. MS	Adjusted mean squares	FR	Feed rate (mm/rev)
Adj. SS	Adjusted sums of squares	MT	Medium temperature (°C)
ANOVA	Analysis of variance	PC	Power consumption (W)
CNC	Computer numeric control	PCR	Parameter contribution rate (%)
CS	Cutting speed (m/min)	RCMX	Round shape cutting tool
CT	Cutting temperature (°C)	RSM	Response surface method
CVD	Chemical vapor deposition	SR	Surface roughness (μm)
DF	Degree of freedom	TOBB	The Union of Chambers and
EN	European norm		Commodity Exchanges of Turkey

machining applications, some applications do not use coolant. Since cutting fluid is not used in the machining method, which it can be describe as dry machining, this method is considered a clean production method. Elimination of the negative effects of cutting fluids on human health and the environment while it has advantages such as reduction of overall processing costs by eliminating filtration, cleaning and disposal costs; and a cleaner working environment [3]. For these reasons, the dry machining method without using cutting fluid is becoming more and more popular. Even if the negative effects of cutting fluids are eliminated in dry machining, it is very difficult to abandon the use of cutting fluids due to high efficiency and performance advantages in machining [4], [5]. In dry machining, there is relatively more friction and adhesion and higher temperatures at the cutting tool and workpiece interface [6]. If a good machining is to be mentioned in the case of dry machining, the correct selection of parameters such as machining process, cutting tool and workpiece material is important [7]. Polycrystalline diamond, ceramic, etc., with high temperature hardness and high wear resistance in dry machining. It would be appropriate to prefer materials such as the material properties of the cutting tool, the geometry of the cutting tool is an important parameter, and it should be selected in the geometry suitable for the work to be done and with optimum properties suitable for the workpiece. Coated tools can also be preferred to increase the performance and life of the tool in machining. The coatings on the tools act as a lubricant, reducing the friction between the tool and the workpiece and preventing the tool from sticking [8]. Because of these effects, it affects the tool life positively. There is a need for the development of new technology tool coatings, which prevent the coating of the tool to be used during long working periods, making it economical as well as improving the product quality [9].

Soft materials such as aluminum are not recommended for dry machining, as they cause chip accumulation on the tool and risk affecting the surface quality during machining [10]. Although dry machining is an environmentally friendly option, it has some disadvantages in processing [11]–[13]. The biggest disadvantage is the high temperature generated during machining, which causes tool wear [14], [15]. In addition, there is a possibility of reducing the tool life and decreasing the surface quality due to the possibility of accumulation of chips generated during machining in the machining area and especially at the tool tip. Due to these disadvantages, it is important to determine the cutting parameters and the machining process correctly [16], to match the material of the workpiece and the cutting tool, and to optimize the cutting process. To summarize the problems related to dry processing [17]. Tool wear that may occur due to friction, poor dimensional tolerance and surface quality, low CS and production speed values to increase tool life, accumulation of chip to low CS, lack of advantages in chip removal, difficult to machine materials [18], [19].

It has been observed that machining operations such as turning, drilling and milling are more suitable for dry machining than closed surface machining, due to the easy evacuation of chip formed in open surface machining. In addition, in closed surface machining such as tapping and drilling, efficient dry machining cannot be performed due to the chip evacuation problem and therefore the possibility of damage to the workpiece surface [20].

2. MATERIAL AND METHOD (MATERYAL VE YÖNTEM)

EN 13262 standard is used to determine the characteristics of train wheels used in European railway networks. In this standard, four different steel grades, ER6, ER7, ER8 and ER9, are defined for use in train wheels. These grades have low carbon content (0.55% C) and pearlitic and ferritic structures. After the train wheels are produced by forging method, they are processed on special vertical CNC lathes due to their geometric shape, size and weight. Since there is not enough lathe in size for the machining of the commercially produced train wheel in the university laboratories, ER7 quality material with the dimensions of 170x50mm was taken from the wheel hub to be used as a test workpiece. The chemical composition of ER7 quality steel used in turning experiments is shown in Table 1. The test workpieces were obtained from Kardemir A.Ş., which manufactures and commercially sells train wheels.

Table 1. The chemical composition of ER7 steel (wt%) (ER7 çeliğinin kimyasal bileşimi (%ağ.)

C	Mn	Si	S	P	Cr	Ni	Cu	Mo	V	Cr+Ni+Mo	H.ppm
0.52	0.80	0.40	0.015	0.020	0.30	0.30	0.30	0.080	0.060	0.50 max	2.0 max

In the experiments, MT-TiCN+Al$_2$O$_3$ CVD coated-RCMX 1606M0 K15 quality tool and suitable tool holder were used in accordance with ISO standards of Korloy company. The experiments were carried out on the TTC-550 CNC lathe located in TOBB Technical Sciences Vocational School Laboratory at Karabük University. Fixed depth of cut (1mm), three different CS (200, 250, 300 m/min) and three different FR (0.15, 0.20, 0.30 mm/rev) were used in the experiments. The temperatures on the cutting tool and workpiece during turning were measured with the Fluke TI400 infrared camera. The infrared camera has automatic focusing, a temperature measuring range of 0 °C to 1200 °C and a measurement accuracy of ±2 °C. KAEL Network Analyzer with three 60/5A current transformers was used to precisely measure the PC of the CNC lathe during turning. After each machining parameter, the SR of the workpiece was measured with the Mahr M300 roughness device. For each measurement, the workpiece was rotated approximately 70° and measured from five different regions and evaluated by taking the average value. The experimental setup is shown in Figure 1.

In the study, an experimental design was made with RSM and SR (Ra), PC (W), temperature (°C) values were taken as basis as quality properties. Control factors were determined as FR(f) and CS (V). Each control factor was defined at three levels and the RSM L9 index was used. RSM-based second-order estimation models have been developed. Analysis of variance (ANOVA) was performed using Minitab software to examine the interaction of the processing parameters separately and with each other.

3. RESULTS and DISCUSSION (SONUÇLAR ve TARTIŞMA)

The study on train wheel material turning, two different variables, CS and FR, and three different values determined according to the preliminary experiments for each variable were used and the results were evaluated on the SR, PC during machining and machining temperature outputs. The cutting depth value was kept constant as 1 mm in the experiments. Experimental results are listed in Table 2. Estimation equations developed using Response Surface Method (RSM) are given in Table 3.
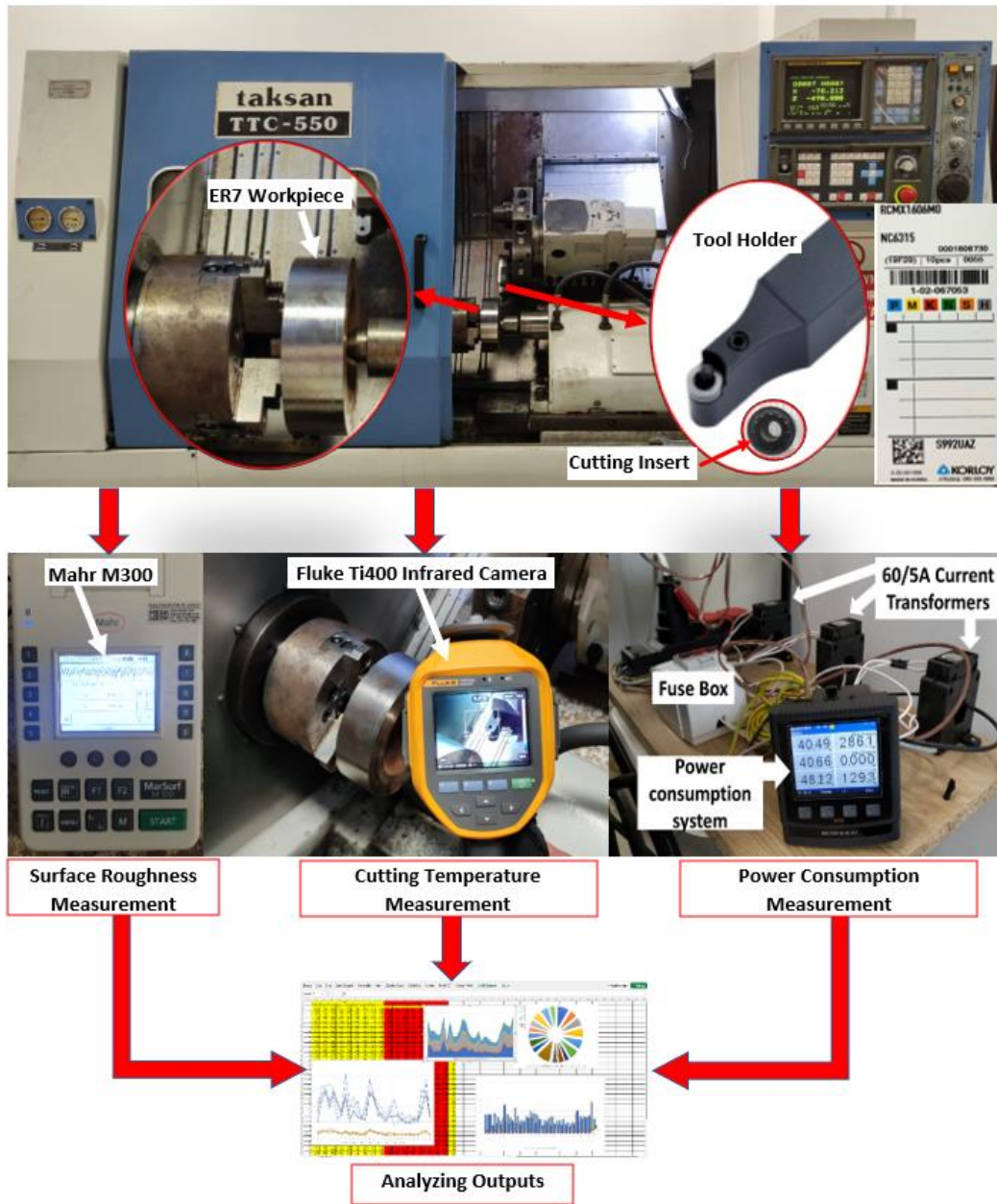
Figure 1. Experimental setup (Deneysel kurulum)

Table 2. Table of experimental and estimated results (Deneysel ve tahmini sonuçlar tablosu)

	Exp. No.	CS (V) [m/min]	FR (f) [mm/rev]	SR (Ra) [µm]	Regression Results SR (Ra) [µm]	PC [W]	Regression Results PC [W]	CT [C]	Regression Results CT [C]
	1	200	0.15	0.635	0.603	342.3	344.078	277	283.556
	2	200	0.2	0.663	0.681	390.3	387.078	376	360.889
RCMX Tool	3	200	0.25	0.752	0.758	434.3	435.744	393	401.556
	4	250	0.15	0.521	0.541	400.3	397.411	406	405.556
	5	250	0.2	0.591	0.619	432.3	437.411	466	470.889
	6	250	0.25	0.729	0.696	485.3	483.078	504	499.556
	7	300	0.15	0.496	0.479	450.3	451.411	461	454.889
	8	300	0.2	0.544	0.557	490.3	488.411	498	508.222
	9	300	0.25	0.638	0.634	530.3	531.078	529	524.889

Table 3. Equations developed by RSM (RSM ile geliştirilen denklemler)

	Ra [µm] = 1.370 − 0.00322*V - 3.73*f + 0.000003*V^2 + 11.62*f^2 + 0.00253*V*f
RCMX	Total Power [W] = 6 + 1.187*V + 703*f + 0.00013*V^2 + 1133*f^2 - 1.200*V*f
	Temperature [°C] = -1527 + 9.7*V + 5073*f - 0.01453*V^2 - 7333*f^2 - 4.8*V*f

3.1. Surface Roughness (Yüzey Pürüzlülüğü)

The roughness values of the surfaces that emerge after machining are very important in terms of manufacturing quality and are an output that is closely followed by the manufacturers. Roughness values of the processed material, toughness, strength, and abrasion resistance, etc. reflects its mechanical properties, as well. The main purpose in machining is to obtain surfaces with as low roughness as possible. For this reason, researchers focused on reducing the SR values.
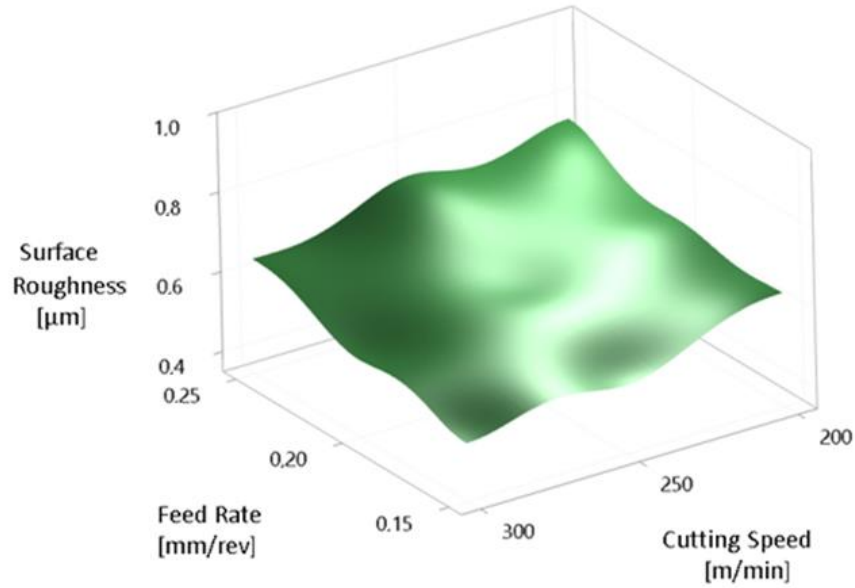
Figure 2. 3D-SR value graph under interactions of process parameters for RCMX cutting tool (RCMX kesici takım için proses parametrelerinin etkileşimleri altında 3B yüzey pürüzlülük değer grafiği)

Figure 3. Graph of SR values obtained according to different parameters (Farklı parametrelere göre elde edilen yüzey pürüzlülüğü değerleri grafiği)

In this study, SR values were measured at different SC and FR after the experiments. These roughness values were taken from three different points on the machined surface and were given as average values. It is seen that the SR values decrease as the CS increases and increase as the FR increases (Figure 2). The test conditions in which the highest SR value is 200 m/min CS and 0.25 mm/rev FR. The experimental conditions at 0.15 mm/rev FR and 300 m/min CS give the lowest roughness values. When the graph given in Figure 3 is evaluated with the RCMX cutting tool, the SR value is 0.496 µm at 0.15 mm/rev FR and 300 m/min CS, and the SR value is 0.544 µm at 0.20 mm/rev FR. It is measured as 0.638 µm at a FR of 0.25 mm/rev. When the FR value increases from 0.15 to 0.20 mm/rev and from 0.15 to 0.25 mm/rev, the increases in the SR value are 9.7% and 28.63%, respectively. About the RCMX cutting tool, the SR value is measured as 0.663 µm at 0.20 mm/rev FR and 200 m/min CS, 0.591 µm at 250 m/min CS and 0.544 µm at 300 m/min CS. When the CS value increases from 200 to 250 m/min and from 200 to 300 m/min, the reductions in the SR value are 10.86% and 17.95%, respectively. The surface roughness increases with increasing feed rate depending on that surface roughness is mainly a function of the feed rate due to increasing load per unit cutting zone by increasing too-chip contact area as as shown in many investigations. Moreover, surface roughness decreases with increasing cutting speed due to decreasing friction coefficient any easier to cut by higher cutting speed [7], [21].

Table 4. ANOVA results according to SR values for RCMX cutting tool (RCMX kesici takım için yüzey pürüzlülük değerlerine göre ANOVA sonuçları)

Source	DF	Adj SS	Adj MS	F-Value	P-Value	PCR (%)
CS - V [m/min]	1	0.023023	0.023023	32.75	0.0110	36.412
FR - f [mm/rev]	1	0.036141	0.036141	51.41	0.0060	**57.158**
V*V	1	0.000109	0.000109	0.16	0.7200	0.172
f*f	1	0.001688	0.001688	2.40	0.2190	2.670
V*f	1	0.000160	0.000160	0.23	0.6650	0.253
Error	3	0.002109	0.000703			3.335
Total	8	0.063230				100

When the variance analysis results given in Table 4 according to the RCMX cutting tool are examined, it is seen that the FR parameter is more effective than the CS parameter. While the effect rate in the FR is 57.158%, this rate is 36.412% for the CS. For a parameter to be statistically significant, the P-value must be less than 0.05 [22]. When the squares of the parameters and the P values of their interaction are examined, it is seen that the results are not significant. On the other hand, the results obtained are significant because the mentioned P values of the parameters are less than 0.05. In the RCMX cutting tool, the results are found to be not significant when the P values obtained from the squares of the parameters and their interaction are examined. CS and FR values are statistically significant. As a result, in cases where good SR is expected, when working with RCMX cutting tools, it will be appropriate to work with 300 m/min and 0.15 mm/rev values to obtain the best SR value. When the error values are examined, it can be said that these values may be caused by bench vibrations, vibrations from the ground or the microstructure of the material. The error value is obtained as 3.335% for the RCMX cutting tool.
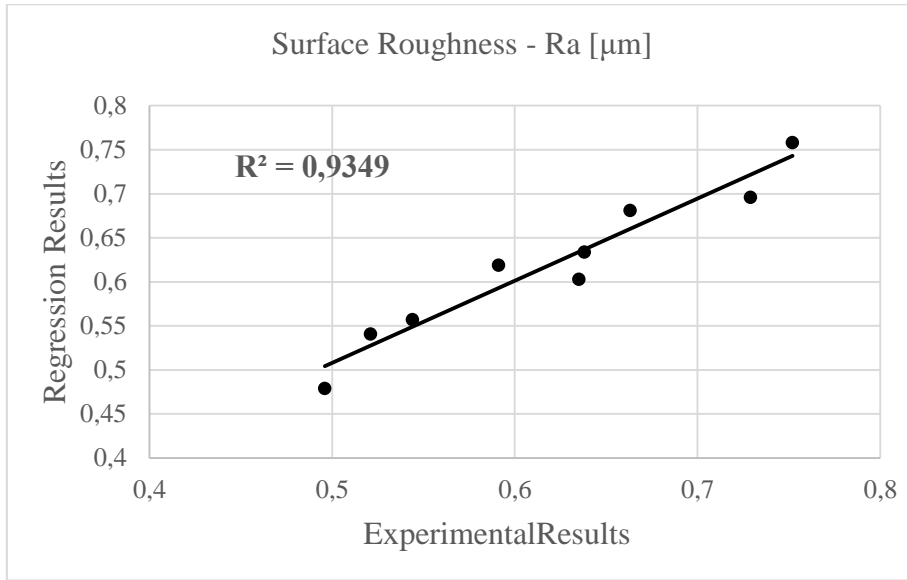
Figure 4. Regression graph of SR results (Yüzey pürüzlülük sonuçlarının regresyon grafiği)

When the graph obtained from the RSM given in Figure 4 for SR is examined, it is seen that the experimental results and the results obtained from the model estimation are in good agreement. R^2 values expressing the agreement of the results were found to be 0.9349.

3.2. Power Consumption (Güç Tüketimi)

The total power value measured during the machining on the CNC lathe where the experiments were carried out was obtained from the sum of the linear power, idle mode power, spindle power and machining power values. According to the tool used during the experiments, the total power values at different CS and FR were measured. The test conditions with the highest power values are 0.25 mm/rev FR and 300 m/min CS (Figure 5). Moreover, the experimental conditions at a CS of 200 m/min and a FR of 0.15 mm/rev give the lowest power values.

Figure 5.3D-PC graph under interactions of process parameters for RCMX cutting tool (RCMX kesici takım için proses parametrelerinin etkileşimleri altında 3B güç tüketim değerleri grafiği)
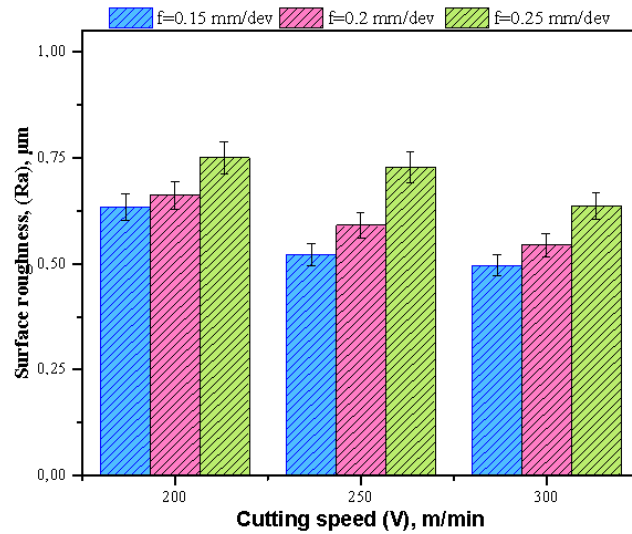
Figure 6. Graph of PC values obtained according to different parameters (Farklı parametrelere göre elde edilen güç tüketim değerleri grafiği)

When the graph given in Figure 6 is evaluated regarding the RCMX cutting tool, the PC value is 450.3 W at 0.15 mm/rev FR and 300 m/min CS, PC value is 490 at 0.20 mm/rev FR. It is measured as 530.3 W at a FR of 3 W and 0.25 mm/rev. The increases in PC are 8.88% and 17.76%, respectively, when the FR value increases from 0.15 to 0.20 mm/rev and from 0.15 to 0.25 mm/rev. The PC value is measured as 434.3 W at a FR of 0.25 mm/rev and a CS of 200 m/min, 485.3 W at a CS of 250 m/min and 530.3 W at a CS of 300 m/min. The increases in PC are 11.74% and 22.10%, respectively, when the CS increases from 200 to 250 m/min and from 200 to 300 m/min. This can attributed that the power consumption increases with increasing feed rate depending on that it is mainly a function of the feed rate due to increasing load per unit cutting zone by increasing too-chip contact area like in surface roughness [23], [24]. Moreover, cutting speed has also rising effect on power consumption due to its increasing influence on spindle speed and spindle power [23].

Table 5. ANOVA results according to PC values for RCMX cutting tool (RCMX kesici takım için güç tüketim değerlerine göre ANOVA sonuçları)

Source	DF	Adj SS	Adj MS	F-Value	P-Value	PCR (%)
CS - V [m/min]	1	15402.7	15402.7	764.47	0.00010	**58.072**
FR - f [mm/rev]	1	11008.2	11008.2	546.36	0.00017	41.503
V*V	1	0.2	0.2	0.01	0.92299	0.001
f*f	1	16.1	16.1	0.80	0.43780	0.061
V*f	1	36	36	1.79	0.27365	0.136
Error	3	60.4	20.1			0.228
Total	8	26523.6				100

When the variance analysis results given in Table 5 regarding the RCMX cutting tool are examined, it is seen that the CS parameter is more effective than the FR parameter regarding the power values. While the rate in FR is 41.503 %, this rate increases to 58.072 in CS. When the squares of the parameters and the P values of their interaction are examined, it is seen that the results are greater than 0.05 and therefore cannot be statistically significant. On the other hand, the results obtained are statistically significant because the mentioned P values of the parameters are much smaller than 0.05. When the P values obtained for the squares of the parameters in the RCMX cutting tool, are examined, it is seen that the results are meaningless. However, it is significant because the P-value obtained for the interaction of the parameters is less than 0.05. The CS and FR values are also statistically significant. As a result, if it is desired to work with lower energy

consumption values, it will be appropriate to work with 200 m/min and 0.15 mm/rev values to obtain the lowest power value in case of working with RCMX cutting tools. When the error values are examined, it can be said that these values may be caused by reasons such as bench vibrations, vibrations from the floor or the microstructure of the material, which are not considered in this study. These error values are obtained as 0.228% for the RCMX cutting tool.
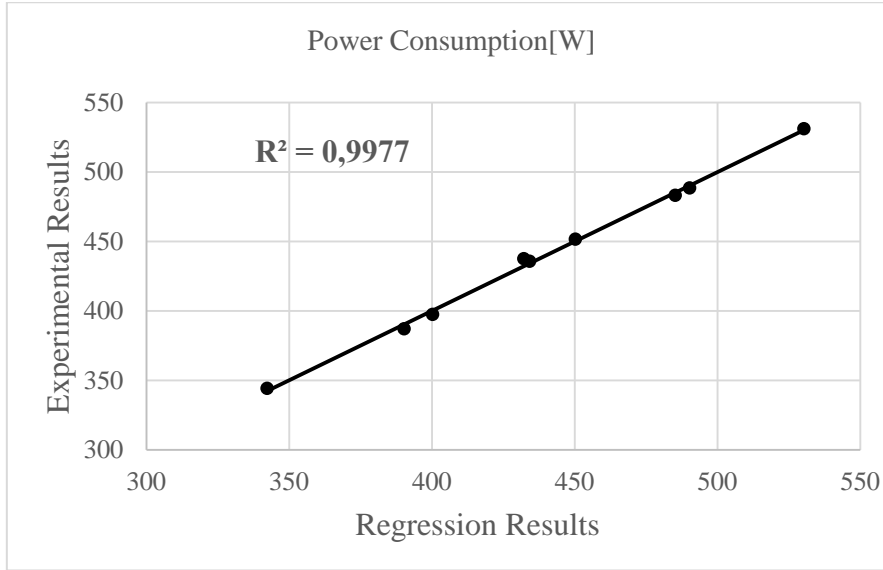
Figure 7. Regression graph of PC results (Güç tüketim sonuçlarının regresyon grafiği)

When the graph obtained from the RSM given in Figure 7 for PC is examined, it is seen that the experimental results and the results obtained from the model estimation are in good agreement. R^2 values expressing the agreement of the results were found to be 0.9977.

3.3.   Cutting temperature (Kesme Sıcaklığı)

In almost all machining processes, mechanical energy converts into heat energy. Some of the heat generated is in the processed material, some of it stays on the tool, and some of it is removed with the material chips. During the experiments, the temperature values that occurred because of heat are measured separately at different CS and FR. The test conditions with the highest temperature value are 300 m/min CS and 0.25 mm/rev FR. The lowest temperature value is found at a FR of 0.15 mm/rev and a CS of 200 m/min. With the increase of the CS, the temperature values also increase (Figure 8). The increase in the FR causes an increase in temperature. The increase in CTs directly affects the tool life.
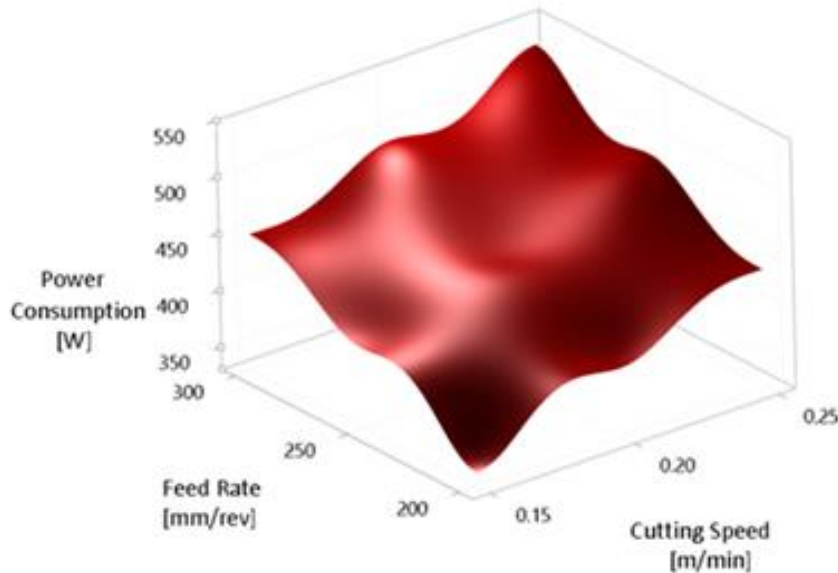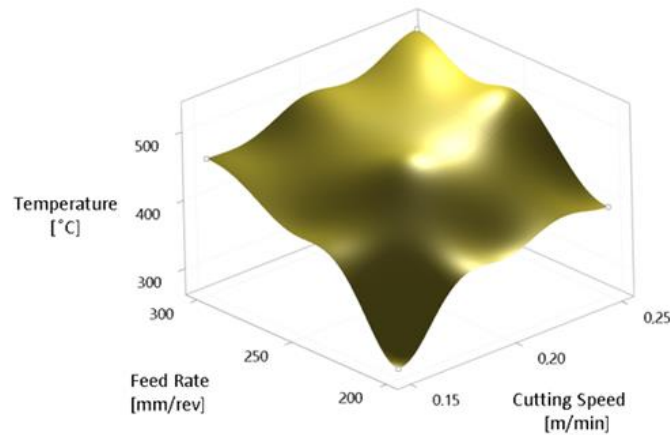

Figure 8. 3D-CT graphs under interactions of process parameters for RCMX cutting tool (RCMX kesici takım için proses parametrelerinin etkileşimleri altında 3B kesme sıcaklığı değer grafiği)
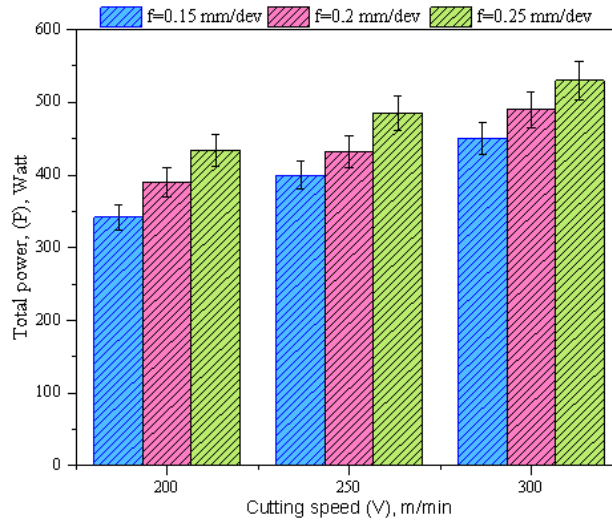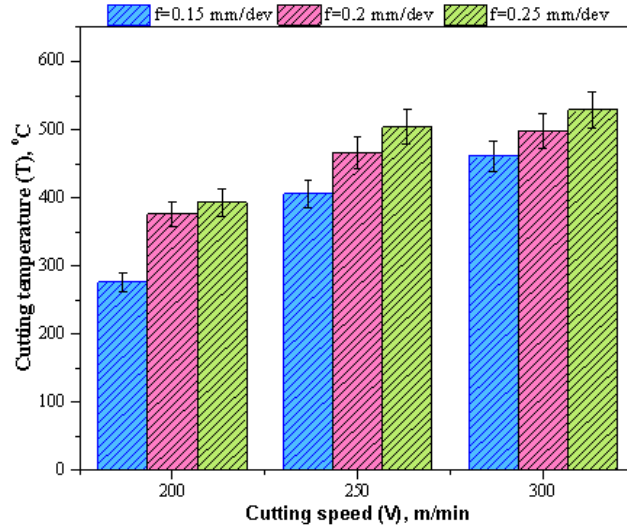
Figure 9. Graph of CT values obtained according to different parameters (Farklı parametrelere göre elde edilen kesme sıcaklığı değerleri grafiği)

Looking at the graph in Figure 9, the temperature value occurring at a FR of 0.15 mm/rev and a CS of 300 m/min is 461 °C, the temperature value is 498 °C at a FR of 0.20 mm/rev and 0.25 mm/rev. At rev FR, it is measured as 529° C. When the FR value increases from 0.15 to 0.20 mm/rev and from 0.15 to 0.25 mm/rev, the increases in temperature value are 8% and 14.75%, respectively. For the RCMX cutting tool, the temperature value was measured as 393 °C at a FR of 0.25 mm/rev and a CS of 200 m/min, 504 °C at a CS of 250 m/min, and 529 °C at a CS of 300 m/min. When the CS value increases from 200 to 250 m/min and from 200 to 300 m/min, the rate of increase in temperature value is 28.24% and 34.61%, respectively. Because of the increased load per unit cutting zone caused by an increase in too-chip contact area, as shown in surface roughness and power, it can be concluded that the cutting temperature rises with increasing feed rate based on the fact that it is mostly a function of the feed rate. Furthermore, cutting speed has a growing impact on cutting temperature as a result of its increasing influence on spindle speed and spindle power, which are both increasing with cutting speed.

Table 6. ANOVA results according to CT values for RCMX cutting tool (RCMX kesici takım için kesme sıcaklığı değerlerine göre ANOVA sonuçları)

Source	DF	Adj SS	Adj MS	F-Value	P-Value	PCR (%)
CS - V [m/min]	1	32560.7	32560.7	178.54	0.001	**64.797**
FR - f [mm/rev]	1	13254	13254	72.68	0.003	26.376
V*V	1	2640.2	2640.2	14.48	0.032	5.254
f*f	1	672.2	672.2	3.69	0.151	1.338
V*f	1	576	576	3.16	0.174	1.146
Error	3	547.1	182.4			1.089
Total	8	50250.2				100

When the variance analysis results given for the RCMX cutting tool in Table 6 are examined, it is seen that the FR parameter is less effective than the CS parameter regarding the temperature values. While the rate in FR is 26.376%, this rate increases to 64.797% in CS. When the P values for two separate parameters and the square of the CS are examined, it is seen that the results are less than 0.05 and therefore statistically significant. On the other hand, the results obtained are statistically insignificant because the square of the FR and the P values for the interaction of cutting

and FR are greater than 0.05. If it is desired to work with lower temperature values, in case of working with RCMX cutting tools, it will be appropriate to work with 200 m/min and 0.15 mm/rev values to obtain the lowest temperature value. The error values can be explained by variables not considered in this study, such as bench vibrations, floor vibrations or the microstructure of the material. These error values were calculated as 1.089% for the RCMX cutting tool.
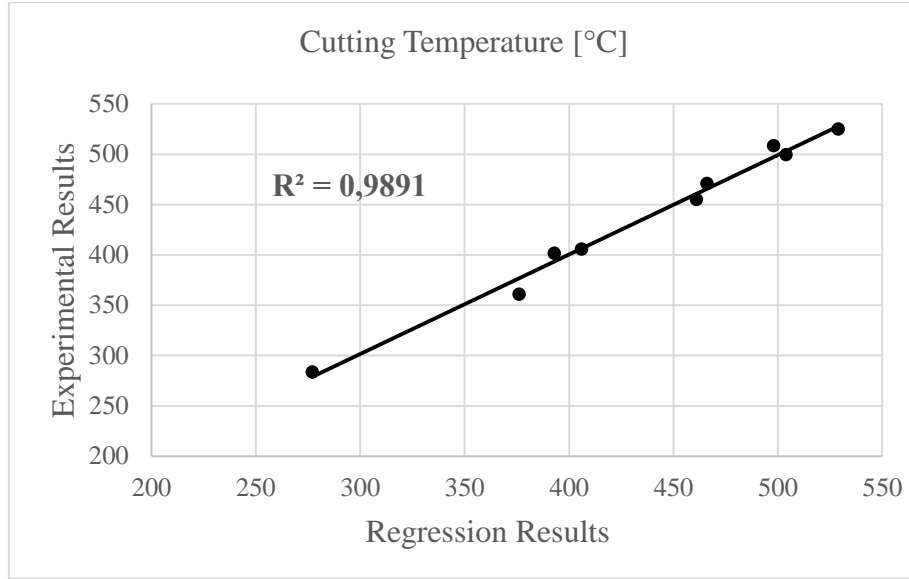
Figure 10. Regression graph of CT results (Kesme sıcaklığı sonuçlarının regresyon grafiği)

When the graph obtained from the RSM given in Figure 10 for CT is examined, it is seen that the experimental results and the results obtained from the model estimation are in good agreement. R^2 values expressing the agreement of the results were found to be 0.9891.

4. CONCLUSIONS (SONUÇLAR)

In this experimental study, the effects of FR and CS parameters on SR, PC and CT values were investigated in the processing of ER7 train wheels with CRMX cutting tool using ANOVA and RSM methods. Appropriate processing parameters were determined by determining the relationship between input parameters and outputs. Experiment results were analyzed using the ANOVA method. Obtained results are given below:

1. According to the analysis of variance, the parameter affecting the SR was the FR with 57.158%. The effect rate of CS is 36.412%. The results for FR and CS are statistically significant as the P-Value value is less than 0.05. In addition, the agreement between the values calculated using the equation obtained by the RSM method and the experimental results was found to be 93.49%. The operating parameters that give the lowest SR value are 0.15 mm/rev FR and 300 m/min CS. As the FR increases, the SR increases, and as the CS increases, the SR decreases.

2. According to the analysis of variance, the parameter affecting the PC was the CS with 58.072%. The impact rate of the FR is 41.503%. The results for FR and CS are statistically significant as the P-Value value is less than 0.05. In addition, the agreement between the values calculated using the equation obtained by the RSM method and the experimental results was found to be 99.77%. The operating parameters that give the lowest PC value are 0.15 mm/rev FR and 200 m/min CS. As CS and FR increase, PC increases.

3. According to the analysis of variance, the parameter affecting the CT was 64.797% CS. The impact rate of the FR is 26.376%. The results for FR and CS are statistically significant as the P-Value value is less than 0.05. In addition, the agreement between the values calculated using the equation obtained by the RSM method and the experimental results was found to be 98.91%. The

operating parameters that give the lowest SR are 0.15 mm/rev FR and 200 m/min CS. As the FR and the CS increase, the CT increases.

REFERENCES (KAYNAKLAR)

1. A. Mazzù, A. Ghidini, L. Provezza, C. Petrogalli, M. Faccoli, Study of the damage induced by thermomechanical load in ER7 tread braked railway wheels, Procedia Structural Integrity, 18: 170–182, 2019.
2. Y. Z. Chen, C. G. He, X. J. Zhao, L. B. Shi, Q. Y. Liu, W. J. Wang, The influence of wheel flats formed from different braking conditions on rolling contact fatigue of railway wheel, Engineering Failure Analysis, 93: 183–199, 2018.
3. V. Gupta, G. Narayanamurthy, P. Acharya, Can lean lead to green? Assessment of radial tyre manufacturing processes using system dynamics modelling, Computers and Operations Research, 89: 284–306, 2018.
4. Y. Touggui, A. Uysal, U. Emiroglu, S. Belhadi, M. Temmar, Evaluation of MQL performances using various nanofluids in turning of AISI 304 stainless steel, The International Journal of Advanced Manufacturing Technology, 2021.
5. T. M. Duc, T. T. Long, P. Q. Dong, Effect of the alumina nanofluid concentration on minimum quantity lubrication hard machining for sustainable production, Proceedings of the Institution of Mechanical Engineers, Part C: Journal of Mechanical Engineering Science, 233(17): 5977–5988, 2019.
6. M. Günay, M. E. Korkmaz, N. Yaşar, Performance analysis of coated carbide tool in turning of Nimonic 80A superalloy under different cutting environments, Journal of Manufacturing Processes, 56: 678–687, 2020.
7. H. Yurtkuran, M. E. Korkmaz, M. Günay, Modelling and optimization of the surface roughness in high speed hard turning with coated and uncoated CBN insert, Gazi University Journal of Science, 29(4): 987–995, 2016.
8. F. Klocke, G. Eisenblätter, Dry cutting - State of research, VDI Berichte, 46(1399): 159–188, 1998.
9. N. Canter, The possibilities and limitations of dry machining, Tribology & Lubrication Technology, 59:, 2003.
10. B. Ozcelik, E. Kuram, E. Demirbas, E. Şik, Effects of vegetable-based cutting fluids on the wear in drilling, Sadhana - Academy Proceedings in Engineering Science, 38(4): 687–706, 2013.
11. M. Kumar Gupta, M. Boy, M. Erdi Korkmaz, N. Yaşar, M. Günay, G. M. Krolczyk, Measurement and analysis of machining induced tribological characteristics in dual jet minimum quantity lubrication assisted turning of duplex stainless steel, Measurement, 187:110353, 2022.
12. N. S. Ross, C. Gopinath, S. Nagarajan, M. K. Gupta, R. Shanmugam, M. S. Kumar, M. Boy, M. E. Korkmaz, Impact of hybrid cooling approach on milling and surface morphological characteristics of Nimonic 80A alloy, Journal of Manufacturing Processes, 73: 428–439, 2022.
13. M. E. Korkmaz, M. K. Gupta, M. Boy, N. Yaşar, G. M. Krolczyk, M. Günay, Influence of duplex jets MQL and nano-MQL cooling system on machining performance of Nimonic 80A, Journal of Manufacturing Processes, 69: 112–124, 2021.
14. T. Kıvak, M. Sarıkaya, Ç. V. Yıldırım, Ş. Şirin, Study on turning performance of PVD TiN coated Al_2O_3+TiCN ceramic tool under cutting fluid reinforced by nano-sized solid particles, Journal of Manufacturing Processes, 56: 522–539, 2020.
15. D. Y. Pimenov, M. Mia, M. K. Gupta, A. R. Machado, I. V. Tomaz, M. Sarikaya, S. Wojciechowski, T. Mikolajczyk, W. Kaplonek, Improvement of machinability of Ti and its alloys using cooling-lubrication techniques: a review and future prospect, Journal of Materials Research and Technology, 11: 719–753, 2021.
16. M. Günay, M. E. Korkmaz, Optimization of honing parameters for renewal of cylinder liners, Gazi University Journal of Science, 30(1):, 2017.
17. S. Dixit, M. Swamy, P. Vikram, J. Bernier, M. T. G. S. Cruz, M. Amante, D. Atri, A. Kumar, Increased drought tolerance and wider adaptability of qDTY12.1 conferred by its interaction with qDTY2.3 and qDTY3.2, Molecular Breeding, 30, 2012.
18. M. Sarıkaya, V. Yılmaz, A. Güllü, Analysis of cutting parameters and cooling/lubrication methods for sustainable machining in turning of Haynes 25 superalloy, Journal of Cleaner Production, 133: 172–181, 2016.
19. V. S. Sharma, M. Dogra, N. M. Suri, Cooling techniques for improved productivity in turning,

International Journal of Machine Tools and Manufacture, 49(6): 435–453, 2009.

20. J. Haider, M. S. J. Hashmi, Health and environmental impacts in metal machining processes, Comprehensive Material Processing, 8: 7–33, 2014.

21. M. E. Korkmaz, M. Günay, Experimental and Statistical Analysis on Machinability of Nimonic80A Superalloy with PVD Coated Carbide, Sigma Journal of Engineering and Natural Sciences, 36(4): 1141–1152, 2018.

22. M. A. Erden, N. Yaşar, M. E. Korkmaz, B. Ayvacı, K. Nimel Sworna Ross, M. Mia, Investigation of microstructure, mechanical and machinability properties of Mo-added steel produced by powder metallurgy method, The International Journal of Advanced Manufacturing Technology, 114: 2811–2827, 2021.

23. A. T. Abbas, F. Benyahia, M. M. El Rayes, C. Pruncu, M. A. Taha, H. Hegab, Towards Optimization of Machining Performance and Sustainability Aspects when Turning AISI 1045 Steel under Different Cooling and Lubrication Strategies, Materials, 12(18):, 2019.

24. A. Shokrani, V. Dhokia, S. T. Newman, Energy conscious cryogenic machining of Ti-6Al-4V titanium alloy, Proceedings of the Institution of Mechanical Engineers, Part B: Journal of Engineering Manufacture, 232(10): 1690–1706, 2018.

A Review on Machinability of Shape Memory Alloys Through Traditional and Non-Traditional Machining Processes

Farij BEN SAOUD[1*] iD, Mehmet Erdi KORKMAZ[2] iD

[1]*Karabük Üniversitesi, Lisansüstü Eğitim Enstitüsü, Makine Mühendisliği A.B.D., Karabük, Türkiye*
[2]*Karabük Üniversitesi, Mühendislik Fakültesi, Karabük, Türkiye*

ABSTRACT

This review article offers consolidated knowledge on the subject of several traditional and non-traditional procedures that are taking place throughout the years to form shape memory alloys (SMAs). At the primary part of the review, the usage of several shape memory alloys was shown. The dialogue then continued towards numerous traditional techniques of operating followed by the obstacles in the running of SMAs utilizing traditional techniques of operating. Moreover, numerous non-traditional processes of operations such WJM (Water jet Machining), cryogenic, WEDM (Wire Electro Discharge Machining), EDM (Electro Discharge Machining), and electrochemical machining explored. As well, Numerous of outcomes reactions that may occur during the operation procedures have been emphasized such as material removal rate (MRR), rate of tool wear, surface roughness (SR), the surface integrity. A consolidated records of various academics and their findings on this issue has been evaluated. After all, the article has been concluded by suggesting a variety of key points seen throughout the review process.

Şekil Hafızalı Alaşımların Geleneksel ve Geleneksel Olmayan İşleme Yöntemleriyle İşlenebilirliği Üzerine Derleme

ÖZET

Bu derleme makalesi, şekil hafızalı alaşımları (ŞHA'lar) üretmek için yıllar boyunca yer alan çeşitli geleneksel ve geleneksel olmayan prosedürler konusunda bilgi sunmaktadır. İncelemenin ilk kısmında, çeşitli şekil hafızalı alaşımların kullanımı gösterilmiştir. Araştırma daha sonra çok sayıda geleneksel üretim tekniğine ve ardından geleneksel üretim tekniklerini kullanan ŞHA'ların çalıştırılmasındaki engellere doğru devam etmiştir. Ayrıca, SJİ (Su jeti İşleme), kriyojenik, TEBİ (Tel Elektro Boşaltma İşleme), EBİ (Elektro Boşaltma İşleme) ve elektrokimyasal işleme gibi çok sayıda geleneksel olmayan işlem süreçleri araştırılmıştır. Ayrıca, talaş kaldırma hızı (TKH), takım aşınma hızı, yüzey pürüzlülüğü (YP), yüzey bütünlüğü gibi operasyon prosedürleri sırasında meydana gelebilecek birçok sonuç reaksiyonu üzerinde durulmuştur. Çeşitli araştırmacıların çalışmaları ve bu konudaki bulguları değerlendirilmiştir. Sonuç olarak makale, inceleme süreci boyunca görülen çeşitli kilit noktalar önerilerek sonlandırılmıştır.

1. INTRODUCTION (GİRİŞ)

By the 1960s, Blair and Willie developed a nickel-titanium alloy containing 53% to 57% nickel, which led to the emergence of a strange case where distorted samples were formed with different strains ranging from 8% to 15%, and these alloys are preparing their original shape after going through a thermal cycle. Hence the name of a shape-memory alloy has appeared. These alloys are characterized by their ability to restore their original condition when heated (to a heat elevated than their transformation temperature). Also, these alloys are distinguished by a low yield strength, which facilitates their formation and transformation into any new form [1]. In other words, (SMAs) are a unique category of compounds which own a capacity to retain their previous appearance after

deformation even after being bent. SMAs could be plastically deformed at a low temperature, but this 'plastic' strain could be gained by raising the heat, known as shape memory effect (SME). By high temperatures, a substantial deformation could gained only by releasing the affected force [2].

The nickel-titanium alloy, known as a Nitinol alloy, is the greatest utilized shape-memory alloy and the highest in price because of its mechanical and unique electrical features, extended fatigue life, and great corrosion resistance. Among the alloys further traded in this field is the copper-aluminum-nickel alloy. Moreover, SMAs may additionally be obtained via using iron zinc, and copper as alloying elements [1-3].

Shape-remembering alloys provide many advantages such as safety, susceptibility to pressure, and provide excellent working conditions such as cleanliness, quietness, and spark-free, and they can work in zero-gravity conditions. Therefore, they are recently used in several applications in various fields such as reciprocating applications (i.e., they are in a permanent state of stopping and working) such as refrigerant circuit valves, fire detection systems, and clamping devices. For example, these reciprocating applications exist in small sizes, such as tiny motors, which are electrically driven machines. It is also used for many purposes in the medical field, like braces, orthodontics, and medical guidewire. Moreover, these alloys were employed in the aerospace industry and in fixed-wing aircraft, where SMAs utilized in the wires (strings) that power the hingeless ailerons. Also, SMAs torque tube utilized to begin spanwise wing twisting of a scaled-down F-18. In all of those implementations, SME is utilized to give actuation through recovering the form that happens when stresses occur [2,4].

These attributes of shape memory compounds are issued by the reversible transformation of the martensite phase, transforming from a solid to a solid-state without diffusion. It is a transition between a crystal structured form represented by austenite and another less organized form martensite. The SMAs are in the austenite phase near relatively high temperatures and shift to a martensite phase when cooled. At the same time, austenite is characterized by a cubic crystal structure, while martensite is designated by a monoclinic crystalline formation, as shown in (Fig. 1)
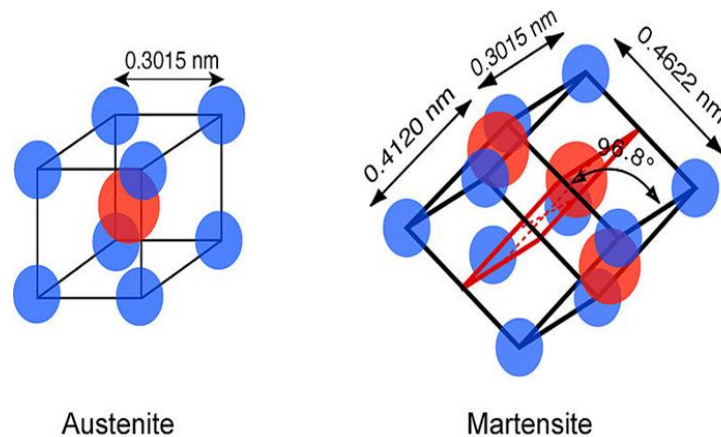
Figure 1. Nitinol austenite and martensite (Nitinol östenit ve martensit) [5].

The transformation from austenite to martensite is carried out through a process of distortion or alteration in the shape of the crystal structure by displacement, where these changes occur in the internal system of the material.

Furthermore, the austenite is stable in the case of low pressures and high temperatures, while martensite is more stable at higher pressures and lower temperatures. The meaning of high or low temperature could be explained more in (Fig. 2). In addition, there is a passage between stage transitions. The austenite and martensite have various start and final temperatures. Thus, temperature variations of 50% martensite to 50% of austenite state are identified as temperature hysteresis [6] (Fig. 2).
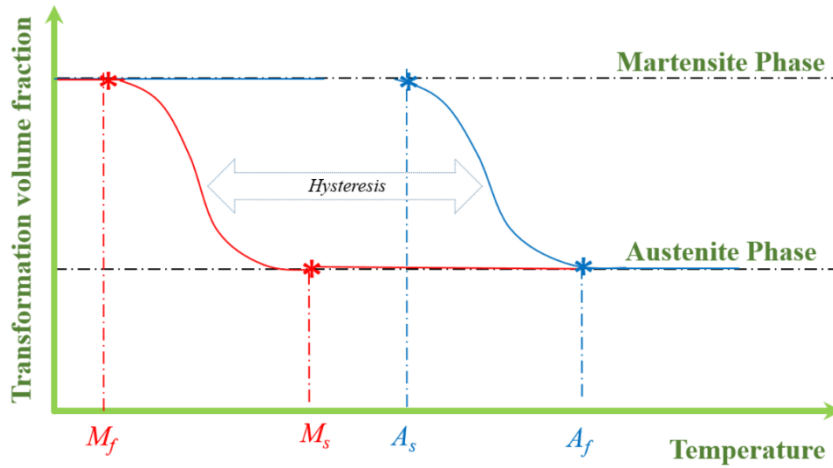
Figure 2. Phase transformation of SMAs (ŞHA'ların faz dönüşümü) [6].

Four transition temperatures describe SMAs: Mf, Ms, As, and Af. Temperatures As and Af are the heats during the transformation of (martensite to austenite) begins and ends, and the temperatures Ms and Mf are the temperatures at which the reverse conversion from austenite to austenite to martensite take place. In contrast, the state of martensite is called the inverse state. When the primary and reverse transformation process is repeated depending on the shape memory alloy property, this may lead to a transition in the temperatures through transformation process starts and ends. This phenomenon is called functional stress, as it is related to varying the fine structure of the material and altering its operating properties as well [7].

The austenite phase crystal structure is shifted with a decrease in the temperature to twinned martensite. This process is beginning from Ms and will finish below Mf. Meanwhile, mechanical stress distorts the twinned martensite to a detwinned structure, and the primary shape is retained inside the SMAs. To regain its original condition, it must go within extra two steps. Firstly, the outside load has to be lifted then heated to an austenite form transformation occurs. This high-temperature period begins from As and takes progression until Af. All these actions create a cycle; thus, the strain recovery depends on the region of the process. The elements that establish these steps are named one-way SMAs. While the final approach, which has a unique property, is termed two ways SME. One-way SMAs have only one initial shape at a higher temperature. However, two recoverable conditions could be produced for two-way SMAs: one of them in the austenite state and the other with a martensite state [6] (Fig. 3). Describe various SMAs for strain, stress, and temperature.
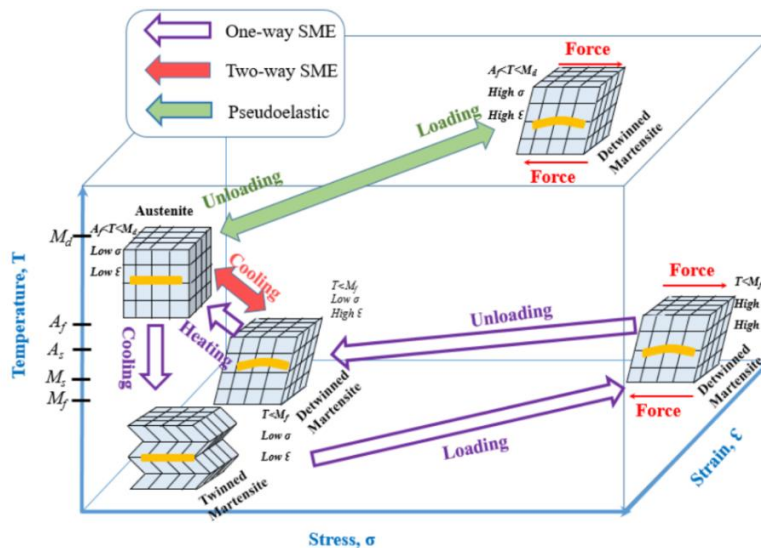
Figure 3. Description of various SMAs for strain, stress, and temperature (Gerinim, stres ve sıcaklık için çeşitli ŞHA'ları tanımlanması) [6].

This article summarizes various operation approaches that could be utilized to form the SMAs and their surface attributes like surface integrity, hardness, generated layer, and residual stress. Also its behavior with various kinds of cutting fluids and dissimilar sorts of cutting tools. However, the behavior and the machinability of shape memory alloys are concerned underneath the variety of conventional, non-traditional, and micro-operating including the consequence of different input factors such as cutting velocity, rate of feed, depth of cutting, style of used coolants, and the variety in the coating types that submitted for cutting instruments.

2. MACHINING OF SHAPE MEMORY ALLOYS (ŞEKİL HAFIZALI ALAŞIMLARIN İŞLENMESİ)

The phrase machining indicates removing undesired substances from the specimen to provide it the wanted appearance with assistance of cutting instruments. Undesired metallic element is discharged from the specimen in a style of chips that are created because of strain hardening of the compound when there is a connection between the cutting tool-specimen, as long as there is a relative movement among the tool and the specimen. Like these manners are regularly known as traditional machining methods, that involve milling, turning, and drilling. The extra, quite-popular manner described by grinding, where cutting operations could be done by abrasive performance, displays much weightage in traditional machining production. Different non-traditional machining processes such as Electro-Discharge (EDM), laser, Water Jet (WJM), and Electrochemical Machining have not owned a connection between the specimen and the shaping tool. There are no cutting tools as in the traditional methods; these methods employ chemical or thermic power for processing. As a result, work hardening or strain hardening, performing quality and cost aims is quite a complicated task. One of the essential matters that require to be dealt with while machining processes is the amount of material that sound be removed besides cutting tool wear. Hence, by studying the influence of engineering machining of SMAs, the subsequent sections illustrate the traditional and non-traditional machining methods to which shape-memory materials might be administered. Viewpoints linked with the operation manner similar feed rate, forming tools, and operation circumstances are analyzed, reviewed, and the results are displayed.

2.1. Traditional Machining of SMAs (Şekil Hafızalı Alaşımların Geleneksel Yöntemle İşlenmesi)

Much of the operation carried out on traditional machining of SMAs concerns Nitinol and Titanium or ternary compounds of NiTi; therefore, the knowledge given turns about those elements. An initial review of the machinability characteristics of NiTi mixtures could penetrate the phenomes that appear when Titanium and Nickel shape memory elements are examined. Titanium's reactivity with the low heat conductivity, shaping tools, significant strength at raised heats, and soft elastic modulus effect in extended temperatures at the tool and chip interface which lead to high dynamic loads, specimen distortions, and decreased tool life [8]. Nickel-based metals and superalloys, similarly to Titanium compounds, exhibit large strength and are supposed hard-to-machine ores. Furthermore, because of their austenitic pattern, nickel superalloys performance hardens immediately while machining and conduce to create connected chips that are unmanageable during operations [9]. The consequences of the earlier characteristics guide to fast flank wear, and notching, and cratering, so they depend on the tool element and the operation circumstances involved.

All the challenges summarized for NiTi alloys individually apply for NiTi alloys. Besides, critical hallmarks of shape memory alloys as pseudoelasticity, pseudo-plasticity, and high ductility of Titanium and Nickel alloys force more challenges during machining these compounds, driving not simply to fast shaping tool defeat but further to lower specimens' quality as a result of extreme burr generation, adhesions on the surface of the shaped part and changes in the microstructure of the sample substance. Operation of SMAs in Circumstances of high stress, strain rates, and temperatures causes surface and sub-surface defects like the creation of a white layer and the rise of microcracks [10].

2.1.1. Turning process (Tornalama işlemi)

Weinert et al. [11] used several tools, including indexable coated, uncoated cemented carbide, CBN, PCD, and ceramic inserts, to operate a shape memory alloy Ni-Ti by turning machine. However, they realized that coated cemented carbide instruments exhibited decreased wear. Further, instruments with eight various bands of TiAlN, TiCN achieved better than yet instruments with more complex coatings such as TiB2. However, uncoated cemented carbide instruments offer massive wear, and ceramic cutting devices cannot machine Nitinol-Titanium mixture irrespective of parameters of cutting. Furthermore, Notch wear was visible on PCD instruments, resulting in unanticipated tool damage, and the wear of CBN instruments was higher than cemented carbide instruments, moreover, in combination with their unusual cost, they were considered as unfavored. Concerning the cutting variables, it was determined that coated cemented carbide instruments with more powerful cutting speeds could be used to machine NiTi as recommended by the related literature and the instrument providers. As a result, the wear of the tool was lessened, and the surface condition is improved at a cutting velocity of (100 m/min).

The turning operating of (β-Ni-Ti) mixture was achieved by wet-dry situations with different machining speeds by Weinert et al.[12]. According to their laboratory issues, the investigators suggested distinguishing three planes for explaining the machinability of the mixture. Through quiet operating velocities equal to or less than (60m/min), as a result, the operating forces were very high, which causes in a case in tool wear including elevated notch wear. Utilizing emulsion as lubricant reduced operating forces and the wear of the tool just for the low cutting velocity rate of (20m/min). During the next step, when operating speeds were ($60 \leq VC \leq 130$m/min), the wear of tool and the operation forces seemed to be unchanged by altering the quickness rate and changing cooling liquid. In the third stage, when the forming speed is higher than (130m/min), the wear and the resulted forces grew significantly for dry states. As a result of its special ductility, a usual burr generation happened when operating NiTi alloys. With the starting of the cutting, the breadth of the burr was lower than the rate of feed, then suddenly it developed quickly until it achieved greater amounts. Nevertheless, the top of burr could create up over numerous millimeters. They noticed that the depth of cutting shall be defined to the tool's cutting-edge radius. Meanwhile, high notch wear occurs when the depth of cutting passes the radius of the cutting-edge. Also, during the turning of TiNi alloy, the poor chip breaking was an extra obstacle.

Ezugwu et al. [13] studied the impact of powerful-pressure coolant applied during machining of (Inconel 90) among carbide inserts (K10 grade) of ISO designation (CNMA & CNMP 20408). The running speeds of (55m/min) with feeds of (0.127 mm/rev) were utilized below both regular and powerful-pressure coolant supplies. Overall examination results explained that more extended tool lives could be obtained among the regular coolant supply than the huge-pressure coolant equipment. Besides, the raised-pressure supply overcame the early breakage of the carbide tools with more powerful velocity and depth of cut; as a result, compared to standard coolant rationing, the tool life is increased. Furthermore, extreme-pressure coolant rationing produced tiny-segmented chips that might be effortlessly removed. In most states, the predominant mode of tool failure was Notching. Tool rejection under powerful-pressure coolant equipment was caused by flank wear in the issue of sharp-nosed tools (CNMA & CNMP 20408). Broad-nosed tools (CNMA & CNMP 1204 12) may have an extended tool life than sharp-nosed tools, which might be caused by the heightened strength of the big nose radius.

A machining test related to the surface integrity characteristics of an Inconel 718 was conducted on a CNC lathe machine by Pusavec et al.[14]. However, the machining operation was handled by utilizing four various coolants, namely: dry, minimum quantity lubrication machining (MQL), cryogenic machining, and the last is an amalgam of cryogenic. After the experiment, it was determined that the cryogenic machining manner achieved the surface with the lowest roughness condition. Additionally seen that cryogenic machining fairly changes the final product microstructure and produces the most downward plastic deformation compared to the other operations on the specimen's machined surface.

Zlatin et al. [15] investigated the operating properties of nickel-based heat-resistant alloys. The high work hardening and the abrasive carbides in the nickel-based microstructure were the primary causes for difficulty operating. Moreover, the determination of a suitable rate of feed is an essential factor, however, was seen that the most extended tool life could be gained from rates of feed ranging in (0.18-0.25 mm/rev). It is a middle ground among the negative impacts of small and elevated feeds.

In other research, Rahman et al. [16] investigated how instrument geometry affects tool life (coated cemented carbides). Equally (PVD, CVD) coated insertions were examined through various feeds of cutting and speeds. Outcomes displayed that with a raise in the side cutting edge angle (SCEA) from (-5° to 15°), and further up to 45°, there was a notable improvement in the life of the tool, though the surface finish SR is negotiated. PVD acts more favorably than multi-CVD-coated carbides. The suitable cutting situation is 45° of (SCEA) with a 30m/min operating speed and feed rate of 0.2 mm/rev.

Arunachalam et al. [17] reviewed the influence of various chip breaker range on the life of the tool by using coated cemented carbides. However, outcomes exhibited that those chip breakers did not cause many effects on the instrument life. Furthermore, events pointed out that coated carbides' acting is more valuable at (SCEA) of 15° than at 45°, promoting Rahman et al.'s findings [16].

2.1.2. Milling process (Frezeleme işlemi)

On the other side, Guo et al. [18] analyzed the milling of a NiTi alloy that employed for biomedical purposes. The authors carried out quasi-static and split-Hopkinson pressure bar compression experiments to estimate the mechanical characteristics of the element. The results illustrated the high strength of the substance beneath static and dynamic statuses registered that NiTi is more difficult to be machine than Ti or Ni-based superalloys. However, they utilized coated carbide inserts, and once again, shorter tool life was recognized compared to milling conventional elements. Furthermore, a rise in feed rate guides to an increment in surface roughness; nevertheless, a high surface roughness resulted from a minimal rate of feeds, and by association, a growing in the flank wear of the instrument also raises the surface roughness. Besides, the high ductility of Ni-Ti is bound for large outlet burrs. Eventually, from the subsurface microstructure and microhardness research, possible to say that tinier rates of feed cause a thicker white layer, suggestive of the phase transformation resulting from extreme loading and temperatures.

Ezugwu et al. [19] tested titanium (Ti6A14V) and nickel-based alloys (Nimonic75 & Inconel 718) at various cutting conditions by applying K20, K40, and P25 of carbide inserts to compare their performances. Outcomes determined that the K20 grade was more reliable than the K40, and P25 because of the compressive strength and comparatively high hot hardness of the K20. Furthermore, K20 has high abrasion resistance due to the low cobalt content. Also, variables such as the low coefficient of thermal expansion and high thermal conductivity of the K20 helps in a more excellent performance by diminishing the thermal shock. In most cases, the dominant forms of the failure of tool are the fracture and chipping. Speeds of 23 m/min, feeds of 0.08 mm/tooth were the optimum cutting situation for (Inconel 718), and the best operating condition for (Nimonic75) achieved by a speed of 27 m/min, feeds of 0.08 mm/tooth. Additionally, sequences recorded that titanium alloys were more manageable than the Inconel 718 & Nimonic75 to be machined, while the most difficult was the (Inconel 718). Ezugwu et al. [20] investigated milling cutting experiments for (Nimonic75) combination utilizing two kinds of cutters: a 70° bevel cutter carbide inserts (P40) also a 45° path angle cutter carbide inserts (K20 & K40). As in the previous study, the K20 offered more remarkably due to their enhanced characteristics than the others. The 70° bevel cutter usage P40 grade was achieved excellently with an unusual tool life of 86 min.

Widespread analysis about the end milling of (Inconel 718) has been held, offered through Alauddin et al.[21], [22] studied the milling operations were by utilizing K20 carbide to investigate cutting requirements, surfaces roughness, and tool life. Of the cutting inspections was seen that the life of tool ranges from 5 to 9.5 min could be reached at speeds of 19.32 to 29 m/min and feeds of 0.091 mm/ tooth with an axial depth of cut 1.0 mm. Furthermore, cutting forces decline by growing

cutting speed while forces rise by either a rising feed or an axial depth of penetration. Alauddin et al. [23] performed tool life experiment throughout end milling operating of Inconel 718. Conclusions recorded a notable variation in the life of tools throughout up and down cut end milling, whereas the life of tools in down-cutting was more useful than in up-cutting.

Some thoughts concern the generation of micro-components using milling [24, 25]. The micro-milling operation has been chosen as complicated geometries needed for micro components in micro-devices and medical treatments. The researchers reviewed the appropriate cutting circumstances and the properties of shape memory alloy machining, such as burr creation during micro-scale; a direct downscaling was unlikely because aspects might vary compared to the methods reviewed in the earlier statements. It showed that micro-operating is as challenging as traditional operating methods, if not even more, where the ranges of appropriate operating circumstances were relatively poor.

2.1.3. Drilling process (Delme işlemi)

Machining shape memory alloys by employing a drilling process impact the tool wear and surface integrity. Weinert et al. [26] drilled NiTi alloy by utilizing cutting tools coated by (TiCN/ TiN) also they submitted a lubricant and inner coolant during machining to reduce the wear of tool. However, it was observed that the high cutting speeds lead to excessive tool wear while the suitable speed for the drilling process was remarked at 30m/min. with improved surface roughness up to 5.9μm. Drilling of tubes made off Ni-Ti alloy that utilized in production parts for medical applications was studied by Petzoldt et al. [27]. They claim that the hardening of work in a subsurface region has an effect during this machining procedure is held. As a consequence, the hardness of the element was built during low cutting rates or high feeds rate. Moreover, no advantages have been seen using coated rather than uncoated cemented carbide. The picking of suitable spindle speed and cutting speed is demanded during drilling operation basically for getting better surface attributes. Mousavi et al. [28] informed the functions governing the drilling of SMAs via fuzzy logic methods. For the drilling of NiTi, a tool diameter of 1-30 mm and a depth of 0.25-3.0 mm were chosen. The range of 20-50 m/min for cutting speed, and 20-6000 rpm for spindle speed were the best machining factors during the drilling process for better surface integrity. Drilling outcomes can be improved by employing tools with tiny diameters. The composition and the sort of drilling tools also influence the drilling operations of SMAs. However, these factors have been researched by Lin et al. [29]. Two compositions of shape memory alloys ($Ti_{50}Ni_{50}$ and $Ti_{49}Ni_{51}$) were drilled with three sorts of twist tools namely HSS, HSS + TiN, and TC under nine surroundings of rotational velocities, and feed rate. The HSS + TiN coated drills displayed more acceptable performance for drilling NiTi when it is compared to other instruments because of their elevated hardness and high wear resistance. Moreover, the composition ($Ti_{50}Ni_{50}$) exhibited better surface integrity of hardness near the drilled hole compared with other elements because of increased plastic deformation of NiTi as illustrated in (Fig. 4).

The necessity of SMAs micro-sized applications is appearing in medical areas such as grooves, micro-slots, and forms with dimensions smaller than 0.5 mm. Because of the superior mechanical features of SMA, it makes a (NiTi) micro-devices a big challenge for designers. As a result, micromachining techniques like micro-drilling are employed to organize these micro-devices. Biermann et al. [30] utilized single-lip and twist drills during their micro-drilling process. They claimed that tool wear increased during single-lip drilling due to adhesion caused by friction between the hole wall and guide pad of tool. The adhesive could be reduced by using a smaller tip angle or by submitting a layers coating of TiN or TiAlN, which assists in declining the friction. On the other hand, the twist drills show no sign of adhesion wears. This is owing to their symmetric construction, that lacks a radial force feature, as well as TiAlN coating. The proper selection of cutting speed is also required for the most optimum utilization of drilling instruments. The velocity shall not be more than Vc= 30 m/min. Moreover, twist tools at a diameter of 1.0 mm attained to a depth of 1200 mm, while single-lip instruments only had a deep of 420 mm.
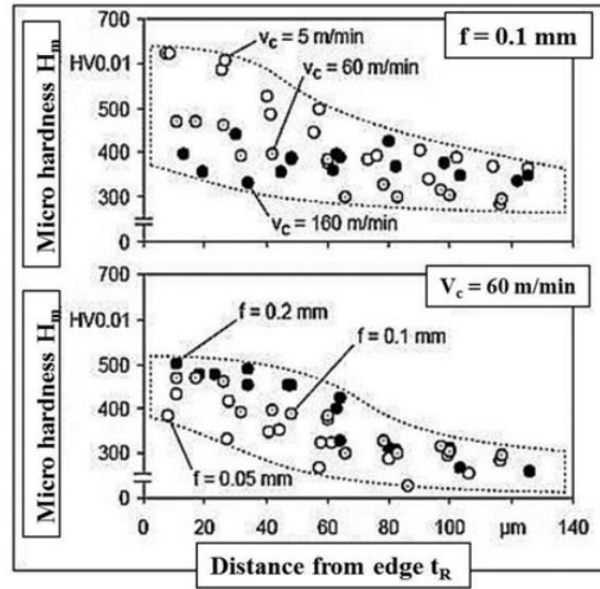
Figure 4. Microhardness in subsurface area while drilling-NiTi under separated cutting parameters (Farklı kesme parametreleriyle delme sırasında yüzey altı bölgesinde mikro sertlik-NiTi) [29].

2.1.4. Grinding process (Taşlama işlemi)

Grinding is typically one of the last finishing techniques on a manufacturing plan; therefore, measurement accuracy and surface quality must constantly be maintained. Roughness of surface and microstructure are being employed to assess the tool efficiency as well as the grinding features of particular elements. Tao et al. [31] employed three types of Ni-Ti+TiH$_2$ compositions with various wt.% as shown in Table 1. In order to measure the surface roughness and the specific energy during grinding machining.

Table 1. NiTi alloy chemical composition and its properties (NiTi alaşımının kimyasal bileşimi ve özellikleri)

Specimen No.	Ni	Ti	TiH2	Pore rate	Density ($g \cdot cm^{-3}$)
1#	55.1	44.9	0.0	37.56 %	4.09
2#	54.9	35.8	9.3	39.39 %	3.97
3#	54.4	17.8	27.8	39.54 %	3.96

The subsequent three grinding settings were used for the process, namely wheel acceleration of 17.5, 20.0 22.5, 25.0 m/s, depth of 0.01~0.09 µm, and specimen infeed rate of 0.3, 0.6, 0.9, 1.2 m/min. However, they claimed that during a very shallow cutting depth of single active grain, the first specimen showed the highest specific energy while the lowest was exhibited by the second sample. When the grit depth of the cut has been elevated to around 0.06 µm, there has been little variation between the different forms of alloys. In addition, as the grit depth of cutting increases, a quite identical tendency can be seen in alloys. Because of the weak grain wear, roughness values climb dramatically with increasing cutting depth, as shown in (Fig. 5).

| Smala cutting depth | Middle cuting depth | Large cutting depth |
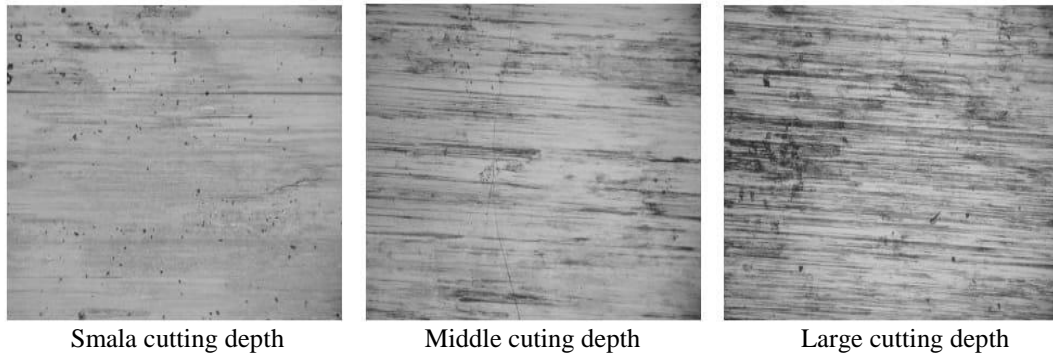
Figure 5. The ground surface's microstructure (Zemin yüzeyinin mikro yapısı) [31].

When the depth of cut was over 0.08 μm, a higher surface roughness has been notalised with significant wear of the abrasive grits' cutting edges, which further limits the capacity to keep its cutting ability.

Production of Ni-Ti alloy in a form of powder by utilizing a high-energy ball grinding approach (Pulverisette 7 premium line) was analyzed by Goryczka et al. [32]. The research was split into two groups. The foremost one was 10 g ground for 100 h, then ground 20 g for 100, 120, and 140 hours. The amount of the phase increased, and the intermediate size of the agglomerates was grown to 700 μm by expanding the sample mass to 20 g and expanding the grinding duration up to 140 h, while the average crystallite size was lowered to just a few nanometers range. Micro-strains have also been minimized as grinding duration was extended. In addition, Mizutani et al. [33] studied the surface quality of Ni-Ti SMA operated by the electrical grinding method (EG-X) based on Electrolytic In-process Dressing grinding in comparison to Thermal Oxidation (TO) surface treatment. In comparison to the standard TO treated surface, the outcomes demonstrated that the electrical grinding process (EG-X) could provide an elevated surface quality.

2.2. Non-Traditional Machining of SMAs (Şekil Hafızalı Alaşımın Geleneksel Olmayan Yöntemle İşlenmesi)

This section of operation regards techniques of elements forming that involve no connection between tools and specimens. As a result, the wear of tools is lessened or wholly diminished, whereas surface integrity could be frequently concerned because of thermal loading. These techniques, such as electric discharge (EDM), laser operating, wire-electric discharge machining (WEDM), (WJM), and electrochemical machining, are extensively applied to SMAs machining particularly for parts with minimal dimensions.

2.2.1. Electrical discharge machining (Elektro erozyonla işleme)

The highly complicated forms could be shaped using high accuracy by electric discharge machining (EDM). In this technique, discharge sparks are employed to meltdown and evaporate the element; a dielectric liquid is also utilized as a medium among the workpiece and electrode [34]. Daneshmand et al. [35] researched the actions of Ni-Ti beneath different electric discharge machining (EDM) parameters. The parameters of (EDM) were arranged such that the pulse on/off time, the discharge current, and voltage. However, the outputs that were examined, namely material removal rate (MRR), rate of tool wear, surface roughness (SR), and relative electrode wear. During this mode, was seen that the most meaningful parameters that alter the (MRR) are the pulse current and the pulse on time. At same time, growth in those two variables grows the element removal rate. Additionally, the growth of pulse current causes an increase in surface roughness. Also, they found that the rate of tool wear raises along with a rise in pulse on time just up to a particular threshold, after which the rate of tool wear begins declining. Besides, they also remarked that by growing the pulse off time, MRR and SR are reduced. Extra investigations on the impact of the machining circumstances during EDM tests on the surface roughness (SR) have been done [36, 37]. These analyses showed that the rise of the working energy leads to worsening surface roughness.

Additionally, a thicker and more irregular melting area was caused by the growth of current, voltage, and pulse on time. Surface roughness SR also depends on the tested material's thermal features, such as melting point and thermal conductivity.

Gangele et al. [38] employed Taguchi's technique to optimize the impact of machining parameters on the surface roughness of Ni-Ti alloy through operating by the EDM method. They noted that the most critical influence on surface roughness was shown to be the pulse-off time. In addition, Jatti [39] applied Taguchi's analysis during EDM machining for three shape memory alloys (NiTi, NiCu, BeCu) to learning the influence of operational factors such pulse on/off duration, gap current/voltage, and electrical conductivity on the output responses like tool wear rate (TWR), material removal rate (MRR). The outcomes revealed that by increasing the gap current, and workpiece electrical conductivity, the MRR increases, although the increase in the gap voltage causes a decrease in MRR. Additionally, the low electrical conductivity of the workpiece yields to lower TWR because of increased heat transmission from tool to workpiece. But, with an increase in gap current, TWR rises. Other ways, the tool wear rate is unaffected by pulses off time or gap voltage, according to the findings. Additionally, Abidi et al. [40] operated a multi-objective genetic algorithm (MOGA-II) to enhance the weights of micro-electrical discharge machining (MEDM) of Ni-Ti alloy to produce superior MRR with great surface condition. Capacitance and electrode material are two critical considerations that influence the (MEDM) process. It was noted that the brass electrode had a higher material removal rate than the tungsten electrode, as well as more tool wear and worse surface quality. On the other hand, the tungsten electrode demonstrated exceptional micro-hole quality as well as a low tool wear rate. Daneshmand et al.[41] explored the impact of tool rotational, AI_2O_3 powder, current, pulse on/off time, and voltage during machining NiTi-60 SMA by the EDM method. And thy pointed out that the AI_2O_3 powder lowers the kinetic energy of ions, and tool rotation can limit the high spread, reducing tool wear. The AI_2O_3 powder loosens plasma channels quicker, and tool rotation reduces pulse off time, grows material removal rate, and reduces processing costs. The material removal rate may increase by raising current intensity and pulse on time while reducing pulse off time and voltage. With high current intensity and voltage, a reduced tool wear rate may be achieved while expanding the pulse on/off time. Surface toughness is also altered by current intensity, voltage, and pulse on/off time. Fu et al. [42] utilized EDM, and laser operations to compare the recast layer of Nitinol shape memory alloy. They revealed that the Electrical discharge machining caused a non-uniform and containing voids recast layer compared to laser cutting. In comparison to EDM, the melt flow formed columnar patterns, which resulted in lower surface integrity of the operated part produced by laser cutting. In addition, EDM created a more rigid recast layer than laser method due to the production of oxides and varied quenching rates.

2.2.2. Wire electrical discharge machining (Tel erozyonla işleme)

There is another type of EDM pronounced as the wire electro-discharge machining WEDM. However, in this method, the substance is consumed from the specimen by employing several sparks caused by a wire. Hsieh et al. [43] examined the operating properties and shape recovery capability of (Ti-Ni-Zr/Cr) SMAs developed with traditional tungsten arc-melting by employing WEDM. They noticed that raising the peak current and pulse on-time improved the SR, also, resulting in higher MRR. The surface quality is determined by the volume of shifted materials on the operated surface, the wire substance, flushing pressure, and dielectric fluid. In another study, R. Chaudhari et al. [44] explored the surface integrity of Nitinol SMA that was machined by the WEDM method. They have chosen the operating factors as pulse-on, off time, and current. Whereas the material removal rate, SR was determined as output parameters. As a result of their examination, they recognized that to achieve a higher material removal rate, elevated discharge energy is needed, which could be gained by increasing the rates of current, and pulse on time. Besides, to obtain a lesser surface roughness (SR), lower discharge energy is demanded that might be performed by decreasing the values of the pulse-off time. Moreover, Praveen et al. [45] examined the influence of current, and pulse on/off time on (MMR) during operating of Cu-Al-Mn

(CAM) SMA by utilizing (WEDM) method. It was discovered that the MRR could be enhanced by raising the current and pulse on time. In contrast, the rise in Pulse off time produces a decline in the MMR measure.

Moreover, the consequence of WEDM factors on the surface integrity of Ti-Ni-Co shape memory alloy was examined by Soni et al. [46]. Pulse on-off duration and servo voltage were the essential factors in Ti-Ni-Co WEDM machining. When the pulse rate was raised over time, the MRR went up, and vice versa. Surface quality was found to be poor in the presence of microvoids, micro-cracks, and micro globules when a specific combination of high pulse on time and low servo voltage was used. The recast layer's minimal thickness was observed by extreme servo voltage and little pulse on time.

WEDM operations were further reviewed by Soni et al. [47] studied the most suitable setting of the WEDM input factors to gain the best outcomes for the material removal rate, and surface integrity of ($Ti_{50} Ni_{45} Co_5$) SMA created using a vacuum arc melt process by the usage of optimization techniques, i.e., Principal Component Analysis (PCA) and Grey Relational Analysis (GRA). In the present study, the suitable setting to obtain higher MRR, and better SR could be fulfilled by applying 125μs, 35μs, and 40V of pulse on/off time, and servo voltage respectively. Bisaria et al. [48] employed WEDM to investigate Ni-rich NiTi alloy's mechanical properties and surface integrity. Spark gap voltage and on-off pulse duration have a big impact on surface roughness and cutting efficiency. By raising the pulse on time and decreasing the pulse off time, surface roughness and cutting efficiency were improved. Many microcracks, craters, voids may be seen on NiTi's surface. The XRD investigation of the NiTi surface is shown in (Fig. 6).

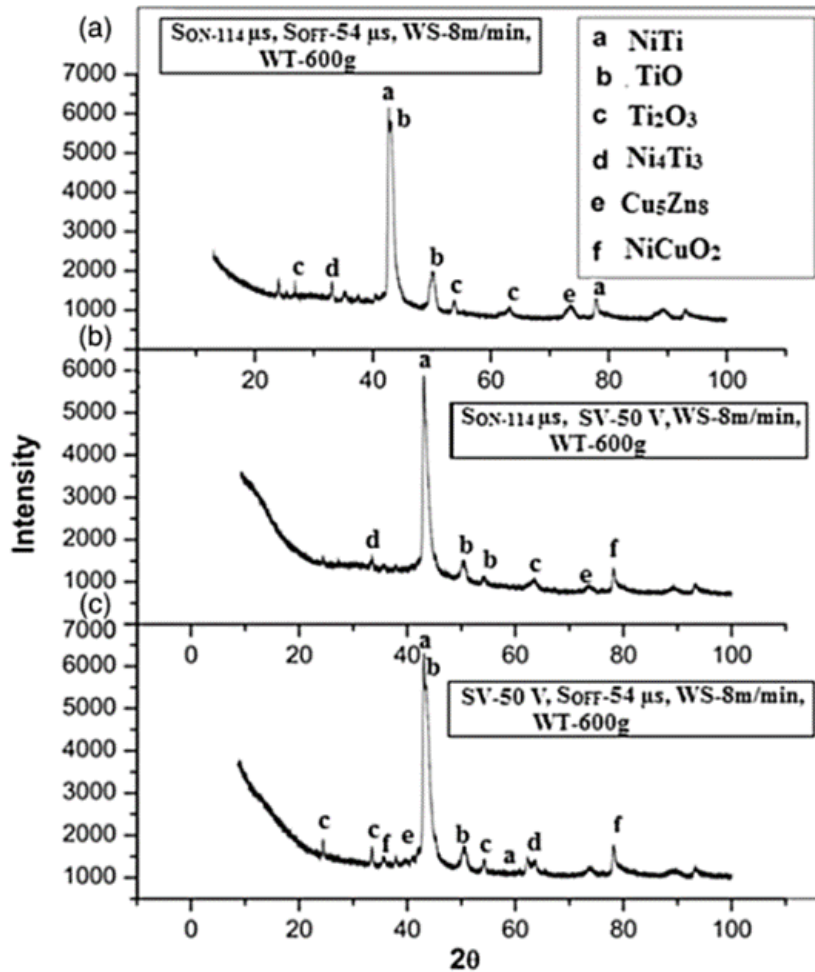Figure. 6. XRD analysis of NiTi's surface. a) 35 V spark gap voltage; b) 52 μs pulse off time; c) 125 μs pulse on time WT: Wire tension, WS: Wire speed.(NiTi yüzeyinin XRD analizi. a) 35 V kıvılcım aralığı voltajı; b) 52 μs darbe kapatma süresi; c) 125 μs darbe süresi WT: Tel gerilimi, WS: Tel hızı) [48].

Due to atom diffusion from the wire and dielectric, the foreign element was carried to the recast layer. TiO, Ti2O3, Ni4Ti3, Cu5Zn3, and NiCuO2 are some of the chemical components and oxides formed by these elements. The chemicals on the machine surface substantially support the EDS findings. The development of Ni and Ti oxides was primarily caused by the strong reactivity of Ni and Ti atoms. The formation of oxides and quenching processes contribute to the hardness of the surface.

2.2.3. Laser machining (Lazer işleme)

Shape memory alloys may also be operated using lasers. Laser operation creates a heat irritated region on the specimen body, similar to electrical discharge machining. Machining of TiNi SMAs was investigated using a femtosecond laser by Li et al. [49] examined the effect of tool path and technique on the manufacture of precision segments. They found that femtosecond laser machining is a primarily thermal mechanism that creates a high ablation rate and notable recast layer. As a result, Lesser beam produces superior cutting quality at a lower cost. Moreover, by using appropriate sideways motion, high quality, recast-free, and exact parts might be created. Too, Tung et al. [50, 51] presented machining of SMAs utilizing laser operating for medical purposes. However, it was announced that the mechanical features would be enhanced, but the private features of SMAs like large hysteresis is tricky. Laser machining tolerances and electropolishing tolerances change the dimensions and geometry.

2.2.4. Water jet machining (Su jeti ile işleme)

Water jet machining (WJM) was also investigated as a non-traditional approach for machining SMAs. Kong et al. [52] described the plain and abrasive (WJM) properties of (Ti-Ni) SMAs. Nevertheless, the investigation showed that abrasive (AWJM) operating has more excellent depth performance in the milling process than (PWJM) running. Also, (AWJM) has a higher thermal impact than (PWJM) because of the increased influence speed of abrasive particles. Temperatures exceeding the austenite transition have been achieved as a result of a compact field collision with a high-velocity abrasive particle, causing the material to melt. This might have an effect on the transition from martensite to austenite. The cracks have started to propagate, and they may originate in the Ti2Ni range rather than the Ti-Ni range. They recommended that the (AWJM) might be a valuable and efficient approach for elements having a complicated crystal structure and phase transition. Frotscher et al. [53] reviewed the different techniques for forming fluffy sheets of Nitani-Titanium-based. However, two methods were employed in their analysis, micro milling and (WJM) operating. However, they determined that in terms of operational value, the cutting time (WJM) process was pretty good. But for the medical application where remarkable accuracy and correctness are needed, their electropolishing was required. Hence after their operations, they got surface with sufficient precision, but the burr resides in the machined part, and de-burring is wanted.

2.2.5. Electrochemical machining (Elektrokimyasal işleme)

Lee et al. [54] served on multiple machining situations to gain the steady electrochemical polishing method for Nitinol based SMAs. They applied acid and the neutral electrolyte in the operating, and they discovered that acid electrolyte is fitting for slow down and accurate operating. At the same time, the neutral electrolyte does not provide precision machining; it generates holes on the nitinol surface. With the most prominent shape, the surface of Nitinol was polished up to a roughness of 0.37 µm, and an acid electrolyte was employed. The adjusted current was 18A, and the pulse off/on time were 200µs and 800 µs. Eventually, the surface roughness of 0.31 µm was achieved. The pulse electrochemical machining has been acquired by Frensemeier et al. [55] to examine the two-way shape memory impact on the Ni-Ti alloys. However, it was found that the more fitting way to operate the (Ni-Ti) alloy is the pulse electrochemical machining because it generated a microstructure that was distortion- and thermal-damage-free and did not oxidize or deform. In pulse electrochemical machining, the use of grooves and hole tools allows for the formation of various protrusion structures on the surface of Ni-Ti. Ao et al. [56] utilized water-free

electrolyte (ethylene glycol–NaCl electrolyte including ethanol) during electrochemical operating to create the microstructure of shape memory alloy (Ni-Ti). They discovered that an ethanol-immersed electrolyte solution could dissolve $TiCI_4$ and so reduce the formation of the oxide. The electrolyte solution containing 20% vol. ethanol produced the best microgroove surface quality. An excessive quantity of ethanol also harmed surface quality and the machined surface.

3. SUMMARY OF TRADITIONAL AND NON-TRADITIONAL MACHINING
(GELENEKSEL VE GELENEKSEL OLMAYAN İŞLEME ÖZETİ)

The formability of SMAs during traditional operations is controlled by the processing settings, coating, and cutting fluids, all of which are illustrated in Table 2. Unconventional machining procedures should be used to address several challenges in the traditional machining process of shape memory alloys, and their recognized specifics are presented in Table 3.

Table 2. Traditional operations of SMAs (SMA'ların geleneksel işlenmesi)

Authors	Material	Tool type	Process	Coolant	Result
K. Weinert, et al. [11]	Ni-Ti alloy	Coated, uncoated cemented carbide, CBN, PCD, and ceramic inserts	Turning	--	It was determined that the coated cemented carbide instruments with cutting velocity of (100 m/min) improved surface condition and lessened the wear of tool.
E. Ezugwu et al. [13]	Inconel 90	Carbide inserts (K10 grade)	Turning	Regular and high-pressure coolant	Examination consequences explained that more extended tool lives could be obtained among the regular coolant supply than the huge-pressure coolant equipment.
F. Pusavec et al.[14]	Inconel 718	--	CNC turning	Dry, MQL, cryogenic, and Amalgam of cryogenic	The cryogenic machining manner achieved the surface with the lowest roughness condition
M. Rahman et al. [16]	Inconel718	(PVD, CVD) coated	Turning	--	Outcomes displayed that with a raise in the side cutting edge angle (SCEA) from (-5° to 15°), and further up to 45°, there was a notable improvement in the life of the tool, though the surface finish SR is negotiated.
E. Ezugwu et al. [19]	(Ti6A14V) and (Nimonic75 & Inconel 718)	K20, K40, and P25 of carbide inserts	Milling	--	The K20 grade was more reliable than the K40, and P25 because of the compressive strength and comparatively high hot hardness of the K20.
E. Ezugwu et al. [20]	Nimonic 75	70° bevel cutter carbide inserts (P40) also a 45° path angle cutter carbide inserts (K20 & K40)	Milling	--	The K20 offered more remarkably due to their enhanced characteristics than the others

M. Alauddin et al. [23]	Inconel 718	Uncoated tungsten carbide inserts	End milling	Dry conditions	The life of tools in down-cutting was more useful than in up-cutting.
Weinert et al. [26]	Ni-Ti alloy	Tools coated (TiCN / TiN)	Drilling	Lubricant and inner coolant	The high cutting speeds lead to excessive tool wear while the suitable speed for the drilling process was remarked at 30m/min. with improved surface roughness up to 5.9μm.
D. Biermann et al. [30]	Ni-Ti alloy	Single-lip and twist drills	Micro-drilling	--	Tool wear increased during single lip drilling due to adhesion caused by friction between the hole wall and the guide pad of tool. The twist drills show no sign of adhesion wears.
Y. Tao et al. [31]	Ni-Ti+TiH$_2$	--	Grinding	--	When the depth of cut was over 0.08 μm, a higher surface roughness has been notalised with significant wear of the abrasive grits' cutting edges, which further limits the capacity to keep its cutting ability

Table 3. Non-traditional operation of SMAs (SMA'ların geleneksel olmayan işlenmesi)

Authors	Material	Process	Parameter	Result
S. Daneshmnd. et al. [35]	Ni-Ti alloy	EDM	Pulse on/off time, discharge current, and voltage	The most meaningful parameters that alter the (MRR) are the pulse current and the pulse on time. By growing the pulse off time, MRR and SR are reduced.
V. Jatti. [39]	(NiTi), (NiCu), (BeCu) alloys	EDM	Pulse on/off duration, gap current/voltage, and electrical conductivity	By increasing the gap current, and workpiece electrical conductivity, the MRR increases. The increase in the gap voltage causes a decrease in MRR. The low electrical conductivity of the workpiece yields to lower TWR.
M. Abidi et al. [40].	Ni-Ti alloy	Micro-electrical discharge machining (MEDM)	Brass and tungsten electrodes	The brass electrode had a higher material removal rate than the tungsten electrode, as well as more tool wear and worse surface quality.

S. Hsieh et al. [43]	(Ti-Ni-Zr/Cr) SMAs	WEDM	Peak current and pulse on time	Raising the peak current and pulse on time improved the SR, also resulting in higher MRR. The volume of shifted materials effect on the surface quality.
R. Chaudhari et al. [44]	Nitinol SMA	WEDM	Pulse-on, off time and current	To achieve a higher MRR, elevated discharge energy is needed, which could be gained by increasing the rates of current, and pulse on time. To obtain a lesser (SR), lower discharge energy is demanded that might be performed by decreasing the values of the pulse-off time.
H. Soni et al. [46]	Ti-Ni-Co	WEDM	Pulse on-off duration and servo voltage	When the pulse rate was raised over time, the MRR went up, and vice versa. Surface quality was found to be poor in the presence of microvoids, micro-cracks, and micro globules when a specific combination of high pulse on time and low servo voltage was used.
H. Soni et al. [47].	$Ti_{50}Ni_{45}Co_5$ SMA	WEDM	Pulse on/off time, and servo voltage	Higher MRR, and better SR could be fulfilled by applying 125μs, 35μs, and 40V of pulse on/off time, and servo voltage respectively
H. Bisaria et al [48]	Ni-rich NiTi alloy's	WEDM	Spark gap voltage and on-off pulse duration	By raising the pulse on time and decreasing the pulse off time, surface roughness and cutting efficiency were improved.
C. Li et al. [49].	TiNi SMAs	Laser operation	Femtosecond laser and Lesser beam	The femtosecond laser creates a high ablation rate and notable recast layer. Lesser beam produces superior cutting quality at a lower cost.
M. Kong et al. [52]	TiNi SMAs	WJM	Plain and abrasive (WJM)	The (AWJM) might be a valuable and efficient approach for elements having a complicated crystal structure and phase transition.
E. Lee et al. [54]	Nitinol based SMAs	Electrochemical polishing	Acid and Neutral electrolyte	The acid electrolyte is fitting for slow down and accurate operating. The neutral electrolyte does not provide precision machining; it generates holes on the nitinol surface.

4. CHALLENGES AND OPPORTUNITIES (ZORLUKLAR VE FIRSATLAR)

In the modern-day, SMAs are new smart elements that could remember and come back to their original form by altering the surrounding conditions. Smart nature, biocompatibility, pseudo-plasticity, high corrosion, and wear resistance are some of the other unique and adaptable qualities of shape memory alloys. Because of their interesting properties, these elements have attracted plenty of attention and interest in a broad range of implementations during the last few years. Machining of these materials is required to be used in various applications. This machining could be performed in both traditional and unconventional ways. However, because of extreme strain

hardening, high toughness, and large cutting pressures, conventional operating of SMAs is challenging, while during non-conventional operating the surface integrity and the accuracy of dimension are greatly enhanced as well as the machining time was reduced. Generally, each machining techniques have impediments that give advantageous or unfavorable results.

5. CONCLUSIONS (SONUÇLAR)

In this article review, several traditional, non-traditional technical techniques of Nitinol - Titanium-based alloys, over with their statements, have been briefly reviewed. Furthermore, the challenges of operation these SMAs typically were also studied. Multiple functions on non-traditional ways of machining such as EDM, WEDM, WJM, and AWJM have been highlighted in this review. Furthermore, the numerous machining methods and the work element were employed by the researcher have been displayed. Finally, subsequent conclusions are formed after reviewing the earlier mentioned literature:

- The significant obstacle faced in the operating of SMAs is the work hardening. However, the most suitable cutting speed range for carbide cutting tools in turning is (15-30m/min). In contrast, coated carbides could be utilized up to (50m/min). Also, the most extended tool life could be provided by ranges of feeds (0.18-0.25 mm/rev), and Positive rake angles are advised to be utilized. A surface with the lowest roughness could be achieved by the usage of a cryogenic machining manner. Usually, the most predominant failure forms are notching and flank wear. Traditional lubricant equipment appears to provide higher life of tool than high-pressure lubricant equipment at most operating situations.

- Cutting speeds (20-30 m/min) and feed rates (0.10-0.15 mm/tooth) were found to be the optimum for most nickel-based composites during milling. Nevertheless, the most applied cutting tool is (K20) carbide grades. Moreover, (CVD) coated instruments function better than (PVD). Down-cutting milling is considered as a favored system since it decreases the influence of work hardening. In addition, the dominant form of instrument breakdown for uncoated carbides is fracture and chipping, Despite the fact that tool crash is influenced by flank wear as well.

- For finer surface integrity in the drilling technique, the range of 20-50 m/min for cutting rate, and 20-6000 rpm for spindle velocity were the most reasonable operating factors.

- The velocity during the micro-drilling process shall not be more than VC = 30 m/min. Due to excessive work-hardening, a slower cut-rate produces chipping of the cutting edge. Faster speeds improve adhesive mechanisms once more.

- Generally, when machining shape memory alloys, the shared act of strain and fatigue hardening has a significant hardening influence and reduces the cutting rate. As a consequence, specimen integrity is reduced, and wear rate is too high, even with modified cutting settings and appropriate cutting equipment. Those properties could as well have an effect on the form of memory characteristics.

- The most substantial parameters that influence the rate of removed materials (MRR) during the EDM test are the pulse current and the pulse on time. In the meanwhile, an increase in these two variables grows the MRR. Additionally, the surface roughness (SR) can be impacted negatively by growing the pulse current and the pulse off time. Finally, structural modifications in the operated surface depend on the machining variables and the thermal features of the tested material, as melting point and thermal conductivity.

- The (EDM) manner is the predominant option in the non-traditional machining of SMAs. It is obviously visible from the number of investigations conducted on that process by various investigators.

- For femtosecond laser machining, the usage of lower beam turns higher quality in the cutting and lower economic cost.

- In comparison to micro-milling processes, the water jet machining was considered more useful in regard to the time of cutting, the thermal attraction of the specimen, and operation costs.
- Finally, high sensitivity to temperature variations, unique chemical reactivity, chip creation, and phase transformation over machining of SMAs considered as causes for engineers to select non-traditional techniques of machining these alloys, essentially to avoid high wastage of element during operating, also has confirmed to be extremely economical as opposed to traditional modes of operating.

6. FUTURE SCOPE (GELECEK KAPSAMI)

The greatest number of public procedures were investigated for traditional operations on SMAs utilizing the turning procedure within dry and cryogenic situations. The turning operation was documented to assess the formability and surface-integrity properties of SMAs like micro-hardness and surface roughness by adjusting cutting quickness, depth, and feed of cutting. During the traditional operation technique, narrow experimentations are implemented to enhance the microstructure and governance of the phase transformation temperature for SMAs.

The application of coating was being used to evaluate tool life and enhancement during the processing of SMAs materials by lowering the temperature during the machining process. Likewise, constructing a texture on the tool rake face is another way to dramatically increase the tool life. Textures may be utilized efficiently to minimize the heat while machining by withstanding the lubrication effect via its groove surface. Like these techniques are not made with SMAs processing. Similarly, research is needed to extend tool life through multilayer coating, tool holder, and insert improvements.

The earlier machinability investigations of non-traditional processes have been done on SMAs that are manufactured by various approaches such as traditional tungsten, vacuum arc melt techniques, melting and remelting methodologies. However, relatively limited studies have been published on the EDM and WEDM operations of shape memory alloys manufactured by powder metallurgy.

REFERENCES (KAYNAKLAR)

1. T. Duerig, K. Melton, Engineering Aspects of Shape Memory Alloys, Butterworths, London, 1989.
2. C. M. Wayman, Some applicatıons of shape-memory alloys, The Journal of The Minerals, Metals & Materials Society, 32: 129-137, 1980.
3. L. Kulinsky, M. J. Madou, BioMEMs for drug delivery applications, MEMS for Biomedical Applications, Woodhead Publishing, 2012.
4. D. J. Hartl, D. C. Lagoudas, Aerospace applications of shape memory alloys, Proc. Inst. Mech. Eng. Part G: Journal of Aerospace Engineering, 4(221): 535-552, 2007.
5. Wikipedia, Nitinol Austenite and martensite small.jpg[Online]. https://en.wikipedia.org/wiki/File:Nitinol_Austenite_and_martensite_small.jpg. [Accessed: 26-Nov-2021].
6. I. Qader, M. Kok, F. Dağdelen, Y. Aydoğdu, A review of smart materials, Journal of Science and Engineering, 3(6): 755-788, 2019.
7. P. Lobo, J. Almeida, L. Guerreiro, Shape memory alloys behaviour: A review, Procedia Engineering, 114: 776-783, 2015.
8. E. Ezugwu, J. Bonney, Y. Yamane, An overview of the machinability of aeroengine alloys, Journal of Materials Processing Technology, 134(2): 233-253, 2003.
9. T. Kıvak, K. Habalı, U. Şeker, The effect of cutting paramaters on the hole quality and tool wear during the drilling of Inconel 718, Gazi University Journal of Science, 25(2): 533-540, 2012.
10. D. Manolakos, A. Markopoulos, A review on the machining of Nickel-Titanium shape memory alloys, Reviews on Advanced Materials Science, 42(1): 28-35, 2015.
11. K. Weinert, V. Petzoldt, D. Kötter, Turning and drilling of NiTi shape memory alloys, CIRP Annals, 53(1): 65-68, 2004.
12. K. Weinert, V. Petzoldt, Machining of NiTi based shape memory alloys, Materials Science and Engineering: A, 378(1-2): 180-184, 2004.

13. E. Ezugwu, Á. Machado, I. Pashby, J. Wallbank, The effect of high-pressure coolant supply when machining a heat-resistant nickel-based superalloy, Lubrication Engineering, 47(9): 751-757, 1991.

14. F. Pusavec, H. Hamdi, J. Kopac, I. Jawahir, Surface integrity in cryogenic machining of nickel based alloy-Inconel 718, Journal of Materials Processing Technology, 211(4): 773-783, 2011.

15. N. Zlatin, J. Christopher, Machining characteristics of difficult to machine materials,influence of metallurgy on machinability, American Society for Metals, 296–307, 1975.

16. M. Rahman, W. Seah, T. T. Teo, The machinability of Inconel 718, Journal of Materials Processing Technology, 63(1-3): 199-204, 1997.

17. R. Arunachalam, M. A. Mannan, Machinability of nickel-based high temperature alloys, Machining Science and Technology, 4(1): 127-168, 2000.

18. Y. Guo, A. Klink, C. Fu, J. Snyder, Machinability and surface integrity of Nitinol shape memory alloy, CIRP Annals, vol. 62, 62(1): 83-86, 2013.

19. E. Ezugwu, E. Machado, Face Milling of Aerospace Materials, Proceedings of the 1st International Conference on Behaviour of Materials in Machining, 1-3 Nov. 1998, England.

20. E. Ezugwu, I. R. Pashby, High speed milling of nickel-based superalloys, Journal of Materials Processing Technology, 33(4): 429-437, 1992.

21. M. Alauddin, M. El Baradie, M.S.J. Hashmi, Modelling of cutting force in end milling Inconel 718, Journal of Materials Processing Technology, 58(1): 100-108, 1996.

22. M. Alauddin, M. El Baradie, M.S.J. Hashmi, Optimization of surface finish in end milling Inconel 718, Journal of Materials Processing Technology, 56(1-4): 54-65, 1996.

23. M. Alauddin, M. El Baradie, M.S.J. Hashmi, Tool-life testing in the end milling of Inconel 718, Journal of Materials Processing Technology, 55(3-4): 321-330, 1995.

24. K. Weinert, V. Petzoldt, Machining NiTi micro-parts by micro-milling, Materials Science and Engineering: A, 301(481-482): 672-675, 2008.

25. R. Piquard, A. D'Acunto, P. Laheurte, D. Dudzinski, Micro-end milling of NiTi biomedical alloys, burr formation and phase transformation, Precision Engineering, 38(2): 356-364 2014.

26. Y. Fu, H. Du, W. Huang, S. Zhang, M. Hu, TiNi-based thin films in MEMS applications: a review, Sensors Actuators A, 112(A): 395-408, 2004.

27. K. Weinert, V. Petzoldt, Machining of NiTi based shape memory alloys, Materials Science and Engineering: A, 378, 180–184, 2004.

28. S. Mousavi, M. Hassani, S. S. Entezami, The control process of Nitinol alloy drilling through fuzzy logic, Majlesi Journal of Mechatronic Systems, 1(2): 1-7, 2012.

29. H. Lin, K. M. Lin, Y. C. Chen, A study on the machining characteristics of TiNi shape memory alloys, Journal of Materials Processing Technology, 3(105): 327-332, 2000.

30. D. Biermann, F. Kahleyss, E. Krebs, and T. Upmeier, A Study on micro-machining technology for the machining of NiTi: Five-axis micro-milling and micro deep-hole drilling, Journal of Materials Engineering and Performance, 20(4-5): 745-451, 2011.

31. Y. Tao, J. Xu, W. Ding, A study on grinding performance of porous NiTi shape memory alloy, Key Engineering Materials, 360(143): 143-147, 2008.

32. T. Goryczka, P. Salwa, Influence of batch mass on formation of NiTi shape memory alloy produced by high-energy ball milling, metals, 11(12): 2-12, 2021.

33. M. Mizutani,, S. Kikuchi, K. Katahira, High precision grinding and surface modification of Ni-Ti shape memory alloy ground by a new electrical grinding technique, J-STAGE, 76(764): 419-421, 2010.

34. M. Manjaiah, S. Narendranath, S. Basavarajappa, Review on non-conventional machining of shape memory alloys, Transactions of Nonferrous Metals Society of China, 24(1): 12-21, 2014.

35. S. Daneshmand, E. Farahmand Kahrizi, E. Abedi, M. Mir Abdolhosseini, Influence of machining parameters on electro discharge machining of NiTi shape memory alloys, International Journal of Electrochemical Science, 8: 3095-3104, 2013.

36. W. Theisen, A. Schuermann, Electro discharge machining of nickel–titanium shape memory alloys, Materials Science and Engineering: A, 378(1-2): 200-204, 2004.

37. S. Zinelis, Surface and elemental alterations of dental alloys induced by electro discharge machining (EDM), Dental Materials, 23(5): 601–607, 2007.

38. A. Gangele, A. Mishra, Surface roughness optimization during machining of NiTi shape memory alloy by EDM through Taguchi's technique, Materials Today: Proceedings, 29: 343-347, 2020.

39. V. Jatti, Multi-characteristics optimization in EDM of NiTi alloy, NiCu alloy and BeCu alloy using Taguchi's approach and utility concept, Alexandria Engineering Journal, 57(4): 2807-2817, 2018.

40. M. Abidi, A. Al-Ahmari, U. Umer, M. S. Rasheed, Multi-objective optimization of micro-electrical

discharge machining of nickel-titanium-based shape memory alloy using MOGA-II, Measurement, 125: 336-349, 2018.

41. S. Daneshmand, V. Monfared, A. A. Lotfi Neyestanak, Effect of tool rotational and Al2O3 powder in electro discharge machining characteristics of NiTi-60 shape memory alloy, Silicon, 9(12): 273-283, 2016.

42. C. Fu, J. Liu, Y. Guo, Q. Zhao, A comparative study on white layer properties by laser cutting vs. electrical discharge machining of Nitinol shape memory alloy, Procedia CIRP, 42: 246-251, 2016.

43. S. Hsieh, S. Chen, H. Lin, M. Lin, S. Chiou, The machining characteristics and shape recovery ability of Ti–Ni–X (X=Zr, Cr) ternary shape memory alloys using the wire electro-discharge machining, International Journal of Machine Tools and Manufacture, 49(6): 509-514, 2009.

44. R. Chaudhari, J. Vora, V. Patel, L. López De Lacalle, D. Parikh, Surface analysis of wire-electrical-discharge-machining-processed shape-memory alloys, Materials (Basel), 530(3): 2-13, 2020.

45. N. Praveen, U. Mallik, A. Shivasiddaramaiah, G. Narendra Reddy, A study on material removal rate of Cu-Al-Mn shape memory alloys in WEDM, Materials Today, 46(7): 2770-2774, 2021.

46. H. Soni, N. Sannayellappa, R. M. Rangarasaiah, An experimental study of influence of wire electro discharge machining parameters on surface integrity of TiNiCo shape memory alloy, Journal of Materials Research, 32(16): 3100-3108, 2017.

47. H. Soni, S. Narendranath, M. Ramesh, Experimental ınvestigation on effects of wire electro discharge machining of Ti50Ni45Co5 shape memory alloys, Silicon, 10: 2483-2490, 2018.

48. H. Bisaria, P. Shandilya, The machining characteristics and surface integrity of Ni-rich NiTi shape memory alloy using wire electric discharge machining, Proc. Inst. Mech. Eng. Part C: Journal of Mechanical Engineering Science, 233(3): 1068-1078, 2019.

49. C. Li, S. Nikumb, F. Wong, An optimal process of femtosecond laser cutting of NiTi shape memory alloy for fabrication of miniature devices, Optics and Lasers in Engineering, 44(10): 1078-1087, 2006.

50. A. Tung, B. Park, D. Liang, G. Niemeyer, Laser-machined shape memory alloy sensors for position feedback in active catheters, Sensors Actuators A: Physical, 147(1): 83-92, 2008.

51. A. Tung, B. Park, G. Niemeyer, D. Liang, Laser-machined shape memory alloy actuators for active catheters, IEEE/ASME Transactions on Mechatronics, 12(4): 439-446, 2007.

52. M. Kong, D. Axinte, W. Voice, Challenges in using waterjet machining of NiTi shape memory alloys: An analysis of controlled-depth milling, Journal of Materials Processing Technology, 211(6): 4959-971, 2011.

53. M. Frotscher, F. Kahleyss, T. Simon, D. Biermann, G. Eggeler, Achieving small structures in thin NiTi sheets for medical applications with water jet and micro machining: A comparison, Journal of Materials Engineering and Performance, 20(4): 776-782, 2011.

54. E. Lee, T. Shin, An evaluation of the machinability of nitinol shape memory alloy by electrochemical polishing, Journal of Mechanical Science and Technology, 25(4): 963–969, 2011.

55. M. Frensemeier, D. Schirra, M. Weinmann, O. Weber, E. Kroner, Shape-memory topographies on nickel–titanium alloys trained by embossing and pulse electrochemical machining, Advanced Engineering Materials, 18(8): 1388-1395, 2016.

56. S. Ao, K. Li, W. Lui, D. Luo, Electrochemical micromachining of NiTi shape memory alloy with ethylene glycol–NaCl electrolyte containing ethanol, Journal of Manufacturing Processes, 53: 223-228, 2020.

Kritik Metan Yoğunluğu Tespit Robotu Prototip Tasarımı ve Üretimi

Oğuzhan ŞENEL[1] ⓘD, Gürcan SAMTAŞ[2*] ⓘD

[1]*Düzce Üniversitesi, Lisansüstü Eğitim Enstitüsü, Düzce, Türkiye*
[2]*Düzce Üniversitesi, Mühendislik Fakültesi, Düzce, Türkiye*

ÖZET

Metan, evsel atıkların çürümesi esnasında metanojen isimli arke bakteriler tarafından üretilen, rengi ve kokusu olmayan bir gazdır. Doğal gazın da ana bileşenlerinden biri olan metan gazı iyi bir yakıttır ve belirli koşullarda patlayıcı özellik gösterebilmektedir. Metan gazına özellikle çöplükler, geri dönüşüm tesisleri ve madenler gibi ortamlarda sıkça rastlanır. Bu ortamlarda kontrolünün sağlanamaması bugüne kadar yüzlerce patlama ve yangına sebebiyet vermiştir. Bu patlama ve yangınlar ciddi can ve mal kayıplarına yol açabilmektedir. Bu çalışmada metan gazının kontrol altında tutulmasını sağlayan mobil bir robot geliştirmek, böylece ülkemizde metan gazı kaynaklı olası patlamaların önüne geçmek amaçlanmıştır. Bu amaç doğrultusunda ortamdaki metan yoğunluğunu ölçerek patlama koşullarını önceden tespit eden ve patlama gerçekleşmeden gerekli birimlere durumu bildiren bir robot tasarlanmış ve üretimi gerçekleştirilmiştir. Çalışmada gaz tespitinden farklı olarak özellikle metan gazının kontrolü üzerine odaklanılmış, robotun tasarımı metan gazının karşılaşıldığı ortamlarda kullanılmaya uygun şekilde yapılmıştır. Olası yangın durumlarında robotun deformasyona uğrama süresini uzatmak adına gövdesi 310 çelik sacdan üretilmiş ve iç yüzeyine seramik fiber ile yalıtım işlemi uygulanmıştır.

Critical Methane Density Detection Robot Prototype Design and Production

ABSTRACT

Methane is a colorless and odorless gas produced by archaeal bacteria called methanogen during the decomposition of household waste. Methane gas, which is one of the main components of natural gas, is a good fuel and can show explosive properties under certain conditions. Methane is frequently encountered in environments such as landfills, recycling facilities and mines. The lack of control in these environments has caused hundreds of explosions and fires to date. These explosions and fires can cause serious loss of life and property. In this study, it is aimed to develop a mobile robot that keeps methane gas under control, thus preventing possible explosions caused by methane gas in our country. For this purpose, a robot was designed and produced, which detects the explosion conditions in advance by measuring the methane density in the environment and notifies the necessary units before the explosion occurs. In the study, unlike gas detection, the focus is on the control of methane gas, and the design of the robot is suitable for use in environments where methane gas is encountered. In order to prolong the deformation time of the robot in case of possible fire, its body is made of 310 steel sheet and its inner surface is insulated with ceramic fiber.

1. GİRİŞ (INTRODUCTION)

Robot terimi Çekçe "zorla çalışma" anlamına gelmektedir ve tarihte ilk olarak Karel Čapek tarafından bir tiyatro oyununda kullanılmıştır. Bu terim dünya tarafından hızla kabul görerek kullanılmaya başlanmıştır [1]. Robot tanımı üzerinde ise henüz bir fikir birliği sağlanamamıştır. Temel olarak robotlar bulunduğu ortam şartlarını algılayabilen, karar alabilen ve aldığı kararları

uygulayabilen makineler olarak ifade edilebilir. Bu özelliklerini kullanarak belirli görevleri yerine getiren robotlar Asimov'a göre üç robot yasasına uymak zorundadır. Bu yasalara göre; bir robot insanlara zarar veremez ya da eylemsiz kalarak zarar görmelerine izin veremez, robotlar birinci yasa ile ters düşmediği sürece insanların verdiği emirlere itaat etmek zorundadır ve birinci ve ikinci yasa ile ters düşmediği sürece robotlar kendi varlıklarını korumak zorundadır [2]. Robotlar savunma sanayi, endüstriyel üretim, temizlik hizmetleri, eğlence sektörü gibi birçok alanda kullanılmaktadır. Arama çalışmalarında belirli madde ve cisimleri bulmada kullanıldıkları gibi zararlı madde ve gazların tespit edilmesinde de görev alabilmektedirler. Yapıları çok sayıda kritere göre değişiklik gösterdiğinden robotlar için genel bir sınıflandırma yapmak oldukça zordur. Robotlar eklem yapılarına, kullanım alanlarına, işlevsel özelliklerine, kontrol yöntemlerine ve çalışma prensiplerine göre çeşitli şekillerde sınıflandırılmaktadır [3]. Robotlar, tarihi gelişimleri açısından ele alındığında endüstriyel ve mobil robotlar olmak üzere iki gruba ayrılabilirler. Mobil robotlar da kendi aralarında sınırlı menzilli ve sınırsız menzilli olmak üzere ikiye ayrılmaktadır [4]. Bu çalışmada tasarımı ve üretimi gerçekleştirilen metan yoğunluğu tespit robotu sınırsız menzilli mobil robotlar kategorisinde yer almaktadır.

Metan patlaması havada %4-%15 arası metan bulunduğu koşullarda gerçekleşmektedir [5]. Bu aralığın üzerindeki metan-hava karışımı alev ile karşılaştığında tutuşarak yanmakta fakat patlayıcı özellik göstermemektedir [6]. En güçlü patlamalar ortamda %9,5 metan ve yeterli miktarda oksijen bulunması ile meydana gelmektedir. Metan gazı havaya kıyasla yaklaşık yarı yarıya daha hafiftir. Bu nedenle sızıntı ve gaz kaçağı durumlarında yukarıya yükselmektedir. Bu durum madenler ve geri dönüşüm tesisleri gibi kapalı alanlarda metan yoğunluğunun ölçülerek kontrol altında tutulmasını güçleştirmektedir. Sızıntının meydana geldiği kapalı alanda hava tahliye kanalları bulunuyorsa sızan gaz zeminde birikmeden yükselerek tahliye olmaktadır. Fakat tahliye kanallarında herhangi bir sorun oluşması durumunda birikerek hızla %4-%15 yoğunluk değerine ulaşabilmekte, rengi ve kokusu olmadığı için bu durum ölçüm cihazları kullanılmadığı takdirde fark edilememektedir. Tasarlanan robot, ölçümleri esnasında metan birikimi oluşmaya başladığını tespit ettiğinde serbest dolaşımı bırakarak bulunduğu yerde alarm durumuna geçmektedir. Alarm durumunda robot iki farklı uyarı işlemini aynı anda gerçekleştirmektedir. Bu işlemlerden ilki sesli uyarı ile bulunduğu bölgeye yakın olan yetkilileri hızlıca bilgilendirmektir. İkinci işlem ise ölçüm sonucu elde ettiği ppm değerini rakamsal olarak ilgili birime göndermek ve gerekli prosedürün uygulanmasını sağlamaktır. Bu iki işlemden biri başarılı olduğu takdirde patlama gerçekleşmeden metanın tahliyesi sağlanarak patlamanın önüne geçilebilecektir. Patlamanın önceden tespit edilebilmesinde tarama yapılan ortamın büyüklüğü ve robotun tarama hızı önem arz etmektedir. Alınan güvenlik önlemleri riski en aza indirse dahi patlama olasılığı her zaman olacaktır. Ortamda görev yapan makine veya operatörlerden kaynaklanan kıvılcım ve yangınlar çöplerin bulunduğu ortamda hızla yayılarak beklenmeyen patlamalara yol açabilmektedir. Bu gibi yangınlarda, yangının başlangıç aşamasında alınan aksiyonlar yangının gidişatı için oldukça belirleyici olmaktadır. Metanın yanma ısısı, ısı kaynağına bağlı olarak 650-750°C arasında değişmektedir [7]. Böyle yüksek sıcaklıklarda yalıtım işlemi uygulanmamış mobil robotların deformasyona uğraması saniyeler sürmektedir. İnsanların aksine robotlar böyle felaket durumlarında korku ve şok gibi hislerin etkisi altında kalmadıklarından çok daha hızlı ve doğru tepkiler verebilmektedir. Bu nedenle yangın güvenliği alanında robotlar ve yapay zekâya güvenmek ve onları ortam koşullarına dayanıklı hale getirmek yerinde bir karar olacaktır.

Mobil robotların güvenlik alanında kullanımı 2000'li yıllara dayanmaktadır. Pektaş, 2010 yılında gerçekleştirdiği çalışma ile mobil bomba imha robotlarını işlevsellik yönünden inceleyerek bir mobil bomba imha robotu prototip tasarımı gerçekleştirmiştir. Çalışmada, modelleme alanında yaşanan zorlukların robotik sektörünün gelişimi ile azalabileceğine vurgu yapmıştır [8]. Özellikle bomba imha alanında mobil güvenlik robotlarının kullanımı zaman içinde artsa da yapılan literatür taramaları sonucu patlayıcı gaz tespiti üzerine az sayıda çalışma ile karşılaşılmıştır. 2014 yılında Raju ve Rani android tabanlı bir otomatik gaz tespit robotu üzerine çalışmışlardır. Raju ve Rani bu çalışmada gaz kaçağı tespiti yapan mini robotun endüstriyel tesislerde kullanımını hedeflemişlerdir [9]. Türkiye'de gaz algılama robotları üzerine ilk çalışma ise Kanlı tarafından yapılmıştır. Bu robot

otonom yürüyüş ile alan içerisinde gezerek gaz ölçümü yapmakta ve gaz tespiti yaptığında alarm durumuna geçmektedir [10]. Bu işlemlerin gerçekleştirilmesinde robotun reaksiyon hızı önem arz etmektedir. Birçok sensör ve sürücü kartı ile uyumlu olması, çıkış sayısının fazla olması ve açık kaynak kodlu olması Arduino mikrodenetleyici platformunu bu tarz uygulamalarda bir adım öne çıkarmaktadır. Arduino Mega modeli, bünyesinde 16MHz sorgu oranına sahip ATmega2560 işlemci barındırmaktadır [11]. İşlemcinin bu düzeyde yüksek hıza sahip olması, çok sayıda sensörden gelen bilgiyi işlerken ve gerekli işlemleri uygularken yaşanan gecikmeleri en aza indirecektir. Öte yandan güçlü bir işlemci ile çok sayıda elektronik aygıtı kontrol etmek için yoğun bir enerji gerekmektedir. Baykal'a göre geliştirilmesi gereken birçok özelliği olmasına rağmen günümüzde yüksek enerji kapasitesine ihtiyaç duyan, yüksek enerji yoğunluğu gerektiren projelerde Lityum-polimer (Li-po) sıklıkla tercih edilmektedir [12]. Li-po batarya hücrelerinin her biri tam dolumda 4.2 V olmak üzere ortalama 3.7 V gerilime sahiptir [13]. Böylelikle 3 hücreli bir Li-po pil toplam 11.1 V gerilime sahip olacaktır.

Bu çalışmada ortamdaki sızıntı metan gazını tespit etmesinin yanı sıra, patlama ihtimalini analiz ederek geri bildirim gönderen mobil bir robot tasarlanmıştır. Robot, ultrasonik mesafe sensörleri yardımıyla etrafındaki engelleri algılamakta ve bu engellerden kurtularak ortam içerisinde hareket etmektedir. Robot, serbest dolaşımdayken gaz sensörü aracılığıyla ortamdaki metan gazının ölçümünü yapmaktadır. Gövdesine uygulanan yalıtım işlemi sayesinde robot yangın ortamında belirli bir süre daha aktif kalarak yangının büyümesini önleyici faaliyetlerde bulunabilecek ve ilgili birime bilgi aktarımı yapabilecektir. Yüksek ısı faktörünü değerlendirerek yangın durumunu tespit eden kritik metan yoğunluğu tespit robotu, yangın bölgesinden ya da yakınından geçen doğalgaz hattını kapatmak ya da itfaiyeye yangın ihbarı yapmak gibi işlemler için bildirim gönderebilecektir.

## 2. MATERYAL VE YÖNTEM (MATERIAL AND METHOD)

2.1. Kritik Metan Yoğunluğu Tespit Robotu Tasarımı (Designing the Critical Methane Density Detection Robot)

Tasarım sürecinin ilk aşamasında dikkat edilmesi gereken birkaç husus bulunmaktadır. Bu hususlardan ilki; robot şasisinin muhtemel ağırlığının hesaplanması ve robotun hareketini sağlayacak olan motorların bu ağırlığı hareket ettirmeye yetecek güçte olmasına dikkat edilmesidir. Yine robotun ağırlığına göre motorların çekeceği sürekli akım ve maksimum akım değerleri hesaplanmalı ve motor sürücü kartı bu değerler referans alınarak seçilmelidir. Göz önünde bulundurulması gereken bir diğer husus ise robotun gövdesinin çelik sacdan üretilecek olmasıdır. Çelik oldukça ağır bir malzeme olduğundan, robotun boyutlarındaki ufak değişimler dahi ağırlığına ciddi etki etmektedir. Bu nedenle motor ve sürücü kartı seçimi yapılmadan önce tasarlanan şasi; bu aygıtların eklenmesiyle ufak değişimler geçirebilecek olsa da boyutlarında büyük oranda artış olmamalıdır.

Bu çalışmada tasarım süreci bu üç hususa dikkat edilerek gerçekleştirilmiştir. Bu doğrultuda ilk olarak kullanılacak olan elektronik aygıtlar ve yalıtım malzemesi belirlenerek boyutları hesaplanmıştır. Mikrodenetleyici kart olarak birçok motor ve motor sürücü kartı ile uyumlu olan Arduino platformu tercih edilmiştir. Böylelikle daha sonra yapılacak olan motor ve sürücü kartı tercihinde seçenek sayısı artmıştır. Projede kullanılacak aygıt sayısı göz önünde bulundurularak diğer Arduino mikrodenetleyici kartı modellerine nazaran daha fazla pin sayısına sahip olan Arduino Mega modeli projeye uygun görülmüştür. Robotun engelleri algılamasını sağlayacak olan 3 adet ultrasonik mesafe sensörü de HCSR04 modeli olarak belirlenmiştir.

Çalışmanın temel amacı; metan sızıntısını henüz patlama koşulları oluşmamışken tespit ederek tahliye işlemi için imkân sağlamaktır. Metan yoğunluğunun %4-%15 aralığına geldiği bir alanda elektronik cihaz kullanmak ya da tahliye işlemi gerçekleştirmek son derece riskli olacaktır. Bu nedenle ortamdaki yoğunluk %4 değerine ulaşmadan, sızıntı tespit edilmeli ve gerekli tahliye işlemi gerçekleştirilmelidir. Çalışma kapsamında metan gazının tespiti ve yoğunluk ölçümünde kullanılacak olan gaz sensörü Arduino uyumlu MQ4 Gaz Sensörü olarak belirlenmiş ve tasarıma dâhil edilmiştir. Bu sensör 300 ile 10000 ppm arası çok düşük yoğunluklarda ölçüm yapabilmektedir. Bu sayede robot aslında eser miktarda sızıntıları dahi fark

edebilmektedir. Fakat her metan sızıntısı metan gazının ortamda birikmesine işaret değildir. Çok hafif olması nedeniyle metan, çoğu durumda ortamda birikmeden yükselerek havalandırma veya farklı bir yol ile tahliye olmaktadır. Metanın birikmediği koşullarda robotun sızıntıyı tespit ederek tesisin iş akışını durdurması istenmemektedir. Bu sebeple havada %0,03 oranına tekabül eden çok düşük yoğunluklar fark edilse de göz ardı edilecektir. Ancak ölçümler 9000 ppm değerini aştığında, sızıntı "ortamda metan birikimine sebebiyet verebilecek durum" olarak değerlendirilecektir. Sensörlerden birinin ortam koşullarından etkilenerek yanlış ölçüm yapması veya bozulması gibi sorunları bertaraf etmek ve ölçümleri karşılaştırarak daha doğru ölçümler elde edebilmek için iki adet gaz sensörü kullanılmıştır. İki sensörden biri 9000 ppm üzerinde bir ölçüm yaptığında robot uyarı verecektir. Robotun yangını algılamasını sağlayacak olan sıcaklık sensörü ise DFRobot markasının DFR0558 modeli olarak belirlenmiştir. Bu sensör ile 1350 °C dereceye kadar olan sıcaklıklar ölçülebilmektedir. Ölçülen sıcaklık değeri fabrika standartları referans alınarak belirlenen değerin üzerinde ise robot bu durumu yangın bildirimi yaparak değerlendirecektir. Her tesisin standart değerleri farklılık gösterebileceğinden çalışmada 70°C referans değer olarak kullanılmıştır. Bu sıcaklık değeri ile karşılaşıldığında SMS bildirimi, kızılötesi sinyaller, bluetooth teknolojisi gibi birçok seçenek ile bildirim yapılabilmektedir. Bu çalışmada kapsam alanının geniş olması nedeni ile iletişim birimi olarak ESP8266 Arduino uyumlu kablosuz ağ modülü tercih edilmiştir. Bu modül aracılığı ile robot görev aldığı tesisin kablosuz ağına bağlanarak veri aktarımı yapabilecektir. Robot, ölçülen sıcaklığı rakamsal olarak aktardıktan sonra bu veri ile yapılacak işlemler doğrudan tesisin imkan ve öncelikleri ile bağlantılı olacaktır. Veri aktarımı ile birlikte acil durum pozisyonunda sesli uyarının gerçekleştirilebilmesi için arduino uyumlu buzzer modülü kullanılmıştır. Bu aygıtların belirlenmesinin ardından çizimleri bilgisayar destekli tasarım programı vasıtasıyla tamamlanmıştır (Şekil 1). Tasarım sürecinde hazır olarak alınan malzemelerin ölçüleri için katalog değerleri referans alınmıştır.
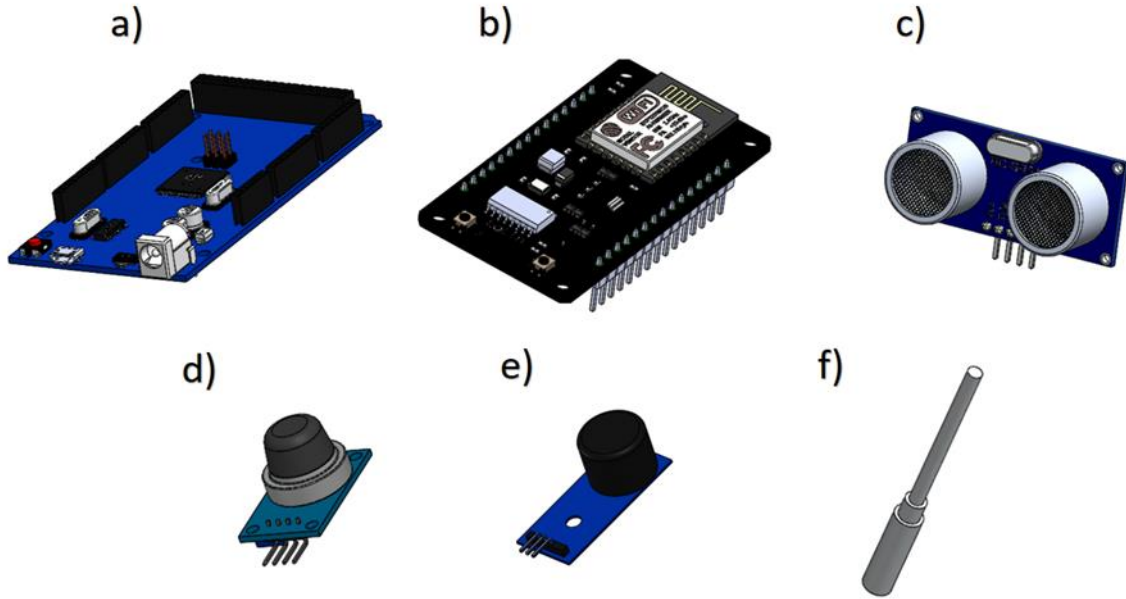

Şekil 1. Elektronik aygıtlar (Electronic devices);
a) Mikrodenetleyici kartı (Microcontroller card)   **b)** Kablosuz ağ haberleşme modülü (Wifi serial module)
c) Ultrasonik Mesafe Sensörü (Ultrasonic sensor)   **d)** Gaz Sensörü (Gas sensor)
e) Buzzer Modülü (Buzzer module)   **f)** Sıcaklık Sensörü (Temperature sensor)

Şasi boyutlarının belirlenmesinde bir diğer etken ise iç yüzeye uygulanacak yalıtım işlemidir. Yangının ilk anlarında sıcaklık 600 °C dolaylarında seyretmektedir. Gövdeye uygulanan yalıtım malzemesi ise 1200 °C gibi yüksek sıcaklıkların yalıtımında kullanılan seramik elyaf battaniyedir. Seramik elyaf battaniye, bir diğer adıyla seramik fiber 96 kg/m^3 ve 128 kg/m^3 yoğunluk olmak üzere ikiye ayrılmaktadır. 96 yoğunluklu seramik fiberin ısı transfer katsayısı 400 °C için 0,09 (w/m.k), 800 °C için 0.15 (w/m.k) olarak bilinmektedir. Gövde yalıtımı için

25mm kalınlığında 96 kg/m^3 yoğunlukta seramik fiber kullanımı tercih edilmiştir. Son malzeme tercihlerinin akabinde şasi tasarımı yapılarak ağırlığı hesaplanmıştır (Şekil 2).
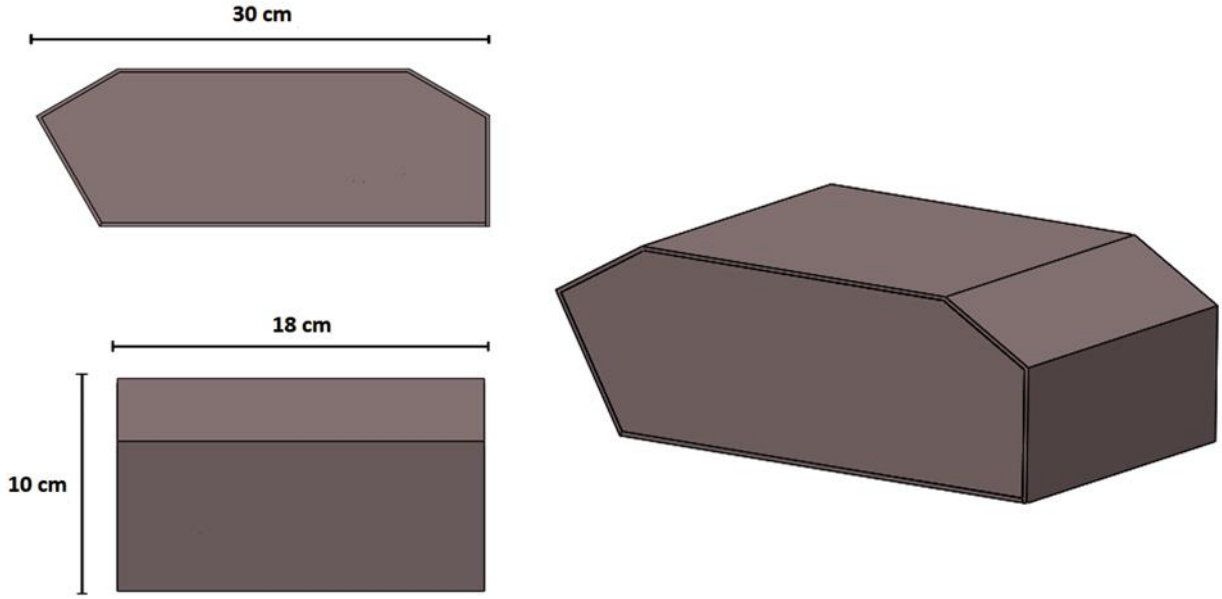
Şekil 2. Şasinin tasarımı ve ölçüleri (Design and dimensions of the chassis)

Tasarım sürecinin ilk aşaması tamamlandıktan sonra şasinin ağırlığı yaklaşık 3,6 kg olarak hesaplanmıştır. Bu ağırlığı hareket ettirmek üzere 19:1 redüksiyon oranına sahip 2 adet 12V redüktörlü DC motor seçilmiştir. Robotun hareketi için bu iki motorun farklı yön ve hızlarda birbirinden bağımsız olarak sürülebilmesi gerekmektedir. Motorların tanesi 8,5kg/cm yük taşıyabilmekte ve maksimum güçte 5,5A akım çekmektedir. Bu doğrultuda sürücü kartı olarak 5-35V gerilim altında kanal başı sürekli olarak 15A, anlık olarak 30A akım verebilen çift motor sürücü kartı seçilmiştir. Seçimlerin ardından motor ve sürücü kartının çizimleri bilgisayar ortamında gerçekleştirilerek tasarıma eklenmiştir (Şekil 3).
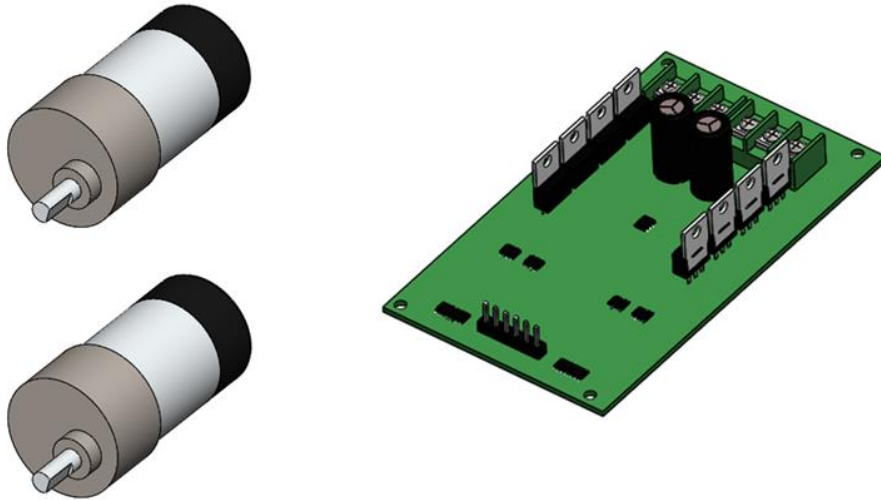
Şekil 3. DC motorlar ve sürücü kartı (DC motors and driver card)

Güç kaynağı olarak 11.1V 35C 4000mAh değerlerine sahip Lityum Polimer (Li-Po) pil tercih edilmiş, bilgisayar ortamında çizimi yapılarak tasarıma dâhil edilmiştir (Şekil 4).

Şekil 4. Lityum polimer pil (Lithium polymer battery)

Motorların her birinin maksimum güçte 5.5A çektiği göz önünde bulundurulursa, diğer elektronik bileşenlerle birlikte robot maksimum güçte ortalama 13A akım çekecektir. Bu durumda maksimum güçte pilin çalışma süresi aşağıdaki eşitlikle hesaplanmıştır.

$$\frac{4000 \; mAh}{13000 \; mA} x 0.7 = 0.215 \; saat = 13 \; dak \tag{1}$$

Eş.1'de 4000 mAh akü kapasitesi ile 13000 mA çekilen akımla pilin çalışma süresi 13 dakika olarak bulunmuştur. Bu süre; robotun, üzerine ağır bir cisim devrilmesi yahut şasenin iki cisim arasına sıkışarak motorların torkunun robotu bulunduğu pozisyondan çıkarmaya yetmemesi gibi olağandışı koşullarda maksimum güçle çalışırken pili tüketme süresidir. Normal kullanımda robotun ilerlediği zeminin eğimi, robotun dur-kalk işleminin artmasına neden olabilecek engel sayısı gibi parametrelere bağlı olarak pilin tükenme süresi değişiklik göstereceğinden net bir süre hesaplanamamaktadır. Ortalama bir fabrika koşulları baz alınırsa normal kullanımda pil ömrünün 2 - 3 saat aralığında olması beklenmektedir. Yapılan son elektronik aygıt seçimleri neticesinde bu aygıtların çizimleri de tasarıma eklenerek nihai şasi görünümü elde edilmiştir (Şekil 5). Eklenen elektronik malzemelerle birlikte yalıtım işlemi öncesi robotun muhtemel ağırlığı 4,1 kg olarak öngörülmüştür.
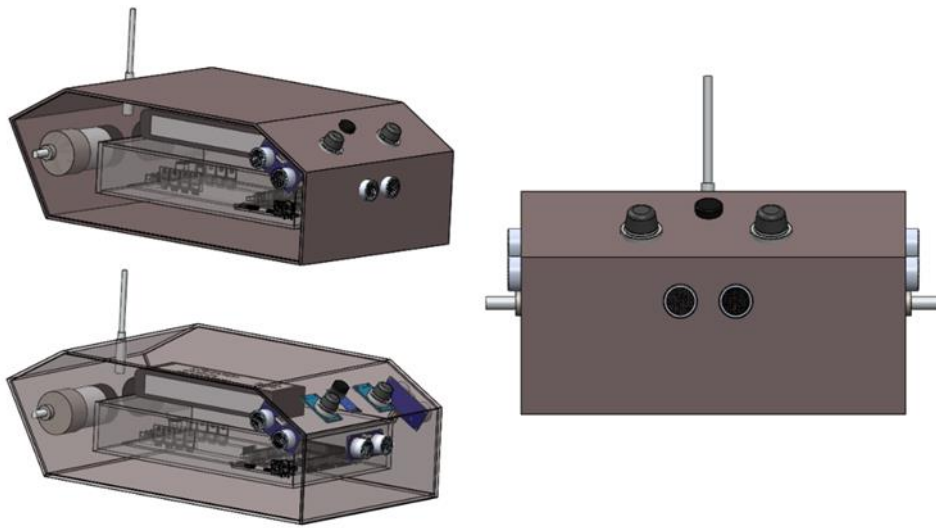
Şekil 5. Elektronik aygıtların şase üzerindeki görünümü (View of electronic devices on the chassis)

Robotun ağırlığı ve çalışma ortamı göz önünde bulundurularak hareketini palet sistemi ile sağlaması uygun görülmüştür. Böylece robotun hareket kabiliyeti fabrika zemininde bulunabilecek

yağ ve benzeri kaygan sıvılardan en az seviyede etkilenmiş olacaktır. Sıradan paletlerin büyük çoğunluğu kauçuk gibi yüksek sıcaklığa ve ateşe dayanımı düşük malzemeden imal edilmektedir. Bu çalışmada robotun paletleri metal zincir olarak tasarlanmıştır (Şekil 6).
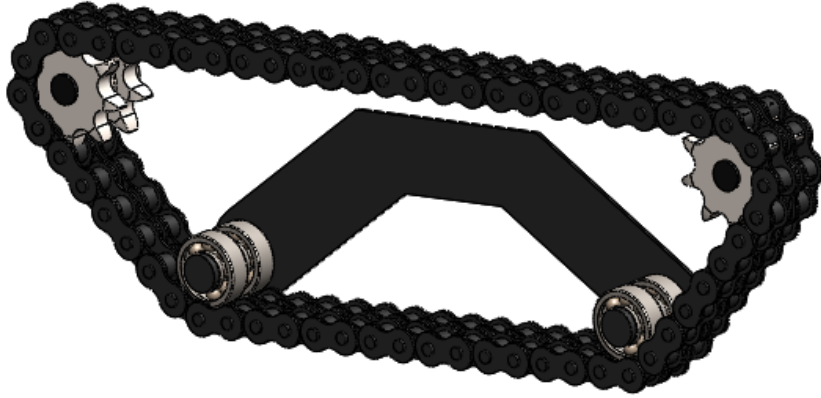
Şekil 6. Palet tasarımı (Pallet design)

Paletin metal bir zincir olarak tasarlanması hem sıcaklığa hem de yırtılma ve delinmelere karşı dayanımı artırmıştır. Tasarlanan iki ayrı paletin ağırlığı toplamda 2,2 kg olarak hesaplanmıştır. Böylece yalıtım işlemiyle birlikte robotun nihai ağırlığı 6,5 kg olarak öngörülmüştür. Bilgisayar ortamında çizimi tamamlanan paletler de eklendiğinde robotun nihai tasarımı elde edilmiştir (Şekil 7).

Şekil 7. Robotun Nihai Tasarımı (Final design of the robot)

2.2. Kritik Metan Yoğunluğu Tespit Robotu Üretimi (Manufacturing the Critical Methane Density Detection Robot)

2.2.1 Şasi Üretimi (Manufacturing the Chassis)

Bilgisayar ortamında tasarım süreci tamamlanan kritik metan yoğunluğu tespit robotunun imalat resimlerinin çıktısı alınarak bükme ve kaynak işlemleri gerçekleştirilmiştir. Kesme ve büküm işlemlerinin ardından imalat resimlerindeki ölçüler baz alınarak motor milleri için 2 adet, ultrasonik mesafe sensörleri için 6 adet ve zil için 1 adet olmak üzere toplamda 9 adet delik açılmıştır. Delme işlemlerinin akabinde şasi elektrostatik toz boya ile boyanmış ve pürüzsüz bir yüzey elde edilmiştir (Şekil 8).
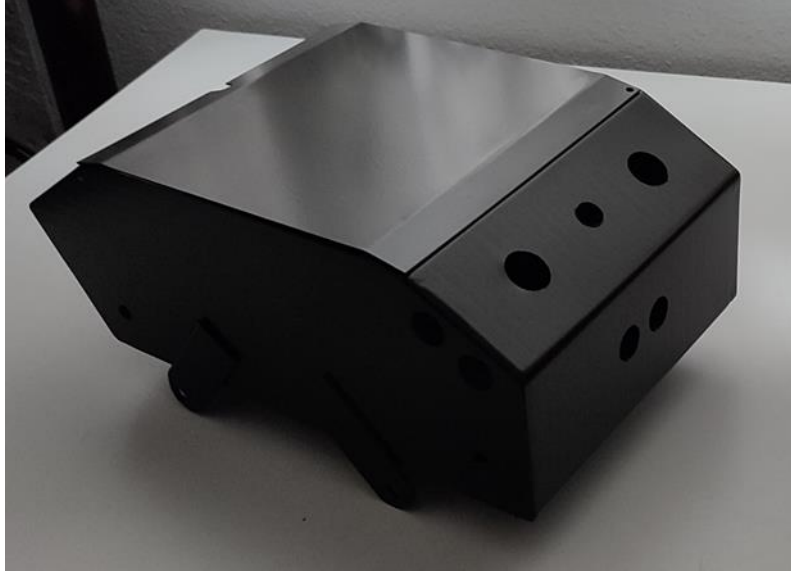
Şekil 8. Hazırlanan şasi (Prepared chassis)

Şasi boyandıktan sonra bilgisayar ortamında tasarımı tamamlanan paletler hazırlanarak şasiye monte edilmiştir (Şekil 9). Paletlerin montajı ile robot yalıtım işleminin uygulanmasına hazır hale gelmiştir.
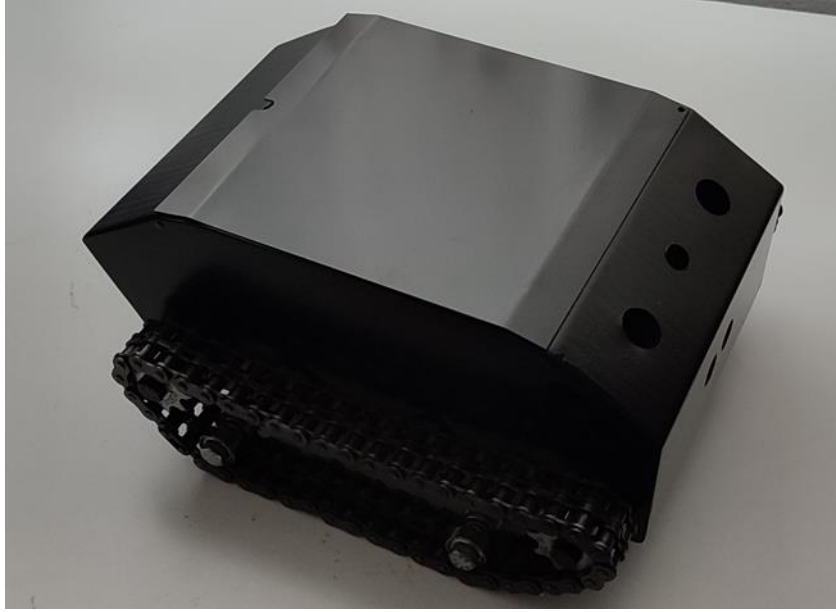
Şekil 9. Palet montajı tamamlandıktan sonra şasinin görüntüsü (Image of the chassis after the pallet assembly is completed)

2.2.2. Yalıtım İşleminin Uygulanması (Application of Insulation Process)

Şasinin üretimi tamamlandıktan sonra iç yüzeyine uygulanan seramik elyaf battaniye ile ısı yalıtım işlemi tamamlanmıştır. Şasinin iç yüzeyine tek katman olarak seramik elyaf uygulanmış, seramik elyafın çelik yüzeye yapışması için yüksek ısı dayanıklı yapıştırıcı kullanılmıştır. Uygulanan ısı yalıtım işlemi sonrası şasinin görüntüsü şekilde verilmiştir (Şekil 10).

Şekil 10. Yalıtım işleminin ardından şasinin görünümü (View of the chassis after isolation process)

2.2.3. Elektronik Malzemeler ve Bağlantıları (Electronic Materials and Connections)

Ultrasonik mesafe sensörleri, gaz sensörleri ve ısı sensörünün bağlantıları şekildeki gibi gerçekleştirilmiştir (Şekil 11).
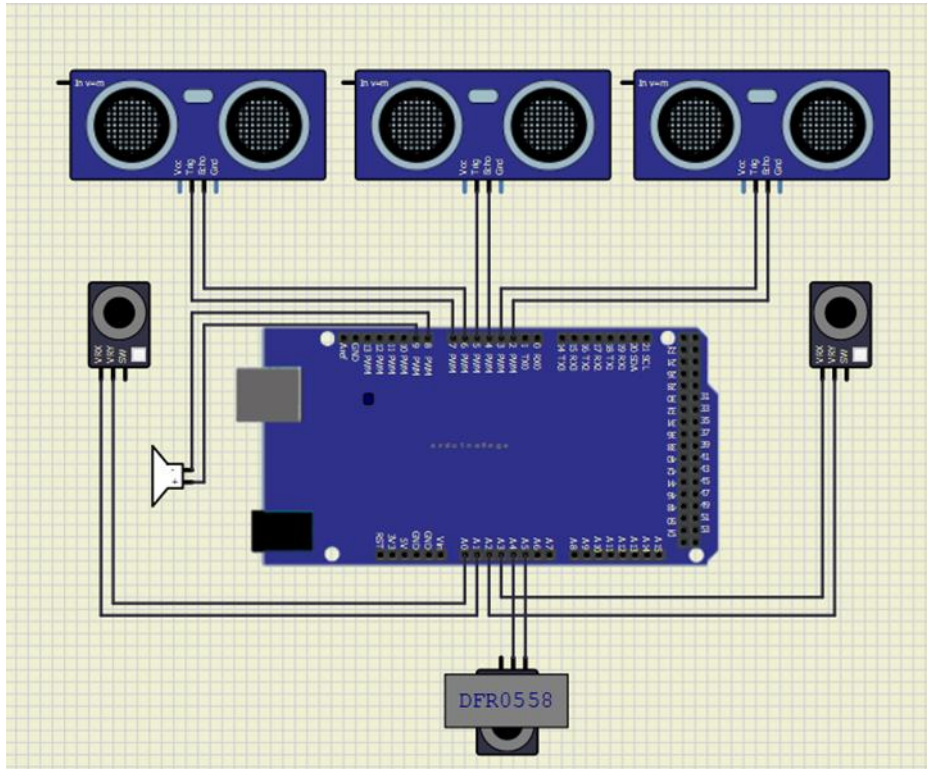
Şekil 11. Sensörler ve buzzer modülünün bağlantı şeması (Connection diagram of sensors and buzzer module)

Çift motor sürücü kartının Arduino ve motor bağlantıları şekildeki gibi gerçekleştirilmiştir (Şekil 12).
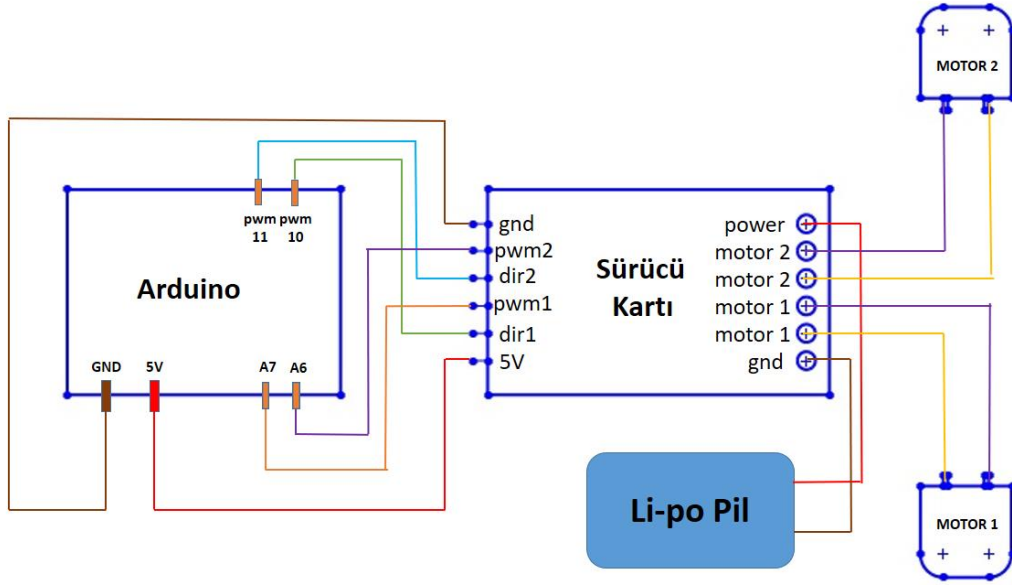
Şekil 12. Sürücü kartı ve motorların bağlantı şeması (Driver board and motors wiring diagram)

Elektronik bağlantıların tamamlanmasıyla robotun son görünümü şekildeki gibidir (Şekil 13).

Şekil 13. Robotun son görünümü (Final view of the robot)

2.2.4. Yazılımın Geliştirilmesi (Software Development)

Yazılım sürecinin ilk aşamasında robotun hareket algoritması belirlenmiştir (Şekil 14). Robotun hareketi belirlenen algoritma üzerine kurgulanarak mikrodenetleyici platformunun derleyicisinde derlenmiş ve mikrodenetleyici karta yüklenmiştir. Sağ ve sola dönüşlerde tek paletin ileri yönlü çalışması yerine paletlerden biri ileri diğeri geri hareket edecek şekilde programlanmıştır. Böylelikle robotun neredeyse olduğu yerde dönecek kadar manevra kabiliyetine sahip olması sağlanmıştır.
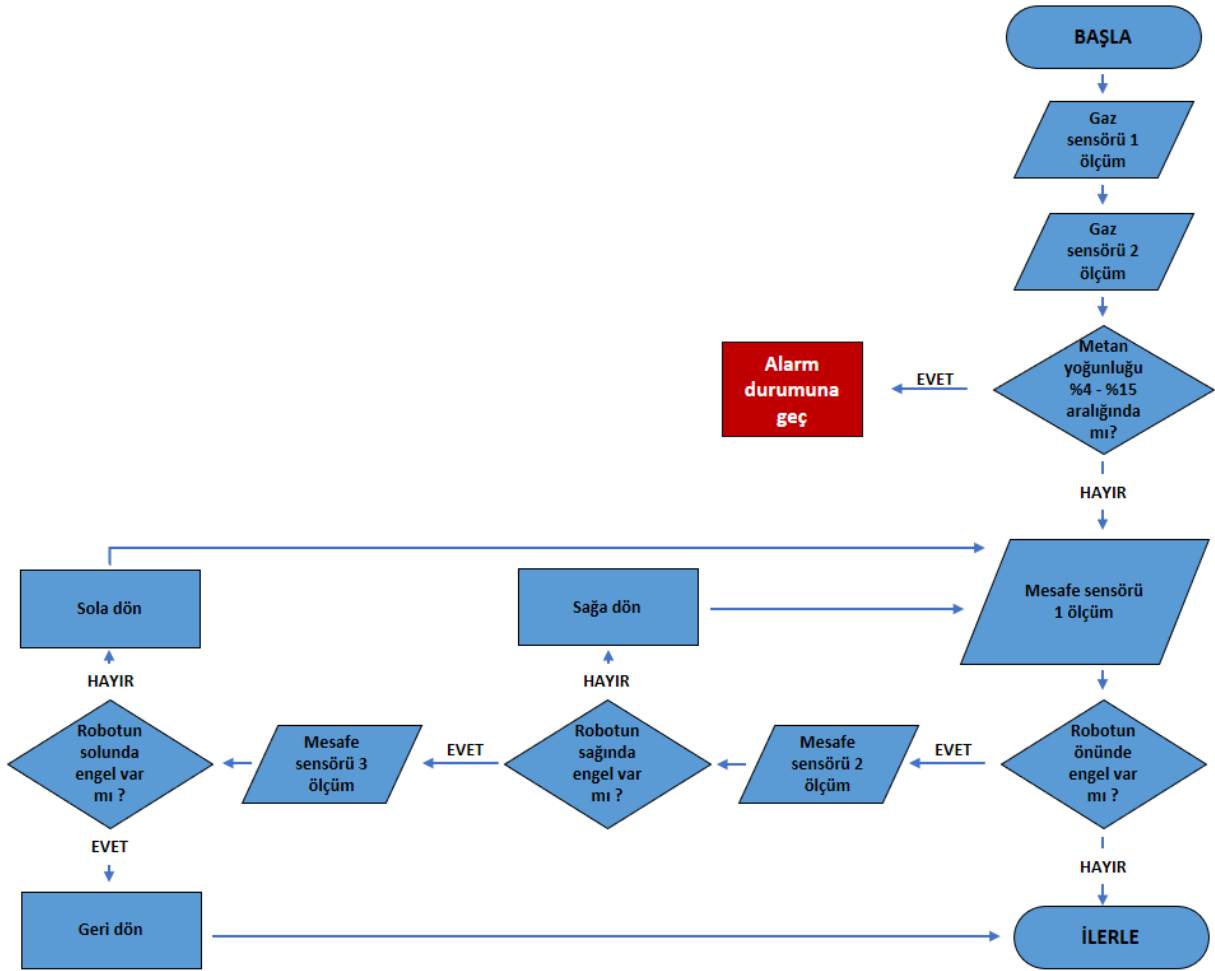
Şekil 14. Robotun hareket algoritması (Motion algorithm of the robot)

Algoritmada belirtilen iş sıralamasında metan yoğunluğunun kontrol edilmesi için robotun bir adım ilerlemesi gerekmektedir. Robotun dar ve üç yönü kapalı bölgelerde hareketi esnasında manevra süresi uzamakta; bu durum metan yoğunluğu ölçümünde gecikmeye sebep olmaktadır. Bu durumun ortaya çıkaracağı risk faktörünün önüne geçmek adına kod bloğunda düzenlemeye gidilerek algoritmadan bağımsız ek yoğunluk ölçümleri eklenmiştir. Ek ölçümler sonucu metan yoğunluğunun tehlikeli düzeyde olduğu tespit edildiği takdirde eklenen yazılım algoritmayı yarıda keserek alarm durumuna geçmektedir.

2.2.5. Sensör Doğruluk Testleri (Sensor Accuracy Tests)

Robotun en temel iki fonksiyonu olan serbest dolaşım ve metan gazı tespitini başarılı bir şekilde gerçekleştirebilmesi için mesafe ve gaz sensörlerinin tutarlı ve doğru ölçümler yapmaları önem arz etmektedir. Engelin yerini ve kendisi ile arasındaki mesafeyi ölçerek bir sonraki ilerleme yönüne karar verebilmesi için robot şasisine biri önde ikisi yanlarda olmak üzere 3 adet ultrasonik mesafe sensörü yerleştirilmiştir. Ultrasonik mesafe sensörü ile mesafe ölçümü yapılırken ses dalgalarından yararlanılmaktadır. Sensör, ses dalgası üreten "trig" bölümü ve kendisine çarpan ses dalgasını algılayan "echo" bölümü olmak üzere iki bölümden oluşmaktadır. Ölçümün yapılması için trig bölümünden bir ses dalgası gönderilerek, ses dalgasının engele çarpıp trig bölümüne dönmesi beklenmiş ve iki işlem arasındaki süre mikro saniye olarak ölçülmüştür. Bu süre zarfında ses dalgası engele kadar gidip geri geldiğinden; ölçülen süre ikiye bölünerek sesin sensörden engele ulaşma süresi hesaplanmıştır. Bu süre, sesin 1 mikro saniyede milimetre cinsinden aldığı yol olan 0.343 değeri ile çarpılarak engel ile sensör arasındaki uzaklık milimetre olarak hesaplanmıştır (Eşitlik 2).

$$Mesafe = \frac{\text{Ölçülen süre}}{2} \times 0.343 \tag{2}$$

Ultrasonik mesafe sensörünün doğruluğunu test etmek adına her sensörün önüne bir engel konulmuş, bu engellerin uzaklıkları dijital kumpas ile 100 mm olarak ayarlanmıştır. Eş.2 kullanılarak sensörler aracılığı ile yapılan mesafe ölçümü sonuçları aşağıdaki tabloda gösterilmiştir (Tablo 1).

Tablo 1. *Sensör doğruluğu test sonuçları (Sensor accuracy test results)*

	Deneme 1 *(mm)*	Deneme 2 *(mm)*	Deneme 3 *(mm)*	Deneme 4 *(mm)*	Deneme 5 *(mm)*
Sensör 1	100	100	101	101	101
Sensör 2	103	102	102	102	102
Sensör 3	103	102	102	102	102

Gaz tespitinde kullanılan sensörlerin doğruluk testleri metanla ilişkisi bulunmayan sıradan bir kapalı ortamda başlatılmıştır. Gaz sensörlerinin ısındıktan sonra daha isabetli ölçümler vermesi sebebiyle teste başlamadan önce 10 saniye sensörlerin ısınması beklenmiş ve sonrasında teste başlanmıştır. Testin ilk aşamasında sıradan kapalı ortam havasında 5 saniye içinde 10 adet ölçüm yapılmıştır (Tablo 2).

Tablo 2. *Standart ortam koşullarındaki metan gazı yoğunluk ölçüm değerleri (Measurement values of methane gas density in standart ambient conditions)*

	Sensör 1 (ppm)	Sensör 2 (ppm)
Ölçüm 1	292.00	289.00
Ölçüm 2	287.00	286.00
Ölçüm 3	287.00	288.00
Ölçüm 4	286.00	287.00
Ölçüm 5	287.00	287.00
Ölçüm 6	288.00	289.00
Ölçüm 7	292.00	292.00
Ölçüm 8	290.00	292.00
Ölçüm 9	289.00	292.00
Ölçüm 10	288.00	288.00

İkinci aşamada her iki sensöre eşit uzaklıktaki kaynaktan içinde yaklaşık %90 metan gazı bulunan doğal gaz karışımı 2 bar basınç ile püskürtülürken aynı işlem uygulanarak 5 saniye içinde 10 adet ölçüm yapılmıştır (Tablo 3).

Tablo 3. *Metan püskürtülmesi sırasındaki metan gazı yoğunluk ölçüm değerleri (Measurement values of methane gas density during methane gas flowing through sensors)*

	Sensör 1 (ppm)	Sensör 2 (ppm)
Ölçüm 1	731.00	729.00
Ölçüm 2	711.00	715.00
Ölçüm 3	719.00	713.00
Ölçüm 4	720.00	719.00
Ölçüm 5	727.00	728.00

Ölçüm 6	728.00	728.00
Ölçüm 7	727.00	726.00
Ölçüm 8	733.00	721.00
Ölçüm 9	731.00	730.00
Ölçüm 10	732.00	735.00

3. SONUÇLAR (CONCLUSIONS)

Bu çalışmada bulunduğu ortamda serbest dolaşım yaparak ortamdaki metan yoğunluğunu ölçen mobil bir güvenlik robotu tasarlanarak üretimi gerçekleştirilmiştir. Şasi içerisindeki elektronik aygıtların olası yangın durumunda belirli düzeye kadar sıcaklıktan korunabilmesi için yalıtım işlemi uygulanmıştır. İzolasyonda kullanılan seramik elyafın çok düşük ısı geçirgenliği olması nedeni ile dışarıdaki ısıyı içeri almamasının yanı sıra robotun içindeki elektronik aygıtların ısısını da içeri hapsettiği gözlemlenmiştir. Bu çalışmada kullanılan motorlar taşıdıkları şasiye göre fazlasıyla yeterli tork gücüne sahip olduklarından normal kullanımda düşük miktarda akım çekmekte, sürücü kartı ve pilde ısınmaya neden olmamaktadır. Isınma potansiyeli daha yüksek bileşenlerin kullanıldığı ve robotun kullanım süresinin daha uzun olduğu çalışmalarda yalıtım işlemi yapılırken robot içerisindeki havanın da ısısını kaybetmeyeceği göz önünde bulundurulmalıdır.

Robotun pilinin tamamen tükenme süresi kullanım koşullarına bağlı olarak değişiklik gösterse de genel olarak 2 saatin üzerinde olduğu gözlemlenmiştir. Fakat Li-po pilin tamamen deşarj olması pil ömrünü ciddi düzeyde kısaltmaktadır. Bu nedenle tamamen tükenmeden yeniden şarj edilmelidir. Kullanım sonunda pilde aşırı ısınmaya rastlanmamıştır.

Mesafe sensörlerinin doğruluk testleri gerçekleştirilirken her sensörün 100 mm uzağına bir engel konularak 5 adet ölçüm gerçekleştirilmiştir. Toplamda 15 ölçüm sonucunda 100 mm – 103 mm aralığındaki değerlere rastlanmıştır. 3 mm yanılma payı kabul edilebilir olarak değerlendirilmiştir. Bunun yanında sensörler ve engeller sabit olmasına rağmen aynı sensörden farklı ölçüm sonuçları alınmıştır. Birinci sensör 2 kez 100 mm, 3 kez 101 mm değerlerini göstermiştir. İkinci ve üçüncü sensörler 1 kez 103 mm, 4 kez 102 mm değerlerini göstermişlerdir. Bu durum sonucunda ortam koşullarının ses dalgalarını etkileyerek ölçüm sonuçlarında az da olsa hatalara sebebiyet verdiğine kanaat getirilmiştir. İlerleyen çalışmalarda üretilen ses dalgalarının gürültülü, tozlu ve yüksek sıcaklıktaki ortamlardaki bozulma oranları ve bu ortamlardaki ölçüm hassasiyetlerinin incelenmesi gerektiği düşünülmektedir.

Gaz sensörlerinin testleri iki aşamada gerçekleştirilmiştir. İlk aşamada standart oda koşullarında yapılan 10 adet ölçümde 286 ile 292 ppm arası değerlere rastlanmıştır. Sensör 300 ppm'in altında ölçüm yapamadığı için 300 ppm'in altındaki bu değerler neticesinde ortamda metan gazı bulunmadığı varsayılmıştır. İkinci aşamada %90 metan içeren doğal gazın 2 barlık basınçla sensörlere püskürtülmesi esnasında 10 adet ölçüm daha yapılmış ve 711 ile 730 ppm arası değerler ile karşılaşılmıştır. Metan gazının patlama aralığına ulaşabilmesi için havada en az %4 yoğunluk oranına, yani 40.000 ppm değerine ulaşması gerekmektedir. Test aşamasında ise sabit hızla sensörlere doğru püskürtülmesine rağmen ölçülen metan değeri 300 ppm dolaylarından 730 ppm dolaylarına yükselebilmiştir. Bu durum metanın hafif olması sebebiyle ortamda hızla dağıldığını kanıtlamaktadır. Ölçülen bu değerler neticesinde metanın ortamda birikmeye başladığı kanısına varılabilmesi için ortam zemininde ulaşması gereken değer 9000 ppm olarak belirlenmiştir.

Robot serbest dolaşımı esnasında ölçtüğü metan değeri 9000 ppm düzeyine ulaştığında bulunduğu yerde sabit kalarak sesli uyarı vermektedir. Böylelikle metan yoğunluğu %0,9'dan %4'e yükselene kadar uyarıyı fark ederek tahliye işlemlerinin gerçekleşmesi içim zaman kazanılmıştır. Fakat uyarının fark edilerek gerekli adımların atılması insan faktörüne bağlıdır. İnsan faktörünü ortadan kaldırarak hata payını en azına indirebilmek adına ileride robotun kablosuz ağ yapılanması bulunan tesislerde kullanılması durumunda bu ağ üzerinden veri aktarımı yapabilmesi için bir kablosuz ağ modülü robota eklenmiştir. Bağlanılmak istenen ağ adı,

ağ şifresi ve verinin gönderileceği adres yazılıma dahil edilmelidir. Kullanılan kablosuz ağ modülünün güvenlik açıklarına sebep olabileceği göz önünde bulundurularak belirlenen şifre ve adresler hiçbir koşulda üçüncü kişiler ile paylaşılmamalı, herhangi bir platformda yayınlanmamalıdır.

Metan gazı kaynaklı patlamalar dünya genelinde ciddi hasar ve kayıplara yol açmaktadır. Robotlar ve yapay zekanın kullanımı ile metan gazı kaynaklı patlamaların büyük çoğunluğunu önlemek mümkündür. Fakat robotların bu alanda etkili kullanımı için bu alanda çok daha fazla çalışmaya ihtiyaç vardır.

TEŞEKKÜR (ACKNOWLEDGMENT)

KAYNAKLAR (REFERENCES)

1. H.P. Moravec, Robot Technology, Encylopedia Britannica, 1998.
2. I. Asimov, Ben Robot, Ithaki Yayınları, İstanbul, 2016.
3. G. Gürgüze, İ. Türköğlu, Kullanım alanlarına göre robot sistemlerinin sınıflandırılması, Fırat Üniversitesi Mühendislik Bilimleri Dergisi, 31(1), 53-66, 2019.
4. A. Dobra, General classification of robots. Size criteria, 23rd International Conference on Robotics in Alpe-Adria-Danube Region, 3-5 September, 2014, Slovakia.
5. M. Durşen, B. Yasun, Yeraltında Bulunan Zararlı Gazlar ve Metan Drenajı, İSGÜM, Ankara, 2012.
6. O. Solak, Türkiye'deki katı atık deponi alanlarında oluşan gazın çevresel ve ekonomik açıdan incelenmesi, Yüksek Lisans Tezi, Hacettepe Üniversitesi Fen Bilimleri Enstitüsü, Ankara, 2015.
7. K. Lambert, Tercüme:Y.D. Gürer, Yanıcılık Sınırları, http://www.cfbt-be.com/images/artikelen/artikel_34_TR.pdf, 2016.
8. Ö. Ö. Pektaş, Mobil bomba imha robotlarının incelenmesi ve prototip robot tasarımı, Yüksek Lisans Tezi, İstanbul Üniversitesi Fen Bilimleri Enstitüsü, İstanbul, 2010.
9. C.M. Raju, N.S. Rani, An android based automatic gas detection and indication Robot, International Journal of Computer Engineering and Applications, 3(1): 55-59, 2014.
10. Ö. Kanlı, Development of gas detection Robot, Master Thesis, Adnan Menderes University Graduate School of Natural and Applied Sciences, Aydın, 2016.
11. J. Hau-Shiue, L. Kai-Yew, Design and control of a two-wheel self-balancing robot using the arduino microcontroller board, 10th IEEE International Conference on Control and Automation (ICCA), 12-14 June 2013, Hangzhou.
12. T. Baykal, Lityum polimer bataryalar için batarya yönetim sistemi geliştirilmesi, Yüksek Lisans Tezi, İstanbul Üniversitesi Fen Bilimleri Enstitüsü, İstanbul, 2013.
13. G. Yalın, Pem yakıt hücresi-lityum polimer batarya hibrit sistemiyle tahrikli mini-İHA üretimi ve enerji yönetim sisteminin modellenmesi, Doktora Tezi, Eskişehir Teknik Üniversitesi Lisansüstü Eğitim Enstitüsü, Eskişehir, 2019.

Investigation of Workpiece and Tool Surface Quality in Electro Discharge Machining of Al 5083 Alloy Produced by Powder Metallurgy

Ahmet Tolunay IŞIK[1] [iD], Ramazan ÇAKIROĞLU[2*] [iD]

[1]*Karabük Üniversitesi, Lisansüstü Eğitim Enstitüsü, Karabük, Türkiye*
[2]*Gazi Üniversitesi, Teknik Bilimler MYO, Ankara, Türkiye*

ABSTRACT

Aluminum alloys are widely preferred in various fields such as aerospace, ship and automotive due to their lightness and relevant production cost. In this study, electro discharge technique was used in the processing of aluminum 5083 alloy (Al5083) produced by powder metallurgy method. The surface quality resulting from the experiments was investigated in terms of Ra, Rz and Rsm. Experimental studies were carried out according to Taguchi L9 orthogonal experimental design, using three different levels of discharge current, pulse on time and pulse off time parameters. As the discharge current increased, Ra and Rz increased, Rsm first decreased and then increased. As the pulse on time increased, Ra and Rz first increased and then decreased, and Rsm increased. When the pulse off time increased, Ra and Rz decreased and Rsm increased. As a result of the analysis of variance (ANOVA) performed to determine the effect rates of the variable parameters on the surface quality, the order of importance of the parameters was found to be discharge current, pulse off time and pulse on time. The effect of discharge current, which is the most effective parameter according to ANOVA, on Ra, Rz and Rsm was calculated as respectively 70.87%, 70.41% and 36.34%. Microscopic images taken from the tool (copper) and workpiece surface show that the craters and peaks formed by the spark effect are formed on both material surfaces.

Toz Metalürjisi ile Üretilmiş Al 5083 Alaşımının Elektro Erozyon ile İşlenmesinde İş Parçası ve Takım Yüzey Yapısının İncelenmesi

ÖZET

Alüminyum alaşımları hafifliği ve uygun üretim maliyetiyle havacılık, gemi ve otomotiv gibi çeşitli alanlarda yaygın olarak tercih edilmektedir. Bu çalışmada toz metalurji yöntemi ile üretilen alüminyum 5083 alaşımının (Al5083) işlenmesinde elektro erozyon tekniği kullanılmıştır. Yapılan deneyler sonucu oluşan yüzey kalitesi Ra, Rz ve Rsm cinsinden incelenmiştir. Deneysel çalışmalar, üç farklı seviyede boşalım akımı, vurum süresi ve vurum aralığı parametreleri kullanılarak Taguchi L9 ortogonal deney tasarımına göre yapılmıştır. Boşalım akımı arttıkça Ra ve Rz artmış, Rsm önce azalmış sonra artmıştır. Vurum süresi arttıkça Ra ve Rz önce artmış sonra azalmış, Rsm ise artmıştır. Vurum aralığı arttığında ise Ra ve Rz azalırken, Rsm değerleri artmıştır. İşleme parametrelerinin yüzey kalitesi üzerindeki etki oranlarının belirlenmesi amacı ile yapılan varyans analizi (ANOVA) sonucu parametrelerin önem sırası boşalım akımı, vurum aralığı ve vurum süresi şeklinde bulunmuştur. ANOVA'ya göre en etkili parametre olan boşalım akımının Ra, Rz ve Rsm'ye etkisi sırasıyla %70.87, %70.41 ve %36.34 olarak hesaplanmıştır. Takım (bakır) ve iş parçası yüzeyinden alınan mikroskopik görüntüler kıvılcım etkisi ile oluşan krater ve tepelerin her iki malzeme yüzeyinde de oluştuğunu göstermektedir.

1. INTRODUCTION (GİRİŞ)

Aluminium alloys are a common type of material used in various fields with high corrosion resistance, high fatigue strength, high thermal and electrical conductivity [1,2]. Aluminium alloys, which can be produced at low cost using the powder metallurgy method, are frequently preferred in

many industries instead of traditional metal materials due to their lightness [3]. However, due to the high ductility and thermal conductivity of the aluminium alloy, burrs occur on the machined surface by conventional methods and wear due to cutting tool adhesion during machining [4]. Electro discharge machining (EDM) technology which is one of the advanced manufacturing methods, is widely used to produce complex shapes without the need for a second finishing process between the conductors, regardless of the hardness of the material [5,6]. Using this technique, aluminium alloy can be easily machined without tool wear when the variable parameters are adjusted appropriately. The tool used in EDM is low cost as it can be selected from easily formable conductive materials [7,8].

EDM technique realise the machining process with the effect of high discharge current and short-term electric sparks in a controlled time interval between two electrically conductive metals. During the machining process, the workpiece and tool material melts or evaporates a little with the effect of the high temperature occurring in the machining area. The insulating liquid used as a dielectric is used both for cooling and to remove the molten materials called debris formed during processing in the processing area [9].

The selection and use of process parameters in EDM technique with a complex processing mechanism is mostly determined by experience [10]. Thus, the manufacturing process will be carried out efficiently and quickly when the processing parameters are optimized. In research into this area, discharge current (Ip), pulse on time (Ton), pulse off time (Toff), reference voltage and dielectric pressure are indicated as the most effective variable parameters on important performance results such as material removal rate (MRR), tool wear rate (TWR) and average surface roughness (Ra) [11,12]. The white layer, craters and peaks that appear on the machined surface after EDM are surface damages during thermal machining [13,14]. Studies on the evaluation of performance results in the machining of aluminium alloys by electro discharge (EDM) can be listed as follows.

Kalyon, investigated the effects of discharge current (6-25 A), pulse on time (50-200 μs) and pulse off time (50-200 μs) parameters on the material removal rate, tool wear rate and average surface roughness results in electro discharge machining of aluminium 6082 alloy. In the Taguchi optimization for the best average roughness value, the author stated that optimum conditions were created at the lowest parameter values (6A,50μs,200μs), so that the washing effect of the dielectric was sufficient and the machining speed could be decrease by shortening the pulse interval [15]. Safiei et al. examined the effects of discharge current (12, 36 A), pulse on time (20, 180 μs), pulse off time (10, 80 μs), reference voltage (40, 60 V) and jump speed (5, 20 mm/sn) parameters on Ra and MRR in machining aluminium 5083 alloy with EDM. The authors stated that with the increase of the pulse on time, which is the most effective parameter, cause a worse surface roughness with the irregular spark rate will increase [16]. Ali et al. investigated the effects of copper, copper-tungsten, graphite and brass tools on the MRR, TWR and Ra in the parameters range of discharge current (2-30 A), pulse on time (100-400 μs), pulse off time (1-9 μs) and reference voltage (21-30 V) during EDM of aluminium LM6 alloy. The authors mentioned that the thermal conductivity and melting point of the tool material affect the performance results [17]. Kakkar et al. examined discharge current (7,9,11 A), reference voltage (30,40,50 V) and pulse on time (50,100,150 μs) variable parameters on the MRR, TWR and Ra in machining Al-SiC metal matrix composite with EDM. The authors reported that MRR increased, TWR and Ra adversely affected with increasing discharge current, pulse on time and reference voltage [18]. Sadagopan and Mouliprasanth investigated the effects of biodiesel, transformer oil and kerosene dielectrics on the TWR and Ra results in the parameters range of discharge current, pulse on time, pulse off time during EDM of aluminium 6063 alloy. The authors reported that dielectrics with low viscosity (4-6 cst) and high flash point (100-170 °C) had better shown MRR, TWR, and Ra [19]. In addition, Guu and Hou studied the effects of discharge current (0.5, 1, 1.5 A) and pulse on time (3.2, 4.8, 6.4 μs) parameters on the machined surface quality (Ra≈0.3-0.075 μm) in machining Fe-Mn-Al alloy with EDM. The negative effects of the discharge energy increases with discharge current and pulse on time, on the surface quality, such as the formation of deep craters, large micro-hole and damage area [20]. Çakıroğlu and Günay used for fatigue prediction of Rz, Rsm and Vickers hardness results

which are affected by discharge current (3-12 A), pulse on time (3-8 µs) and pulse off time (5-7 µs) parameters in the turning of AISI L2 cold work tool steel with EDM. The authors reported that Rz and Rsm increased with discharge current and pulse on time, while Rz decreased at the highest value of pulse on time. Also, the authors in these study suggested obtaining low Rz and high Rsm results in order to improve the fatigue life in their study [21].

In the literature, it has been observed that studies mostly focused on the evaluation of the average surface roughness (Ra) in the machining of aluminium alloys with the EDM method. However, it is important to examine other roughness criteria as the Ra value is not fully sufficient to control the functionality of parts manufactured by machining. In this study, electro discharge machining experiments were carried out on Al5083 alloy produced by powder metallurgy method at different variable parameters. The quality of the machined surfaces was evaluated in terms of roughness criteria average surface roughness (Ra) which gives a general description of height changes, average surface roughness depth (Rz) which gives information about rarely high peaks and deep valleys that cannot be detected in the Ra parameter and average peak width (Rsm) which gives general information about the width of the hills and valleys that cannot be detected in height parameters such as Ra and Rz.

2. MATERIAL AND METHOD (MATERYAL VE YÖNTEM)

2.1. Experimental Setup (Deney Düzeneği)

The main purpose of this study is to determine the effects of variable parameters on surface roughness values (Ra, Rz and Rsm) in the processing of pure Al5083 alloy produced by powder metallurgy method with EDM. In the experimental study, Furkan brand "K1 Z-NC EDM" die-sinking type electro erosion bench located in Gazi University Technical Sciences Vocational School campus was used. The electro erosion bench and the images taken during the experiment and the test equipment are given in Figure 1.
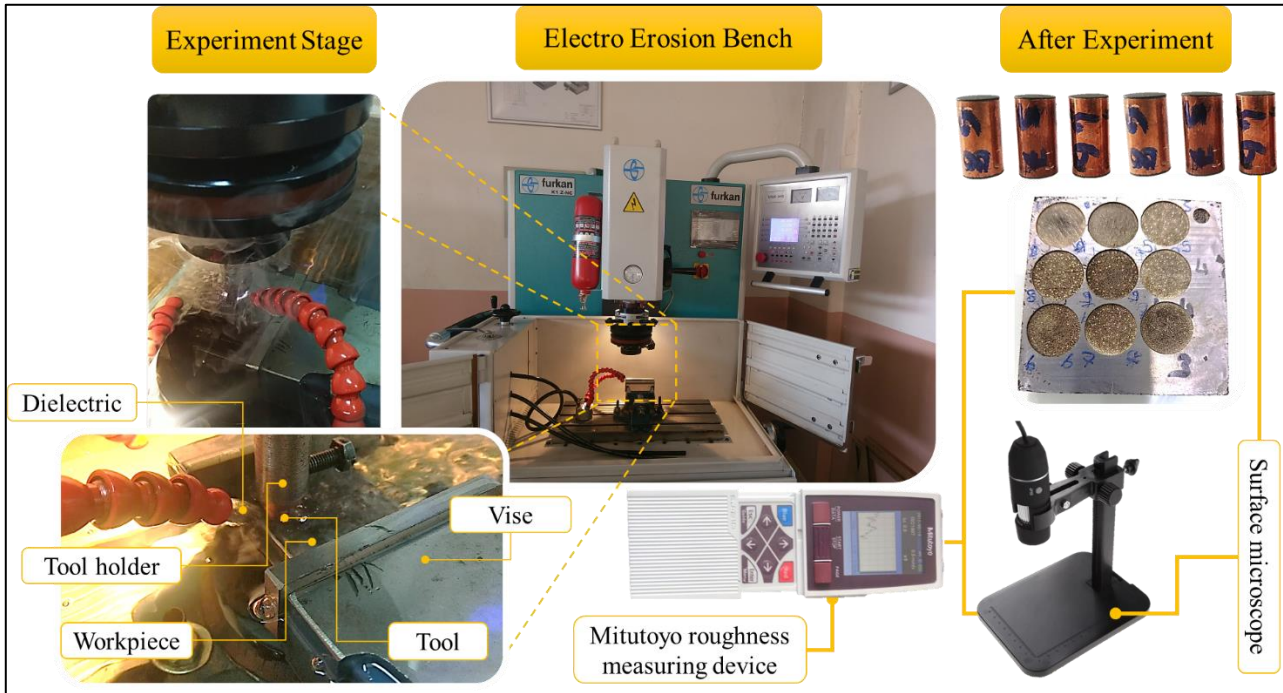
Figure 1. Die-sinking type Z-NC EDM and experimental equipment (Dalma tipi Z-NC elektro erozyon tezgahı ve deneysel ekipmanlar)

2.2. Workpiece, Tool and Dielectric Properties (İşparçası, Takım ve Dielektrik Özellikleri)

Aluminum alloy Al5083 with 10 mm thickness and 60x60 mm dimensions was used as the workpiece material. Al5083 material was produced using powder metallurgy method. In the production method, ground aluminium alloy powders with an average diameter of 45 µm were compressed in a 30x30 mm hot work tool steel powder metal mold at 700 MPa pressure at 500 °C.

The chemical composition of the workpiece material Al5083 is given in Table 1 and its technical characteristics are given in Table 2. Al5083 alloy has properties suitable for use in the aerospace and automotive industries.

Table 1. Chemical composition of Al 5083 alloy (Al5083 alaşımının kimyasal kompozisyonu)

Elements	Si	Fe	Cu	Mn	Mg	Zn	Ti	Cr	Other	Al
wt. [%]	0.4	0.4	0.1	0.4-1.0	4.0-4.9	0.25	0.15	0.05-0.25	max. 0.15	92.4-95.6

Table 2. Technical characteristics of Al 5083 alloy (Al5083 alaşımının teknik özellikleri)

Properties	Value (Max.-Min.)
Yield Strength (MPa)	125-145
Tensile Strength (MPa)	275-350
Elongation (%)	22
Hardness (Vickers)	87
Density (g/cm^3)	2.66
Electrical Resistance (Ω.cm)	0.00000598
Melting Temperature (°C)	590.6-638
Thermal Conductivity (W/mK)	117
Specific Heat (J/g°C)	0.900

Electrolytic copper material with a diameter of 15 mm and a length of 30 mm was used as the tool (electrode) material. The tool electrode was cut with the help of a wire saw, and the burrs formed after the process were cleaned by sanding. The advantage of copper material in EDM is stated as high electrical conductivity and carbon sequestration ability. During EDM, carbon-based dielectric ionizes and carbon atoms deposition on the tool (anode) material and form a protective layer against wear. The technical characteristics of the tool material are given in Table 3.

Table 3. Technical characteristics of electrolytic copper material (Elektrolitik bakır malzemenin teknik özellikleri)

Properties	Value (Max.-Min.)
Hardness (Vickers)	90
Density (g/cm^3)	8.89
Electrical Resistance (Ω.cm)	0.00000172
Melting Temperature (°C)	1083
Thermal Conductivity (W/mK)	391.05
Specific Heat (J/g°C)	3.894

Colorless, odorless, high flash point (102 °C), high corrosion resistance, high chip carrying ability and low viscosity (1,910 mm^2/s) standard EDM fluid was used as a dielectric which is used for cleaning the debris from the machining area and as a coolant. During the experiment, the dielectric was sent to the processing zone continuously in the form of lateral washing with a pressure of 30 kPa.

2.3. Experiment Design and Selection of Parameters (Deney Tasarımı ve Parametrelerin Seçimi)

Determination of variable parameters for determining performance results is an important step in experimental design. When the literature is examined, it is seen that there are many variables that affect the performance of the EDM. Discharge current, pulse on time and pulse off time which are used as the most common and most effective were used as variable parameters in the experiments. As a result of the preliminary experiments carried out to minimize tool wear, the pulse on time parameters at the highest discharge current were determined. The experimental design was created according to the Taguchi L9 orthogonal array, and at three different levels of three different variable parameters. Variable and fixed parameters are given in Table 4.

Table 4. Variable and fixed machining conditions (Değişken ve sabit işleme koşulları)

Parameters	Levels			Unit
	1	2	3	
Variable Parameters				
Discharge current (Ip)	6	9	15	A
Pulse on time (Ton)	75	150	300	μs
Pulse off time (Toff)	50	100	150	μs
Fixed Parameters				
Dielectric pressure	30			kPa
Open circuit voltage	130			V
Reference voltage (gap)	60			V
Discharge time	1			sec
Back off	1,2			mm
Machining depth	1			mm
Power supply (DC)	250-233			V

2.4. Determination of Performance Results and Statistical Analysis of Results (Performans Sonuçlarının Belirlenmesi ve İstatistiksel Analizi)

After the manufacturing stage in the industry, the surface quality and roughness of the final product is an important criterion in terms of quality control. In this study,

- Average surface roughness (Ra), the arithmetic mean of the absolute value of deviations from the mean line ($Z(x)$) along the sample length (lr) (Equation 1).

$$Ra = \frac{1}{lr} \int_0^{lr} |Z(x)| \, dx \tag{1}$$

- Average surface roughness depth (Rz), the sum of the highest peak and the deepest valley in a sample length is defined as Rz_i. Rz is obtained by averaging the Rz_i values calculated along the evaluation length (Equation 2).

$$Rz = \frac{1}{n} \sum_{i=1}^{n} Rz_i \tag{2}$$

- Average peak width (Rsm), average of Xs values calculated over the evaluation length. Xs, the width of the highest and deepest points that intersect the mean line on the x-axis defined within the sample length (Equation 3) [22].

$$Rsm = \frac{1}{n} \sum_{i=1}^{n} Xs_i \tag{3}$$

were determined as performance results in terms of contribution to the literature and industry. Mitutoyo brand Surftest SJ-210 model roughness device was used to measure the surface roughness values. Measurements were taken from three different places of each test sample and the average was calculated. The surface roughness device was used at λc:0.8 nm and λs:2.5 μm measurement conditions. In addition, images were taken with a digital camera to evaluate the surface topography of the powder metallurgy samples and the tool (electrode) after processing.

Statistical analysis was carried out by analysing the mean values of the variable parameters and the effect plots of the signal to noise ratios. In the Taguchi method, a method of approach is used to calculate the deviation between the experimental results and the optimum value. In order to minimize the Ra and Rz results from the surface roughness results, the "small is better" approach (Equation 4) was used in the Taguchi methodology. In order to maximize the Rsm result, due to its effect on fatigue the "large is better" approach was used in the Taguchi methodology (Equation 5), thus the signal-to-noise (S/N) ratios of the result data were determined. ANOVA (analysis of variance) was used to calculate the contribution rates and percentages of variable parameters to the performance results [23].

Small is better:

Signal to noise ratio, $\eta = -10 \log \left(\frac{1}{n} \sum_{i=1}^{n} y_i^2 \right)$ (4)

Large is better:

Signal to noise ratio, $\eta = -10\log\left(\frac{1}{n}\sum_{i=1}^{n}1/y_i^2\right)$ (5)

3. EXPERIMENT RESULTS AND DISCUSSION (DENEY SONUÇLARI VE TARTIŞMA)

In this study, the effect of variable parameters on the surface roughness of aluminium 5083 alloy by EDM was investigated. The roughness results and signal/noise ratios obtained as a result of the experiments are given in Table 5.

Table 5. Experiment results and S/N ratios (Deney sonuçları ve S/G oranları)

Exp. No	Ip [A]	Ton [µm]	Toff [µs]	Ra [µm]	S/N ratio (Ra)	Rz [µm]	S/N ratio (Rz)	Rsm [µm]	S/N ratio (Rsm)
1.	6	75	50	10.980	-20.8120	63.575	-36.0657	488.575	53.7786
2.	6	150	100	9.309	-19.3781	60.683	-35.6613	367.967	51.3162
3.	6	300	150	6.546	-16.3195	44.252	-32.9186	411.833	52.2944
4.	9	75	100	11.421	-21.1541	65.190	-36.2837	328.167	50.3219
5.	9	150	150	11.870	-21.4890	67.397	-36.5728	323.000	50.1841
6.	9	300	50	13.717	-22.7452	82.485	-38.3274	396.450	51.9638
7.	15	75	150	12.619	-22.0205	76.038	-37.6206	350.600	50.8962
8.	15	150	50	18.205	-25.2038	108.708	-40.7252	462.725	53.3065
9.	15	300	100	17.128	-24.6741	101.266	-40.1092	544.700	54.7231

The effects of variable parameters on Ra, Rz and Rsm can be seen in the graphs created in Minitab 19 program using Equation 4 and Equation 5 (Figure 2-4). The highest value of the calculated signal/noise ratio shows the most effective experiment or the most effective variable parameter values for surface roughness. When the main effect graphs are examined, according to the "small is better" approach, the best Ra 6 A Ip, 300 µs Ton and 150 µs Toff processing condition, the best Rz 6 A Ip, 75 µs Ton and 150 µs Toff processing condition; According to the "large is better" approach, the best Rsm can be obtained at 15 A Ip, 300 µs Ton and 50 µs Toff machining condition.

In Figure 2, it is seen that Ra improves with decreasing discharge current, increasing pulse on time and pulse off time. The negative effect of the discharge current on the average surface roughness is known [24–26]. Pulse on time as expands the diameter of the plasma channel during machining as also increases the surface roughness by increasing the discharge energy. High discharge energy causes more melting and evaporation of the workpiece material [27]. With increasing plasma channel diameter and greater melt density, the cleaned material in the pulse off time often creates peaks at less elevation. This can be seen as a reducing factor in the average surface roughness.
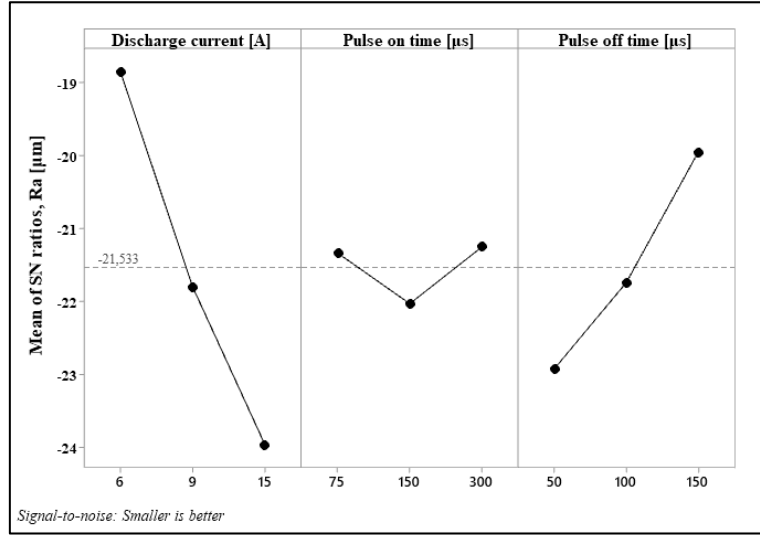
Figure 2. S/N ratio plot for average surface roughness (Ra) (Ortalama yüzey pürüzlülüğü (Ra) için S/N oranları grafiği)

In Figure 3, it is seen that Rz improves with decreasing discharge current and pulse on time and increasing pulse off time. The effect of the discharge current on Rz should be greater than for other roughness results. The discharge current is the most effective variable on the depth of surface roughness due to the increase in the intensity of the spark [28]. In contrast to the average surface roughness in the figure, a lower Rz result was obtained at the lower value of the pulse on time. In addition, an increase in Rz is observed at high pulse on time compared to 150 μs level. The Rz result is a performance result calculated by averaging the highest peaks. The density of low-level peaks does not affect this result.
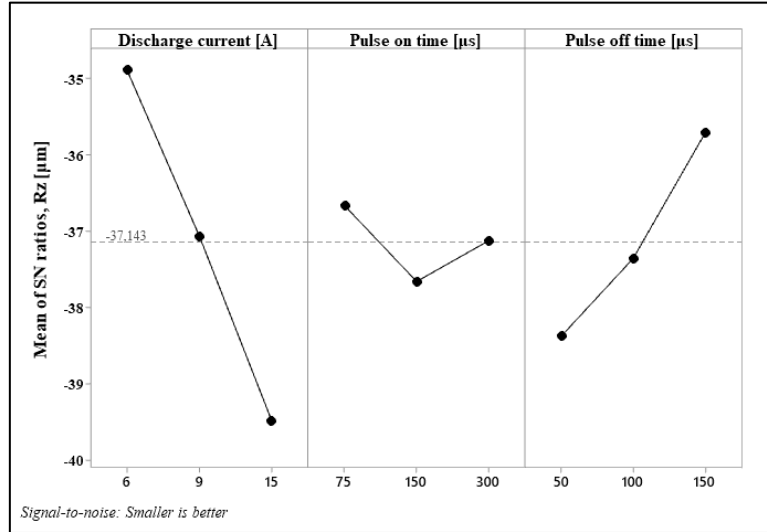

Figure 3. S/N ratio plot for average surface roughness depth (Rz) (Ortalama yüzey pürüzlülüğü yüksekliği (Rz) için S/N oranları grafiği)

In Figure 4, it is seen that Rsm increases with decreasing pulse off time and increasing pulse on time. Rsm obtained in the experimental study is calculated as the mean width of the highest peaks and troughs [21]. It cleans the debris from the dielectric processing zone in the pulse off time. The increased pulse off time takes out more of the recast melt during cleaning. This situation creates new peaks and craters and has a reducing effect on Rsm. However, in the literature, it is mentioned that the surface roughness worsens as a result of poor cleaning of the spillage when the pulse off time is not sufficient [29]. The low discharge current in the experimental study reduces the discharge energy and erodes less surface, thus increasing the average width of craters and peaks. The increased discharge energy with high discharge current increases the amount of molten material and causes the formation of larger craters, thus increasing the Rsm.
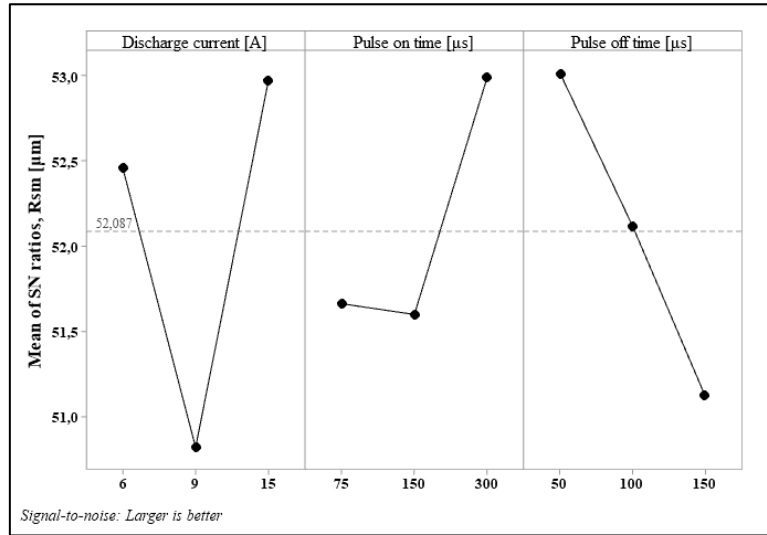
Figure 4. S/N ratio plot for average peak width (Rsm) (Ortalama tepe genişliği (Rsm) için S/N oranları grafiği)

Analysis of variance was used to determine statistically significant variable parameters and their contribution to surface roughness. ANOVA results for surface roughness of variable parameters are presented in Table 6. In the table is given as P effect of the processing conditions (P ≤ 0.05 as boundary condition), DF degrees of freedom, SS sum of squares and MS mean of squares [30]. The F-value indicates a value in the confidence interval for the contribution of the processing conditions to the model for the result to be modelled for prediction. At larger F value, it can be interpreted that the machining condition causes a large change on the performance result.

In the analysis of the F-value in Table 6, the most important parameter affecting Ra, Rz and Rsm is the discharge current. In the P-value analysis, it is seen that Ip has a significant effect for Ra and Rz, while other variable parameters have no significant effect on the result data (Ra, Rz, Rsm).

Table 6. ANOVA results for surface roughness (Yüzey pürüzlülüğü için ANOVA sonuçları)

Source	DF	SS	MS	F-Value	P-Value	PCR (%)
Ra						
Ip	2	74.354	37.177	19.95	0.048	70.87
Ton	2	3.182	1.591	0.85	0.539	3.03
Toff	2	23.647	11.823	6.35	0.136	22.54
Error	2	3.726	1.863			3.55
Total	8	104.91				100.00
Rz						
Ip	2	2334.11	1167.06	56.86	0.017	70.41
Ton	2	182.04	91.02	4.43	0.184	5.49
Toff	2	757.73	378.86	18.46	0.051	22.86
Error	2	41.05	20.53			1.24
Total	8	3314.93				100.00
Rsm						
Ip	2	17014	8507	1.71	0.369	36.34
Ton	2	8263	4131	0.83	0.546	17.65
Toff	2	11599	5799	1.17	0.462	24.78
Error	2	9942	4971			21.24
Total	8	46817				100.00

The ratio (%) contribution of the variable parameters (PCR) on Ra, Rz and Rsm is shown graphically in Figure 5 as a result of the analysis of variance. When the graphs are examined, Ip 70.87%, Ton 3.03% and Toff 22.54% has effect on Ra, Ip 70.41%, Ton 5.49%, Toff 22.86% has

effect on Rz, Ip 36.34%, Ton 17.65%, Toff 24.78% has effect on Rsm. The mean effect on the experimental study was determined as 59.21% for Ip, 8.72% for Ton and 23.39% for Toff.
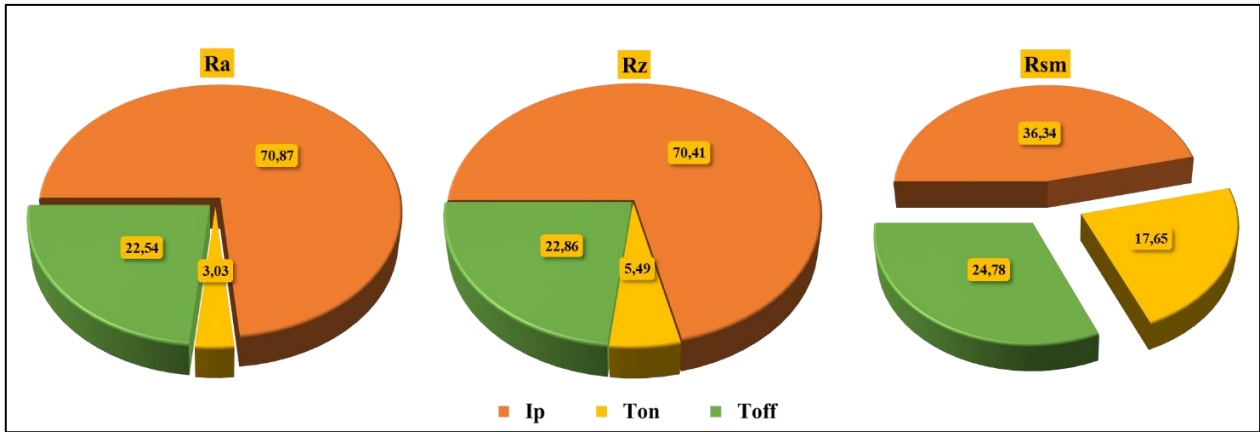

Figure 5. Percent effect plot of variable parameters on Ra, Rz and Rsm (Değişken parametrelerin Ra, Rz ve Rsm üzerine yüzde etki grafiği)

After the experiments, the images taken from the machined surface of the workpiece material are separated in detail in Figure 6 according to the processing conditions. Figure 6 shows traces of burning and recast material, micro-hole or crater-like structures formed on the workpiece surface [31]. These structures are encountered in the recast layer (white layer), which is a typical result of the electro-erosion process [32]. The recast layer is a hard-brittle structure, the thickness of which varies according to the melting point of the electrode, discharge energy and pulse off time [33]. This layer consists of dielectric material and electrode (tool or workpiece) material that cannot be ejected in the pulse off time, which rapidly cools and solidifies [34]. As seen in Figure 6, the crater width increases as the pulse on time increases due to the expansion in the plasma channel. With the effect of the experimental design, it is seen that this expansion increases with the increase in the pulse off time in the 6A, 9A and 15 A discharge current experiments.
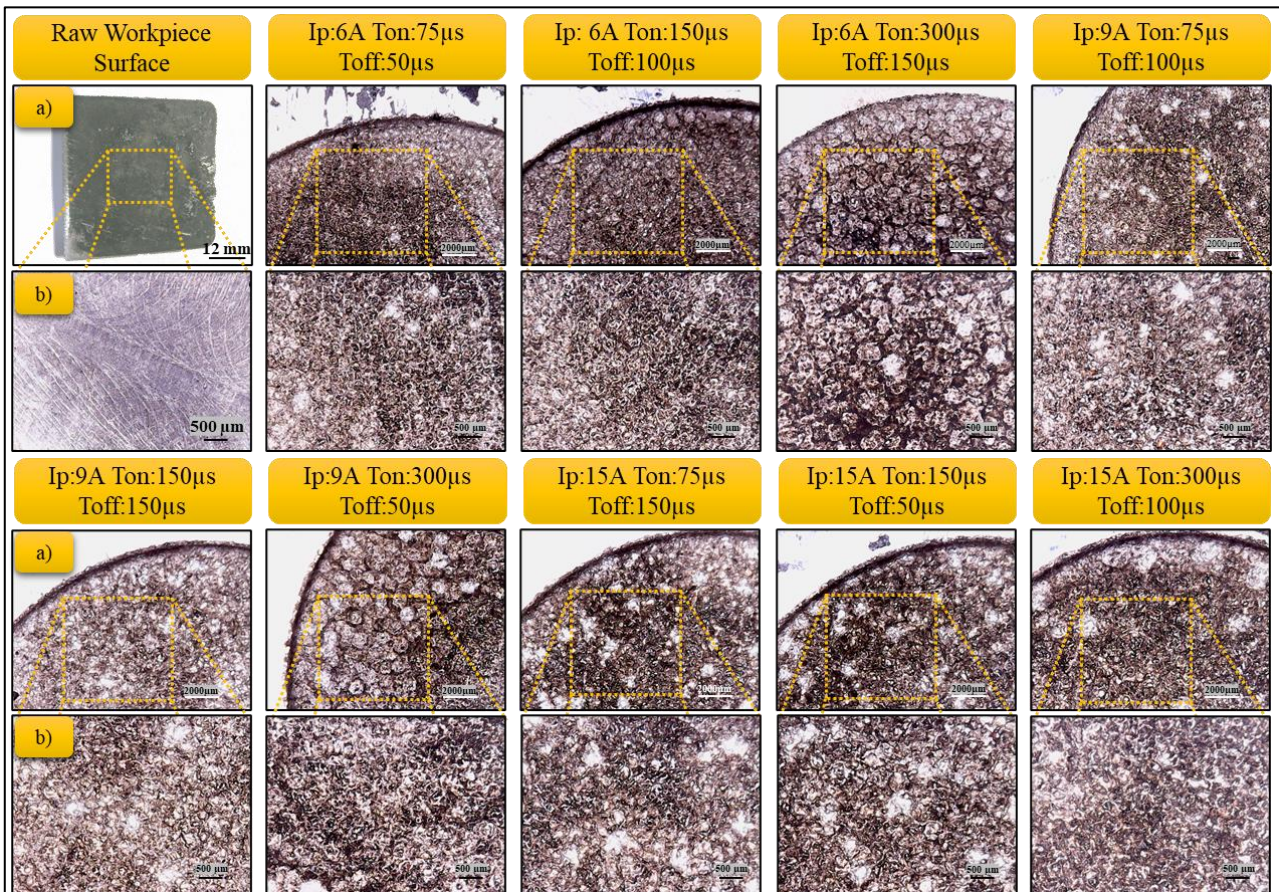
Figure 6. Surface images of workpiece material in a) 2000 μm, b) 500 μm scale (İş parçası malzemesinin yüzey görüntüleri a) 2000 μm ölçeğinde, b) 500 ölçeğinde)

Electro-erosion machining is a two-way advanced manufacturing technique in which the workpiece and tool material are wear. Machining takes place with electrons moving from the workpiece to the tool (electrode) surface and ions moving from the dielectric to the workpiece (cathode) [35]. Thus, it is possible to see craters and microcracks in the electrode material after EDM. After the experiments, the images taken from the machining surface of the tool material (electrode) are separated in detail in Figure 7 according to the machining conditions. When the tool images are examined, the pulse on time and pulse off time cause the craters to expand on the tool electrode surface as well as on the workpiece surface. In addition, the color difference between the unused tool and the used tool can be opened as short circuits and burns caused by spark energy as a result of the carbon from the dielectric penetrating the surface of the positive pole copper electrode during processing [36].
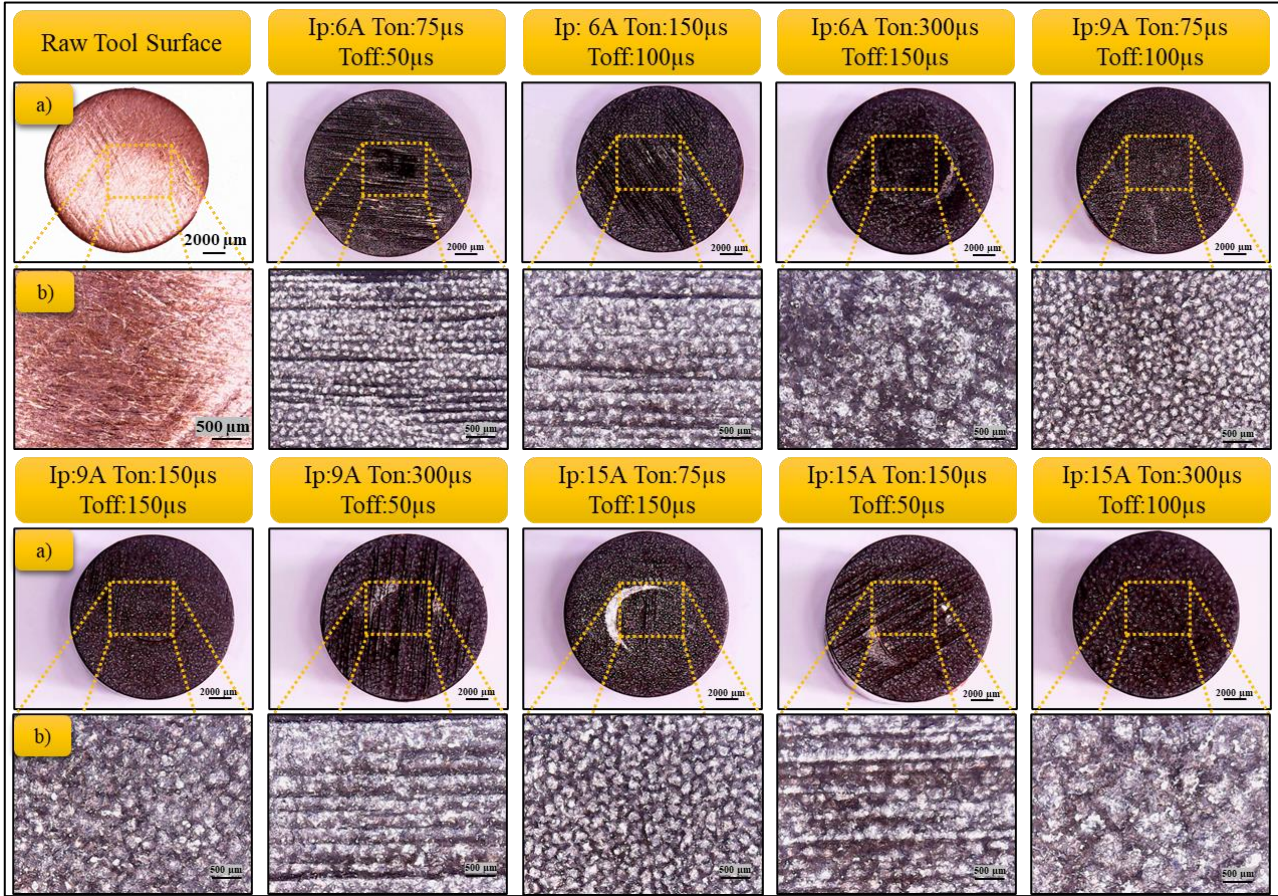

Figure 7. Surface images of tool material in a) 2000 μm scale, b) 500 μm scale (Takım malzemesinin yüzey görüntüleri a) 2000 μm ölçeğinde, b) 500 μm ölçeğinde)

4. CONCLUSIONS (SONUÇLAR)

In this study, the surface roughness of the Al5083 material processed by the die-sinking type electro discharge machining method was investigated. In the study, the effects of variable parameters such as discharge current (Ip), pulse on time (Ton) and pulse off time (Toff) on the obtained Ra, Rz and Rsm surface roughness results were statistically investigated. The effects of the processing parameters on the surface quality were interpreted with the images taken from the machining surface. The results obtained after the experimental study are summarized below as a list.

- The signal to noise ratio for Ra increased by 35.24% in the range from -25.2038 to -16.3195 for Rz increased by 19.86% compared to the variables in the range from -40.7252 to -

32.9186 for Rsm increased by 9.04% compared to the variables in the range from 50.1841 to 54.7231.

- In the experimental study, while the discharge current was the most effective (average 59.21%) parameter on Ra, Rz and Rsm, the mean effect of pulse on time and pulse off time were 8.72% and 23.39%, respectively.
- In the electro discharge machining technique, the workpiece wears out as well as the tool material. Tool material wear increases with increasing discharge current and decreases with increasing pulse on time and pulse off time.
- The surface roughness of the workpiece material increases for Ra and Rz as Ip increases and Toff decreases; first increasing and then decreasing as Ton increases. Rsm first decreased and then increased as Ip increased, increased as the pulse on time increased, and decreased as the pulse off time increased.
- Since Ra and Rz are based on depth values in roughness, the energy of the spark has a bad effect on the surface roughness depth. However, an increase in Ra and Rz was observed in the experimental study at low and high pulse on time. Thus, it was concluded that in the case of a high pulse on time, with increasing plasma channel diameter, denser melt is cleaned in the pulse off time and the height of the peaks and craters decreases.
- High Rsm is a preferred roughness result due to its effect on fatigue. In the experimental study, the pulse off time increased the Rsm by increasing the crater width, and the Rsm decreased as the pulse off time increased. This has been interpreted as the formation of new peaks and craters by further cleaning of the recast melt in the high pulse off time.
- Best Ra at 6 A Ip, 300 μs Ton and 150 μs Toff processing condition, best at Rz 6 A Ip, 75 μs Ton and 150 μs Toff processing condition; the best Rsm can be obtained at 15 A Ip, 300 μs Ton and 50 μs Toff processing condition.

REFERENCES (KAYNAKLAR)

1. TMMOB Metalurji Mühendisleri Odası, Alüminyum raporu, Metalurji, 137: 1–43, 2004.
2. G. Önal, A. Ünüvar, T. Şimşek, 5083 Al-Mg alaşımında mekanik özellikler üzerine korozyon etkisinin araştırılması, Gazi Üniversitesi Mühendislik Mimarlık Fakültesi Dergisi, 20(2): 191–196, 2013.
3. A. Kaya, M. Aslan, N. F. Yilmaz, H. Kurt, Al-Mg-SiC kompozitlerin görünür yoğunluklarının Taguchi analizi, El-Cezeri Fen ve Mühendislik Dergisi, 7(2): 773–780, 2020.
4. M. C. Santos, A. R. Machado, W. F. Sales, M. A. S. Barrozo, E. O. Ezugwu, Machining of aluminum alloys: a review, The International Journal of Advanced Manufacturing Technology, 86 (9): 3067–3080, 2016.
5. Y. Sun, L. Jin, Y. Gong, X. Wen, G. Yin, Q. Wen, B. Tang, Experimental evaluation of surface generation and force time-varying characteristics of curvilinear grooved micro end mills fabricated by EDM, Journal of Manufacturing Processes, 73: 799–814, 2022.
6. M. P. Groover, Fundamentals of Modern Manufacturing, 4. Ed., John Wiley & Sons, 2010.
7. N. M. Kumar, S. S. Kumaran, L. A. Kumaraswamidhas, An investigation of mechanical properties and material removal rate, tool wear rate in EDM machining process of AL2618 alloy reinforced with Si3N4, AlN and ZrB2 composites, Journal of Alloys and Compounds, 650: 318–327, 2015.
8. L. Selvarajan, R. Sasikumar, N. Senthil Kumar, P. Kolochi, P. Naveen Kumar, Effect of EDM parameters on material removal rate, tool wear rate and geometrical errors of aluminium material, Materials Today: Proceedings, 46: 9392–9396, 2021.
9. O. Poyrazoğlu, Elektriksel kıvılcımla aşındırma metodu ile işleme edm elektroerozyon tekniği, TEKEV, Ankara, (1994).
10. P. N. Singh, K. Raghukandan, B. C. Pai, Optimization by Grey relational analysis of EDM parameters on machining Al–10%SiCp composites, Journal of Materials Processing Technology, 155–156: 1658–1661, 2004.
11. C. R. Sanghani, G. D. Acharya, A review of research on improvement and optimization of performance measures for electrical discharge machining, Journal of Engineering Research and Applications, 4 (1): 433–450, 2014.
12. W. König, Fertigungsverfahren 3: Abtragen, Generieren und Lasermaterialbearbeitung, 4. Ed., Springer-Verlag, Berlin Heidelberg, (2007).

13. I. Ayesta, O. Flaño, B. Izquierdo, J. A. Sanchez, S. Plaza, Experimental study on debris evacuation during slot EDMing, Procedia CIRP, 42: 6–11, 2016.

14. T. Koyano, S. Suzuki, A. Hosokawa, T. Furumoto, Study on the effect of external hydrostatic pressure on electrical discharge machining, Procedia CIRP, 42: 46–50, 2016.

15. A. Kalyon, Alüminyum 6082 alaşımının pirinç elektrot ile işlenebilirliğinin optimizasyonu, El-Cezeri Fen ve Mühendislik Dergisi, 6(1): 118–130, 2019.

16. W. Safiei, M. R. R. M. Amin, Experimental investigation of EDM die sinking process parameters on Aluminium alloy 5083 using design of experiment, International Journal of Engineering Technology and Sciences, 4(1): 138–144, 2017.

17. M. M. Ali, S. Laily, B. Manshoor, N. Syahrian, R. Izamshah, M. Hadzley, M. Muhamad, Performance of copper, copper tungsten, graphite and brass electrode on MRR, EWR and SR of aluminium LM6 in EDM die sinking, Journal of Advanced Research in Applied Mechanics, 6(1): 30–36, 2015.

18. K. Kakkar, N. Rawat, A. Jamwal, A. Aggarwal, Optimization of surface roughness, material removal rate and tool wear rate in EDM using Taguchi method, International Journal of Advance Research, Ideas and Innovations in Technology, 4(2): 16–24, 2018.

19. P. Sadagopan, B. Mouliprasanth, Investigation on the influence of different types of dielectrics in electrical discharge machining, The International Journal of Advanced Manufacturing Technology, 92(1): 277–291, 2017.

20. Y. H. Guu, M. T.-K. Hou, Effect of machining parameters on surface textures in EDM of Fe-Mn-Al alloy, Materials Science and Engineering: A, 466(1): 61–67, 2007.

21. R. Cakiroglu, M. Günay, Elektro erozyonla tornalama yöntemiyle işlenen soğuk iş takım çeliğinin yorulma ömrünün tahmini, Politeknik Dergisi, 24(2): 495–502, 2021.

22. TS 6956 EN ISO 4287, Geometrical product specifications (GPS)-Surface texture: Profile method-Terms, definitions and surface texture parameters, Türk Standardı, İsviçre, 1–22, 1997.

23. Y.-C. Lin, Y.-F. Chen, D.-A. Wang, H.-S. Lee, Optimization of machining parameters in magnetic force assisted EDM based on Taguchi method, Journal of Materials Processing Technology, 209(7): 3374–3383, 2009.

24. S. H. Lee, X. Li, Study of the surface integrity of the machined workpiece in the EDM of tungsten carbide, Journal of Materials Processing Technology, 139(1): 315–321, 2003.

25. E. Pujiyulianto, Suyitno, Effect of pulse current in manufacturing of cardiovascular stent using EDM die-sinking, The International Journal of Advanced Manufacturing Technology, 112(11): 3031–3039, 2021.

26. H. Ramasawmy, L. Blunt, Effect of EDM process parameters on 3D surface topography, Journal of Materials Processing Technology, 148(2): 155–164, 2004.

27. H. T. Lee, T. Y. Tai, Relationship between EDM parameters and surface crack formation, Journal of Materials Processing Technology, 142(3): 676–683, 2003.

28. A. A. Khan, M. Y. Ali, M. M. Haque, A study of electrode shape configuration on the performance of die sinking EDM, International Journal of Mechanical and Materials Engineering, 4 (1): 19–23, 2009.

29. F. Yerui, G. Yongfeng, L. Zongfeng, Experimental investigation of EDM parameters for TiC/Ni cermet machining, Procedia CIRP, 42: 18–22, 2016.

30. M. Günay, E. Yücel, Application of Taguchi method for determining optimum surface roughness in turning of high-alloy white cast iron, Measurement, 46(2): 913–919, 2013.

31. Y. H. Guu, K.-L. Tsai, L.-K. Chen, An experimental study on electrical discharge machining of manganese–zinc ferrite magnetic material, Materials And Manufacturing Processes, 22 (1): 66–70, 2007.

32. V. Prakash, Shubham, P. Kumar, P. K. Singh, A. K. Das, S. Chattopadhyaya, A. Mandal, A. R. Dixit, Surface alloying of miniature components by micro-electrical discharge process, Materials and Manufacturing Processes, 33(10): 1051–1061, 2018.

33. R. Davis, A. Singh, S. Kachhap, Experimental investigation of the effect of input control variables in near dry electric discharge drilling process, Materials Today: Proceedings, 18: 3027–3033, 2019.

34. J. E. A. Qudeiri, A. Zaiout, A.-H. I. Mourad, M. H. Abidi, A. Elkaseer, Principles and characteristics of different edm processes in machining tool and die steels, Applied Sciences, 10(6): 2082, 2020.

35. A. Equbal, A. K. Sood, Electrical discharge machining: an overview on various areas of research, Manufacturing and Industrial Engineering, 13: 1–6, 2014.

36. N. Mohri, M. Suzuki, M. Furuya, N. Saito, A. Kobayashi, Electrode wear process in electrical discharge machinings, CIRP Annals, 44(1): 165–168, 1995.

Influence of Glass Fiber Ratio on Drillability Characteristics of PA66 Polymer for Aerospace Applications

Gonca Uslu[1*] (iD), Muzaffer Demirhan[1] (iD), Nafiz Yaşar[2] (iD), Mehmet Erdi Korkmaz[3] (iD)

[1]*Karabük Üniversitesi, Lisansüstü Eğitim Enstitüsü, Karabük, Türkiye*
[2]*Karabük Üniversitesi, TOBB Teknik Bilimler MYO, Karabük, Türkiye*
[3]*Karabük Üniversitesi, Mühendislik Fakültesi, Karabük, Türkiye*

ABSTRACT

This study examined the machinability of polyamide 66 (PA66) reinforced with glass fiber (GF) at 10%, 20%, and 30%. Cutting speeds of 40, 80 and 120 m/min and feed rates of 0.06, 0.09, and 0.12 mm/rev were used to examine thrust force (Fz) and surface roughness (Ra). Drilling operations were done using uncoated HSS and TiAlN coated HSS cutting tools. The goal of this research is to investigate the effect of cutting parameters (spindle speed and feed rate) and reinforcement ratios on thrust force (Fz) and surface roughness during cutting operations (Ra). Statistical analysis was used to determine the contribution of the cutting parameters to the results that were under investigation. For the purpose of examining the hole quality and damage mechanisms, scanning electron microscopy (SEM) was performed. The surface roughness values obtained in the 30% glass fiber added PA66 material drilled with an uncoated cutting tool were quite high. A high fiber rupture rate on the hole surfaces, matrix fragmentation, and other difficulties resulted in increased thrust force.

Cam Elyaf Oranının Havacılık ve Uzay Uygulamaları için PA66 Polimerinin Delinebilirlik Özelliklerine Etkisi

ÖZET

Bu çalışmada %10, %20 ve %30 cam elyaf (GF) ile güçlendirilmiş poliamid 66'nın (PA66) işlenebilirliği incelenmiştir. İtme kuvvetini (Fz) ve yüzey pürüzlülüğünü (Ra) incelemek için 40, 80 ve 120 m/dak kesme hızları ve 0,06, 0,09 ve 0,12 mm/dev ilerleme hızları kullanılmıştır. Kaplamasız HSS ve TiAlN kaplı HSS kesici takımlar kullanılarak delme işlemleri yapılmıştır. Bu araştırmanın amacı, delme işlemleri sırasında kesme parametrelerinin (işmili hızı ve ilerleme hızı) ve takviye oranlarının itme kuvveti (Fz) ve yüzey pürüzlülüğü (Ra) üzerindeki etkisini araştırmaktır. İncelenen sonuçlara kesme parametrelerinin katkısını belirlemek için istatistiksel analiz kullanılmıştır. Delik kalitesi ve hasar mekanizmalarını incelemek amacıyla taramalı elektron mikroskobu (SEM) ile incelemeler yapılmıştır. Kaplamasız kesici takımla delinmiş %30 cam elyaf katkılı PA66 malzemesinde elde edilen yüzey pürüzlülük değerleri oldukça yüksektir. Delik yüzeylerinde yüksek lif kopma oranı, matris parçalanması ve diğer zorluklar, artan itme kuvvetiyle sonuçlanmıştır.

1. INTRODUCTION (GİRİŞ)

As a matrix in polymer composite materials, polyamides, epoxy resins, polyesters, phenolic resins, and vinyl ester resins are commonly utilized due to their high strength and low density as well as their outstanding chemical stability and exceptional corrosion resistance [1]. These materials, on the other hand, are reinforced with various types of fibers [2], including glass, carbon, basalt, and aramid, because they have a poor hardness and a proclivity to creep at high temperatures, and hence require reinforcement [3,4]. Because of their superior mechanical and thermal qualities are well suited for use in aviation and maritime applications [5,6]. Furthermore, they offer a high filling capacity, a low and well-distributed internal tension in products, and are simple to process when it comes to filling materials. There is no stress accumulation at the interface

between the reinforcements and the matrix as a result of the smooth spherical surfaces of these microparticles. As reinforcements, they are particularly well suited, particularly when coupled qualities such as isotropy or low melt viscosity are required [7]. A more promising alternative is to employ composite materials that are reinforced with fibers, which are becoming increasingly popular [8], particularly in the aerospace and aviation industries as well as the automobile, sporting goods, and marine industries [9,10]. Composite materials are named as heterogeneous materials that are formed by combining the properties of at least two different materials in a single and new material, rather than using single materials with limited properties [11]. Composite materials have properties such as stiffness level, fatigue and shrinkage level, resistance to pressure and tendency, sensitivity to high temperature and high corrosion resistance due to the different properties of at least two different materials [12]. Apart from these, it exhibits good tribological properties such as low density, high hardness, and high resistance to breakage. For this reason, it is widely used in many fields such as construction, space technologies, automotive industry, maritime, nuclear industry, robotic technology, health sector and chemicals, especially in the defense industry and aviation industry [1]. Composite materials are highly resistant to temperature, as well as being light, robust and resistant to impacts, allowing work to be carried out in many areas. It determines the basic properties of matrix, fiber, ball, interface and microstructure composite materials [13]. The fiber material is the component that can determine the strength and load-bearing properties of composites [14]. Glass fiber reinforced composites (GFRP) are obtained by using methods such as molding under pressure and vacuum, hand laying. The dimensions of the place to be used in the production phase and the geometric shape are also taken into consideration. Machining methods such as turning, drilling and milling are used to finalize composites produced in various conditions [15]. However, GFRP composites are not the isotropic structure found in metals and alloys. Therefore, various problems occur in the machining of GFRP composite. During the processing of fiber reinforced composites, it is important to increase the level of surface quality and increase the life of the tool. Machining costs have a significant impact on the cutting force and the quality level of the machined surfaces. The surface quality has a great influence on the mechanical properties of the composite material [16]. Therefore, the quality of the surface is one of the most important issues to be considered during the turning phase. Machining variables and also fiber length and proportions must be at appropriate values and ratios for the surface quality to be at the best level [17]. Drilling generally constitutes finishing, and the higher the reject rate of parts due to these holes, the higher the part defects and scrap material. Therefore, high quality drilling is always desired [18].

Taguchi technique and multiple regression analysis were employed by Latha et al. to model delamination during the drilling of GFRP composites with carbide drills, according to their findings. The researchers' findings revealed that the feed rate and drill bit diameter were the most significant input elements that could have an impact on delamination [19]. Krishnaraj et al. conducted a survey on the optimization of machining parameters for drilling thin Carbon fiber reinforced polymer (CFRP) laminates, which they published in the journal Composites Engineering. They stressed that the circularity of the hole is the most important aspect, and that feed rate was the most influencing factor on the thrust force, delamination, and hole diameter (all of which were measured) [20]. Gaitonde et al. investigated the effects of drilling parameters on thrust forces, hole sizes, and circularity in PA66 matrix-glass fiber reinforced composites with a 30 percent glass fiber content [21]. They discovered that the tip angle of the drill can have an effect on the thrust force and the roundness of the hole while drilling a hole. In order to decrease the thrust force, they advised a point angle of 115° when the drill had an 85° point angle to ensure the least amount of roundness error was produced. When drilling a 30 percent GFR polypithylamide matrix composite, Fçc and Ayparças discovered that the material of the cutting tool can have an impact on the surface roughness of the composite. In their research, they discovered that carbide drills created holes with lower surface roughness than holes produced with high-speed steel (HSS) drills [22].

However, while most of the literature is concerned with mechanical characteristics or machinability, most of the testing has been done with constant parameters. Although the drillability

of PA66 reinforced with GF was evaluated at 10 percent, 20 percent, and 30 percent reinforcement ratios, cutting speeds, and feed rates using uncoated and TiAlN coated HSS drills for Fz and Ra, the results showed that the drillability was poor.

2. MATERIAL AND METHOD (MATERYAL VE YÖNTEM)

The polyamide 66 material utilized in this investigation was manufactured by adding 10%, 20%, and 30% glass fiber. Drilling of GFRP Composite with various fiber ratios at the cutting speeds of 40-80-120 m/min and feed rates of 0.06-0.09-0.12 mm/rev was used to examine the effects of fiber ratio, cutting speed, and feed rate on Fz and Ra (Figure 1). The experiments were carried out at three distinct levels of feed rate and cutting speed, which were established by taking into account the cutting tool recommendation as well as relevant research [23,24].

Figure 1. Experimental Setup (Deneysel düzenek)
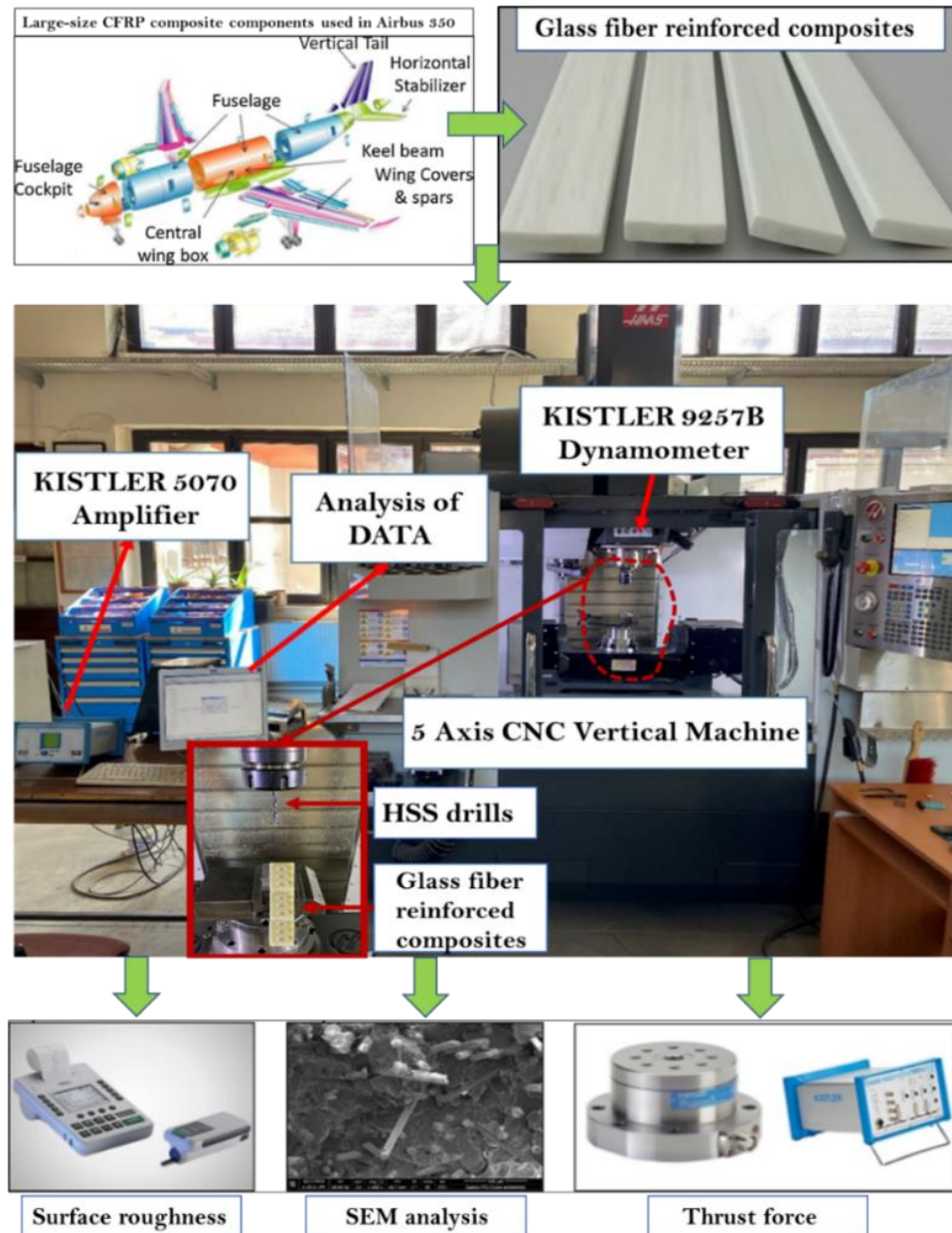
It was decided to make GFRP and GBRP composites with varying reinforcement ratios and test the mechanical properties of these composites. A high-strength engineering thermoplastic known as Polyamide 66 (PA66) is used as the matrix material. It has good corrosion and abrasion resistance, self-lubricating characteristics, low impact resistance, and exceptionally high strength. The images

of the glass fiber (glass fiber GF) reinforcement elements that were supplied and used in the composite are shown below. The coated aminosilane is reinforced with average chopped length 11 mm of diameter 4.5 mm PA2 types of short glass fibers (glass fiber industry, Turkey) as well as short glass fibers (glass fiber industry, Turkey) coated again surface aminosl.

The thrust force was measured with a piezoelectric dynamometer (Kistler 9257), which is connected to the 5070-A multichannel charge amplifier and Dynoware 2825A-02-01 software. The surface roughness of the holes was measured in order to determine the impact of the type of cutting tool used and the cutting parameters used in the cutting process. The hole surface roughness was measured using a Mahr brand MarSurf M 300 type profilometer.

3. RESULTS AND DISCUSSION (SONUÇLAR VE TARTIŞMA)

During drilling, the cutting tool removes chip from the resin rich region on the outside of the GFRP composite. The thrust force causes rapid elastic loading of the workpiece material. The GFRP's anisotropy causes a decrease of stiffness, which causes force fluctuation. The perpendicular-to-fiber cutting zone causes a force signal variance when the cutting tool touches the fibers and advances. Moving from 0.06 mm/rev to 0.09 mm/rev boosted Fz values by almost 22%, and from 0.09 mm/rev to 0.12 mm/rev increased them by nearly 44%. These changes show that feed rate is more important than cutting speed. 30 percent GFRP had a higher Fz than 10% reinforcement at the same cutting speed and feed rate. The other feed rates and cutting speeds showed a similar tendency, with Fz values increasing with the glass fiber ratio. The glass fiber ratio increases with strength and hardness. The test results with coated drills (Figure 2d-e-f) show lower Fz values than uncoated cutting instruments (Figure 2a-b-c). Coated drills have a lower friction coefficient than uncoated cutting instruments. This coating has a high hardness value and hence allows for high-speed work [10]. The low coefficient of friction enables for easy chip evacuation. This is good for chip development. It also works effectively at high temperatures due to its low thermal conductivity. So it has good tool life and wear resistance at high temperatures [9].

All increases in cutting speed were reduced by approximately 8% compared to the uncoated cutting tool. The feed rate decreases by 11% compared to the uncoated cutting tool. Using a coated tool improves Fz value. The thrust force increases with increasing glass fiber ratio. Increasing the glass fiber ratio increases the material's elastic modulus and thus the thrust force. This impact is accompanied by a reduction in the contact area between the cutting tool and the workpiece, as well as a reduction in the specific cutting energy [11]. When feed rates increased at all the other parameters constant, the forces increased as well. Following the findings of previous studies [12,13], our results were found to be associated with increased uncut chip thickness and shear area. Ra values decrease with cutting speed (Figure 2g-2l). Like the thrust force, the observed discrepancy can be explained by increased tool-to-workpiece friction with increasing cutting speed. It also aids in chip removal. By increasing feed rate from 0.06 to 0.09 mm/rev at 40 m/min cutting speed, the Ra values improve by roughly 10% and 25%. The same feed rate increment increases the Ra levels by 50% and 30% at 80 m/min and 120 m/min, respectively.
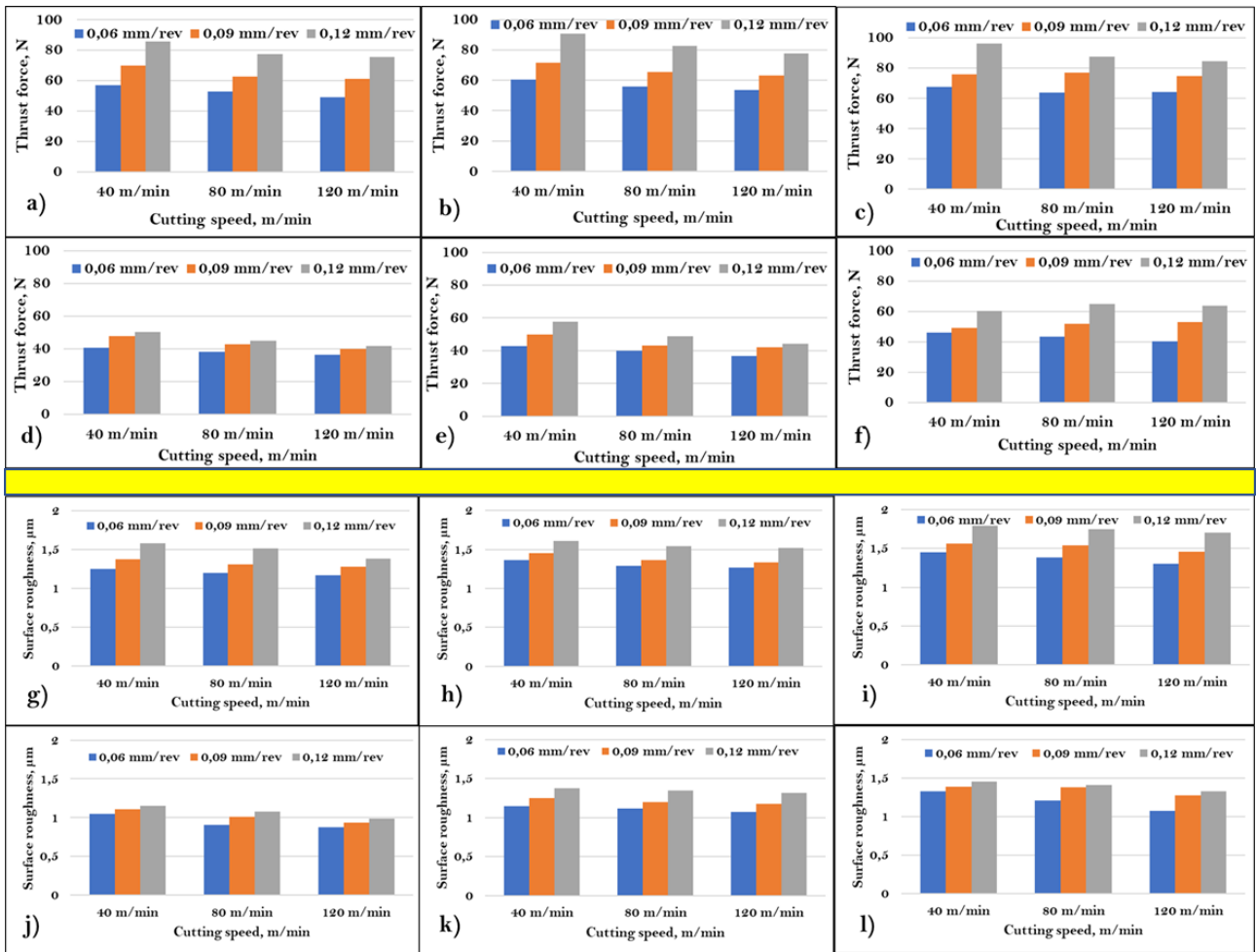
Figure 2. Thrust force variation for a) 10%GFR-uncoated, b) 20%GFR-uncoated, c) 30%GFR-uncoated, d) 10%GFR-coated, e) 20%GFR-coated, f) 30%GFR-coated, and Surface roughness variation, g) 10%GFR-uncoated, h) 20%GFR-uncoated, i) 30%GFR-uncoated, j) 10%GFR-coated, k) 20%GFR-coated, l) 30%GFR-coated (İtme kuvveti değişimi, a) %10 GFR kaplamasız, b) %20 GFR kaplamasız, c) %30 GFR kaplamasız, d) %10 GFR kaplamalı, e) %20 GFR kaplamalı, f) %30 GFR kaplamalı ve Yüzey pürüzlülük değişimi, g) %10GFR kaplamasız, h) %20GFR kaplamasız, i) %30GFR kaplamasız, j) %10GFR kaplamalı, k) %20GFR kaplamalı, l) %30 GFR kaplamalı)

There is an average of 8% increase in Ra value when the feed rate increased from 0.06 to 0.09 mm/rev at 40 m/min cutting speed, and an average of 10% increase by 0.12 mm/rev increase. In the light of these results, it is seen that the feed rate is a more efficient factor on Ra than the cutting speed. SEM images obtained from the hole surfaces depending on the cutting speed are given in Figure 3. In addition, it was observed that 30% GFRP reached higher Ra values than 10% GFRP at the same cutting speed and feed rate. Similarly, for different feed rates and cutting speeds, Ra values increased with increasing glass fiber ratio. Ra values increased with increasing glass fiber ratio, indicating a similar tendency for various feed rates and cutting speeds. Figure 3d-3f shows the hole surface varies with the glass fiber ratio. Under the same cutting conditions, the uncoated drill has higher Ra values than the coated drill. This is explained by the coated drill's strong wear resistance, low friction coefficient, and the elimination of chips between the tool and the workpiece. Ra grew with the glass fiber ratio. Due to the glass fiber ratio and difficult cutting, this increase in surface roughness could be read as an increase in material strength [14]. Uncoated cutting tools also produce a higher Ra value. The matrix material binds to the hole surface and reduces surface damage at low feed rates (Figure 3g-i). Surface roughness is exacerbated by matrix fragmentation caused by high temperatures and high feed rates [15]. As seen in Figure 3j to 3l, the coated tool generates a superior surface by lowering friction and thus heating. Based on these findings, fast cutting speed and low feed rate improve surface quality at low glass fiber ratios. The best surface quality was 0.88 m in testing with coated cutting tools at 120 m/min and 0.06 mm/rev.
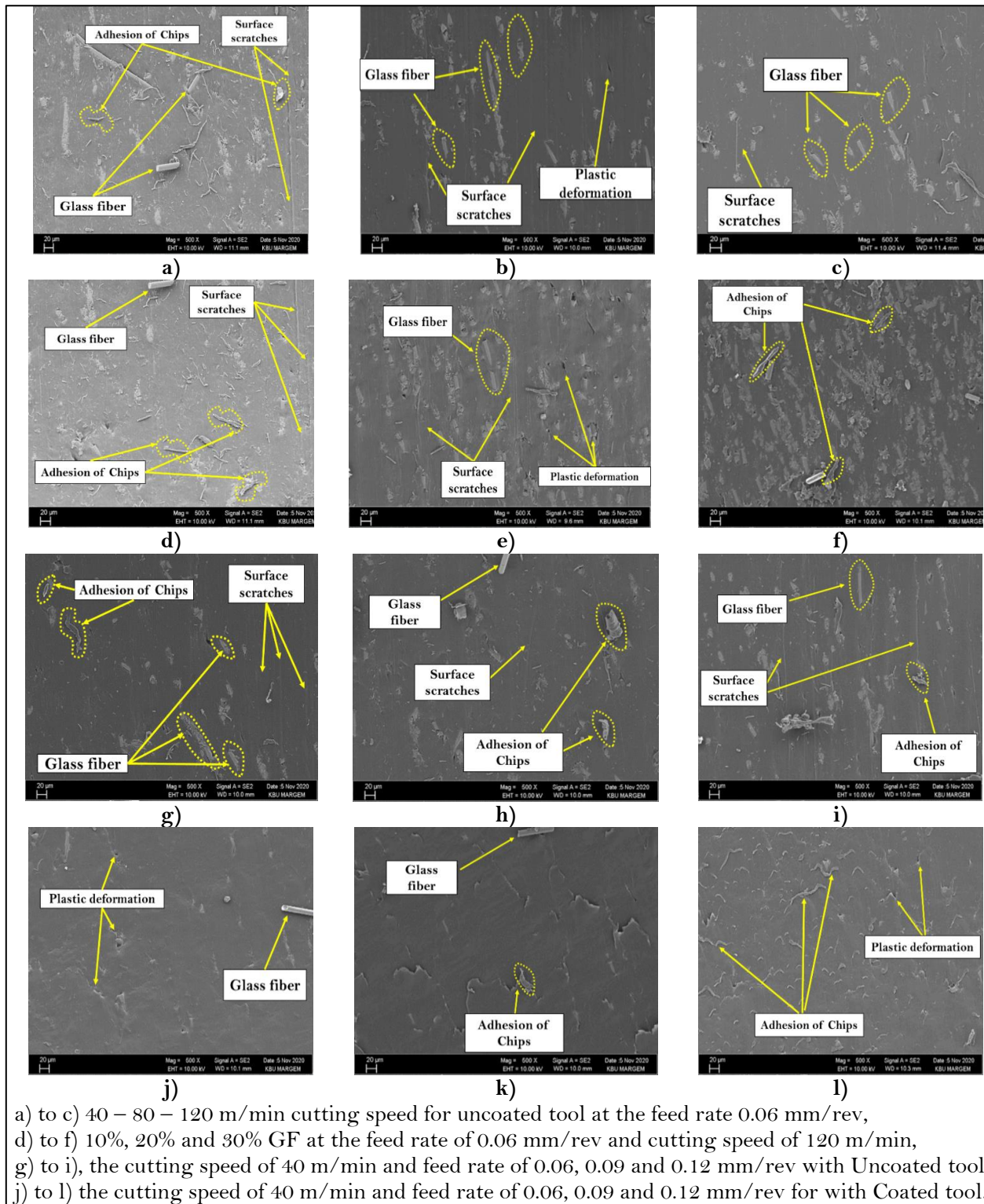
a) to c) $40-80-120$ m/min cutting speed for uncoated tool at the feed rate 0.06 mm/rev,
d) to f) 10%, 20% and 30% GF at the feed rate of 0.06 mm/rev and cutting speed of 120 m/min,
g) to i), the cutting speed of 40 m/min and feed rate of 0.06, 0.09 and 0.12 mm/rev with Uncoated tool
j) to l) the cutting speed of 40 m/min and feed rate of 0.06, 0.09 and 0.12 mm/rev for with Coated tool.

Figure 3. SEM images of hole surfaces (Delik yüzeylerinin SEM görüntüleri)

4. CONCLUSIONS (SONUÇLAR)

In this research, the machinability of single-reinforced and hybrid glass fiber-reinforced polymer composites (PA66) were investigated. To begin, polymer composites reinforced with varying ratios of carbon fibers were created. Later, machined samples were created to determine the influence of cutting parameters and reinforcement ratio on the thrust force and hole surface roughness of the fabricated samples. The materials utilized in the fabrication and the quality of the machined holes was both evaluated using scanning electron microscopy (SEM). Following are the conclusions that may be drawn from this research:

• Drilled with an uncoated cutting tool, the 30% glass fiber added polyamide 66 (PA66) material had very high surface roughness values. Adding 30% glass fiber to polyamide 66 (PA66) material causes fiber rupture on hole surfaces, matrix fragmentation, etc. The inaccuracies enhanced surface roughness.

• The SEM photos show that as the glass fiber ratio increases, the surface roughness increases due to the material's durability and forced drilling. The coated tool is tougher than the uncoated tool, allowing for easier drilling and improved surface quality.

• As a result of the drilling tests, it has been established that PA66 based fiber reinforced polymer composites are prevalent. In this paper, a generic approach for fabricating various types of composites is provided from the beginning of the fabrication process through the end of the drilling operation. This approach will be used frequently in the future for a wide range of technical components, and the characteristics identified during this study will be used to guide the process.

• The study's novelty and future advice is that an appropriate combination of glass fiber should be favored for optimal machinability and mechanical properties of GF/GB reinforced polymers rather than employing only glass fiber reinforcement.

REFERENCES (KAYNAKLAR)

1. S. Sharma, J. Singh, M.K. Gupta, M. Mia, S.P. Dwivedi, A. Saxena, S. Chattopadhyaya, R. Singh, D.Y. Pimenov, M.E. Korkmaz, Investigation on mechanical, tribological and microstructural properties of Al–Mg–Si–T6/SiC/muscovite-hybrid metal-matrix composites for high strength applications, Journal of Materials Research and Technology, 12: 1564–1581, 2021.
2. U. Koklu, S. Morkavuk, C. Featherston, M. Haddad, D. Sanders, M. Aamir, D.Y. Pimenov, K. Giasin, The effect of cryogenic machining of S2 glass fibre composite on the hole form and dimensional tolerances, The International Journal of Advanced Manufacturing Technology, 115: 125–140, 2021.
3. R. Singer, A.M. Ollick, M. Elhadary, Effect of cross-head speed and temperature on the mechanical properties of polypropylene and glass fiber reinforced polypropylene pipes, Alexandria Engineering Journal, 60: 4947–4960, 2021.
4. U.A. Khashaba, M.S. Abd-Elwahed, I. Najjar, A. Melaibari, K.I. Ahmed, R. Zitoune, M.A. Eltaher, Heat-Affected Zone and Mechanical Analysis of GFRP Composites with Different Thicknesses in Drilling Processes, Polymers, 13, 2246, 2021.
5. P. Foraboschi, Strengthening of Reinforced Concrete Beams Subjected to Concentrated Loads Using Externally Bonded Fiber Composite Materials, Materials, 15: 2328, 2022.
6. M.B. Rahman, L. Zhu, Low-Velocity Impact Response on Glass Fiber Reinforced 3D Integrated Woven Spacer Sandwich Composites, Materials, 15: 2311, 2022.
7. M. Li, G. Gan, Y. Zhang, X. Yang, Thermal damage of CFRP laminate in fiber laser cutting process and its impact on the mechanical behavior and strain distribution, Archives of Civil and Mechanical Engineering, 19: 1511–1522, 2019.
8. A. Iqbal, G. Zhao, J. Zaini, M.K. Gupta, M. Jamil, N. He, M.M. Nauman, T. Mikolajczyk, D.Y. Pimenov, Between-the-Holes Cryogenic Cooling of the Tool in Hole-Making of Ti-6Al-4V and CFRP, Materials, 14: 2021.
9. M. Danish, M.K. Gupta, S. Rubaiee, A. Ahmed, A. Mahfouz, M. Jamil, Machinability investigations on CFRP composites: a comparison between sustainable cooling conditions, The International Journal of Advanced Manufacturing Technology, 114: 3201–3216, 2021.
10. J. Xu, T. Lin, J.P. Davim, On the Machining Temperature and Hole Quality of CFRP Laminates When Using Diamond-Coated Special Drills, Journal of Composites Science, 6: 45, 2022.
11. R. Hsissou, R. Seghiri, Z. Benzekri, M. Hilali, M. Rafik, A. Elharfi, Polymer composite materials: A comprehensive review, Composite Structures, 262: 113640, 2021.
12. P. Alam, D. Mamalis, C. Robert, C. Floreani, C.M. Ó Brádaigh, The fatigue of carbon fibre reinforced plastics - A review, Composites Part B: Engineering, 166: 555–579, 2019.
13. B.V. Lingesh, B.M. Rudresh, B.N. Ravikumar, Effect of Short Glass Fibers on Mechanical Properties of Polyamide66 and Polypropylene (PA66/PP) Thermoplastic Blend Composites, Procedia Materials Science, 5: 1231–1240, 2014.
14. M.M.B. Hasan, A. Abdkader, C. Cherif, F. Spennato, Fibre hybrid composites consisting of discontinuous waste carbon fibre and continuous glass filaments developed for load-bearing structures

with improved impact strength, Composites Part A: Applied Science and Manufacturing, 126: 105610, 2019.

15. N. Khanna, C. Agrawal, D.Y. Pimenov, A.K. Singla, A.R. Machado, L.R.R. da Silva, M.K. Gupta, M. Sarikaya, G.M. Krolczyk, Review on design and development of cryogenic machining setups for heat resistant alloys and composites, Journal of Manufacturing Processes, 68: 398–422, 2021.

16. Y. Singh, J. Singh, S. Sharma, T.-D. Lam, D.-N. Nguyen, Fabrication and characterization of coir/carbon-fiber reinforced epoxy based hybrid composite for helmet shells and sports-good applications: influence of fiber surface modifications on the mechanical, thermal and morphological properties, Journal of Materials Research and Technology, 9: 15593–15603, 2020.

17. G.L. Umesh, N.J. Krishna Prasad, B.M. Rudresh, M. Devegowda, Influence of nano graphene on mechanical behavior of PA66/PA6 blend based hybrid nano composites: Effect of micro fillers, Materials Today: Proceedings, 20: 228–235, 2020.

18. N. Yaşar, M. Günay, Experimental investigation on novel drilling strategy of CFRP laminates using variable feed rate, Journal of the Brazilian Society of Mechanical Sciences and Engineering, 41: 150 2019.

19. [B. Latha, V.S. Senthilkumar, K. Palanikumar, Modeling and optimization of process parameters for delamination in drilling glass fiber reinforced plastic (GRFP) composites, Machining Science and Technology, 15: 172–191, 2011.

20. V. Krishnaraj, A. Prabukarthi, A. Ramanathan, N. Elanghovan, M. Senthil Kumar, R. Zitoune, J.P. Davim, Optimization of machining parameters at high speed drilling of carbon fiber reinforced plastic (CFRP) laminates, Composites Part B: Engineering, 43: 1791–1799, 2012.

21. V.N. Gaitonde, S.R. Karnik, J.C.C. Rubio, W. de Oliveira Leite, J.P. Davim, Experimental studies on hole quality and machinability characteristics in drilling of unreinforced and reinforced polyamides, Journal of Composite Materials, 48: 21–36, 2012.

22. F. Ficici, Z. Ayparcasi, Effects of cutting parameters on delamination during drilling of Polyphthalamide (PPA) matrix composite material with 30% glass fiber reinforcement, Acta Physica Polonica A, 127: 1118–1120, 2015.

23. J.P. Davim, P. Reis, C.C. António, Experimental study of drilling glass fiber reinforced plastics (GFRP) manufactured by hand lay-up, Composites Science and Technology, 64: 289–297, 2004.

24. Ş. Yazman, The effects of back-up on drilling machinability of filament wound GFRP composite pipes: Mechanical characterization and drilling tests, Journal of Manufacturing Processes, 68: 1535–1552, 2021.